

Technische Universität München
Lehrstuhl für Physikalische Chemie

**Identical location transmission electron microscopy in
combination with rotating disc electrode measurements –
the activity of fuel cell catalysts and their degradation**

KATRIN G. SCHLÖGL

Vollständiger Abdruck der von der Fakultät für Chemie der Technischen Universität
München zur Erlangung des akademischen Grades eines

Doktors der Naturwissenschaften

genehmigten Dissertation.

Vorsitzender: Univ.-Prof. Dr. H. Gasteiger

Prüfer der Dissertation:

1. Prof. Dr. M. Arenz, University of Copenhagen/Dänemark
2. Univ.-Prof. Dr. U. K. Heiz
3. Univ.-Prof. Dr. K.-O. Hinrichsen

Die Dissertation wurde am 06.06.2011 bei der Technischen Universität München
eingereicht und durch die Fakultät für Chemie am 13.07.2011 angenommen.

Je suis de ceux qui pensent que la science a une grande beauté. Un savant dans son laboratoire n'est pas seulement un technicien: c'est aussi un enfant placé en face de phénomènes naturels qui l'impressionnent comme un conte de fées.

I am among those who think that science has great beauty. A scientist in his laboratory is not only a technician: he is also a child placed before natural phenomena which impress him like a fairy tale.

Marie Curie (1938)

Contents

List of Acronyms	vii
Abstract	ix
1 Introduction	1
2 Experimental Background and Methods	5
2.1 Cyclic Voltammetry	5
2.2 Electrochemical Reactions	6
2.3 Electrocatalysis and Kinetics	7
2.4 Rotating Disc Electrode	9
2.5 Determination of the Electrochemical Active Surface Area	11
2.6 Catalytic Activity towards the ORR	13
2.7 Reversible Hydrogen Electrode	14
2.8 Differential Electrochemical Mass Spectrometry	14
2.9 Identical Location Transmission Electron Microscopy	15
3 Experimental Details	21
3.1 Working Electrode Preparation	21
3.2 Electrochemical Cell Design	23
3.3 Procedure of Experimental Measurements	24
4 Potential Cycling Degradation Measurements	27
4.1 Removing Impurities of Industrial Electrocatalysts	28
4.2 Degradation Behavior changes with Scan Rate	29
4.3 The Choice of Electrolyte influences Catalyst Stability	29
4.4 Traces of Chlorides cause increased Degradation	31
4.5 Degradation Behavior depends on Convection and Catalyst Loading	33
4.6 Conclusion	36
5 IL-TEM Investigation of the Degradation of Standard Electrocatalysts	37
5.1 Degradation Mechanisms of Platinum Nanoparticles in Fuel Cells	38
5.2 Degradation Behavior of Standard Electrocatalysts	40
5.2.1 Dependence of Catalyst Loading	43

5.2.2	Influence of Support Properties	48
5.2.3	Impact of Temperature Pre-Treatment and Particle Size	50
5.2.4	Effect of Alloying Platinum with Cobalt	55
5.2.5	Summary	56
5.3	Degradation Behavior at elevated Temperatures	59
5.4	Conclusion	66
6	Different Concepts towards High-Performance Catalysts	67
6.1	Supported Platinum Clusters as Model Electrocatalyst	68
6.1.1	Size-selected clusters as heterogeneous model catalysts under applied reaction conditions	68
6.1.2	Electrochemically induced nanocluster migration	75
6.2	Improved Catalyst Durability by Support Modifications	85
6.2.1	IL-TEM investigations on the degradation mechanism of Pt/C electrocatalysts with different carbon supports	85
6.3	Bimetallic Particles for Electrocatalysis	93
6.3.1	AuPt core-shell nanocatalysts with Pt bulk activity	93
6.3.2	Adsorbate-Induced Surface Segregation for Core-Shell Nanocatalysts	99
6.3.3	Degradation of Carbon-Supported Pt Bimetallic Nanoparticles by Surface Segregation	105
6.4	Conclusion	109
7	Conclusion	111
	List of Figures	I
	List of Tables	III
	References	V
	Acknowledgements	XIII
	Curriculum Vitae	XV
	Publication List	XVII

List of Acronyms

CCD	Charge-Coupled Device
CE	Counter Electrode
CV	Cyclovoltammogram
DEMS	Differential Electrochemical Mass Spectrometry
ECA	Electrochemical Surface Area
EDX	Energy Dispersive X-ray Spectroscopy
HER/HOR	Hydrogen Evolution/Oxidation Reaction
HOMO	Highest Occupied Molecular Orbital
H _{upd}	Underpotentially deposited Hydrogen
HSA	High Surface Area
ICP-OES	Inductively Coupled Plasma Optical Emission Spectroscopy
IL-TEM	Identical Location Transmission Electron Microscopy
LUMO	Lowest Unoccupied Molecular Orbital
MEA	Membrane Electrode Assembly
PEMFC	Proton Exchange Membrane Fuel Cell
ORR	Oxygen Reduction Reaction
RDE	Rotating Disc Electrode
RE	Reference Electrode
RHE	Reversible Hydrogen Electrode
SCE	Saturated Calomel Electrode
SHE	Standard Hydrogen Electrode
TEM	Transmission Electron Microscopy
TOC	Total Organic Carbon
TOF	Turnover Frequency
UHV	Ultra-High Vacuum
WE	Working Electrode
XRD	X-ray Diffraction

Abstract

As an alternative to conventional combustion engines, the Proton Exchange Membrane Fuel Cell using hydrogen as a fuel is a promising concept owing to its potential independence from fossil fuels, high efficiency and zero emissions. Concerning its commercial viability, the fundamental problem of high system cost per power output and lifetime is closely related to finding more active and stable catalysts for the oxygen reduction reaction. In the presented work, several methods are combined to examine the parameters and processes responsible for both activity and degradation of platinum-based catalysts. Degradation mechanisms are scrutinized by means of electrochemical measurements with the rotating disc electrode in combination with a recently developed TEM technique, which allows for the comparison of identical locations before and after accelerated stress tests.

Kurzzusammenfassung

Die mit Wasserstoff betriebene Proton Exchange Membrane Brennstoffzelle stellt aufgrund ihrer potentiellen Unabhängigkeit von fossilen Energieträgern, ihrem hohen Wirkungsgrad und fehlendem Schadstoffausstoß eine vielversprechende Alternative zum konventionellen Verbrennungsmotor dar. Das grundlegende Problem der zu hohen Systemkosten und zu geringen Lebensdauer für kommerzielle Anwendungen ist eng mit der Entwicklung aktiverer und stabiler Elektrokatalysatoren für die Sauerstoffreduktion verknüpft. In der vorliegenden Arbeit werden verschiedene Methoden kombiniert, um die Parameter und Prozesse zu untersuchen, welche für die Aktivität und Degradation platinbasierter Katalysatoren verantwortlich sind. Zur Aufklärung vorliegender Degradationsmechanismen werden elektrochemische Messungen mit der rotierenden Scheibenelektrode in Kombination mit einer neu entwickelten TEM Methode eingesetzt, welche es ermöglicht, identische Stellen vor und nach beschleunigten Degradationstests zu untersuchen.

Chapter 1

Introduction

Powering automobiles with fossil fuels is dependent on the availability of crude oil reserves. As these resources are limited and in fact many chemicals are produced from crude oil as well, in the future oil will become too valuable to be primarily used for transportation. Consequently alternatives have to be found. One possible option is the storage and generation of onboard electric energy and the use of electric power-trains [1]. In this concept, proton exchange membrane fuel cells (PEMFCs) using hydrogen as a fuel have received much attention in recent years. A fuel cell is an electrochemical device that converts chemical energy of a reaction directly into electricity. Its efficiency is thus not limited by the Carnot Cycle. The typically gaseous reactants are thereby continuously supplied to the cell. Given their high efficiency and low emissions, fuel cells provide a promising alternative to power produced from fossil fuels [1].

In a PEMFC, the two electrodes are separated by means of an electrically insulating but ionically conductive solid membrane, the polymer electrolyte membrane. The anodic reactant is hydrogen which is oxidized to protons. At the cathode, oxygen is reduced with the protons transported through the proton conductive membrane to form water. With water being the only exhaust, oxygen from ambient air and the potential application of regeneratively produced hydrogen also environmental requirements can be met. A major challenge in the use of PEMFCs is the need for better materials to make fuel cells cost-effective and more durable [2]. The major part of performance loss in a PEMFC can be assigned to the slow kinetics of the oxygen reduction reaction which includes the breakage of the strong O-O bond and the transfer of four electrons [3]. For this reason, cathode catalysts for a more efficient activation of the oxygen reduction reaction have to be found. Platinum exhibits the highest activity towards this reaction in comparison with other pure metals [2]. However, minimizing the amount of the expensive metal in order to lower the costs of the fuel cell is an important issue. Accordingly, the development of highly active, cheap and stable fuel cell catalysts for the oxygen reduction reaction

is a fundamental aspect in the research on PEMFCs.

The standard oxygen reduction reaction (ORR) catalyst used in current fuel cells consists of platinum nanoparticles supported on a high surface area carbon. In order to meet the requirements for large-scale applications, the catalytic activity per mass of platinum has to be increased by a factor of >4 [4]. In this respect, there are two promising approaches: first of all, the amount of expensive platinum can be reduced by increasing the specific surface area per mass. Therefore, the particle size is scaled down which can additionally lead to benefits from a change in the electronic structure [5]. Secondly, exchanging part of the platinum particles by cheaper materials is an option. It has been shown that alloying platinum with other transition metals like cobalt, nickel or copper considerably increases the specific activity together with a reduction of cost (due to the decreased platinum amount) [6, 7, 8, 9].

In addition to activity issues, the long term stability is crucial for the applicability of an electrocatalyst in a fuel cell [10, 11]. In this regard, modifications of the particle size and structure, but also the optimization of the catalyst support plays an important role.

Most studies investigating the performance and durability of electrocatalysts are performed with fuel cell stacks or membrane electrode assemblies (MEAs). In such studies, the cell voltage depends not only on the cathodic reaction, but also on the anodic reaction, the operating conditions and the preparation of the MEA. Half-cell experiments in an electrochemical cell, which were applied in this thesis, facilitate a separate investigation of the anode and cathode, respectively, and reduce the complexity of the system. These investigations enable to focus on the function of the catalyst itself. For the determination of the electrocatalytic activity of fuel cell catalysts, this method has proven to be very efficient [12, 13, 4] and the durability of electrocatalysts can be determined by applying accelerated stress tests [11].

Catalyst degradation goes along with a loss in accessible active surface area of the catalyst [14]. By means of rotating disc electrode (RDE) measurements in combination with identical location transmission electron microscopy (IL-TEM), not only the decrease in active surface area is measured but also an insight into mechanistic details of the degradation process is gained. The recently developed IL-TEM technique provides the opportunity to observe identical regions before and after an accelerated stress test. Additionally, as the TEM grid itself is applied as working electrode, it is not necessary to irreversibly remove the catalyst from the electrode or out of the MEA. Consequently, this technique is superior to conventional degradation studies of electrocatalysts and is suitable to scrutinize degradation processes [15].

In the presented work, several methods are combined to examine the parameters and processes responsible for both activity and stability of oxygen reduction reaction (ORR) electrocatalysts. For this purpose, half-cell measurements in an electro-

chemical cell are conducted and further analyzed.

The thesis is structured as described in the following: first of all, the mainly employed methods are introduced together with the necessary experimental background. Then, the experimental details are given before the setup as well as the measurement procedures are discussed with respect to disturbing influence factors and reproducibility. By this means, some important insights like the dependency of the loss of active surface area on the scan rate, contaminations or the kind of electrolyte are obtained. In the following chapter, after introducing possible degradation mechanisms, the durability of commercial standard cathode electrocatalysts is scrutinized by using RDE measurements in combination with IL-TEM. Thereby, the occurring degradation mechanisms are studied in detail and related to different properties of the catalysts.

Besides standard electrocatalysts, also new promising concepts were developed and investigated. In the following chapter, an approach using well-defined platinum clusters, produced in a laser vaporization source and deposited on carbon substrates, as electrocatalyst is demonstrated. Since the cluster size, cluster density and the kind of carbon can be adjusted and the complexity of the system is minimized, this well-defined system serves as model electrocatalyst for the study of degradation mechanisms and influences thereon. The characterization of these electrocatalysts and first results regarding their activity and stability are given.

Furthermore, the modification of the carbon support with transition metals induces a stabilization effect. This finding was proven by means of RDE measurements for an industrial catalyst in comparison with a non-modified one. The results for the corresponding microscopic processes, obtained by IL-TEM studies, are discussed. Afterwards, the concept of applying bimetallic core-shell particles as cathode electrocatalysts is examined by means of synthesized AuPt core-shell particles and a commercial Pt₃Co/C electrocatalyst. For the highly active AuPt core-shell particles, a new upscalable synthesis route was developed and optimized based on the characterization by means of RDE and TEM measurements. Furthermore, it is shown that it is possible to modify the alloy catalyst Pt₃Co/C, generating a core-shell structure. Therefore, a suitable treatment in carbon monoxide atmosphere inducing surface segregation has to be applied. However, the reversal segregation process is demonstrated to occur during operation conditions of a fuel cell which raises doubts concerning the application of alloy catalysts with non-noble transition metals. In the end, the results are summarized and conclusions are drawn.

Chapter 2

Experimental Background and Methods

In this chapter, the applied methods are introduced and some basic theoretical background is given. First, general aspects concerning cyclic voltammetry, electrochemical reactions, electrocatalysis and kinetics and the technique of the rotating disc electrode are presented. Then, the methods to determine the electrochemical active surface area (ECA), the activity towards the oxygen reduction reaction (ORR) and the reversible hydrogen electrode (RHE) are specified. Furthermore, differential electrochemical mass spectrometry (DEMS) and in detail identical location transmission electron microscopy (IL-TEM) are described.

2.1 Cyclic Voltammetry

Cyclic voltammetry is the method of choice for the initial investigation of electrochemical systems and has also been proven to be useful in obtaining information about complicated electrode reactions [16]. Due to the fact that the potentials of occurring processes are determined, this electroanalytical method is also often referred to as "electrochemical spectroscopy". In this respect, faradaic processes involving charge transfer across the metal-solution interface as well as nonfaradaic processes like adsorption and desorption can be observed. During cyclic voltammetry, the potential $E(t)$ of the working electrode (WE) is periodically swepted between a lower limit E_{min} and an upper limit E_{max} describing a triangular waveform (see also figure 2.1a):

$$E(t) = E_{min/max} \pm \nu t \quad (2.1)$$

The scan rate ν is the rate of change of the potential with time. The responding current passing the WE is recorded as a function of the respective potential resulting

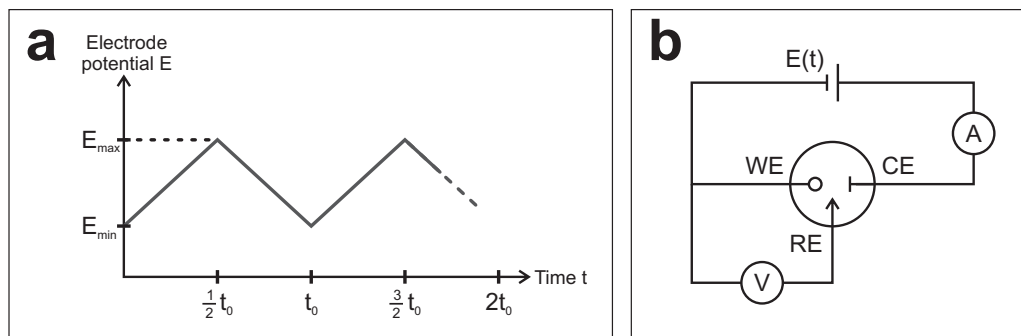


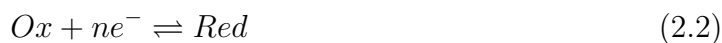
Figure 2.1: (a) In cyclic voltammetry, the potential is periodically swept (following a periodicity of t_0) between a lower E_{min} and an upper limit E_{max} , describing a triangular waveform. (b) In a three-electrode-setup, the circuit is separated into two circuits: one where the current flows (containing the counter electrode CE) and another one where the potential is determined (involving the reference electrode RE).

in a current-potential plot, called cyclovoltammogram (CV).

Typically, cyclic voltammetry is conducted in a three-electrode-setup in order to guarantee an exact control of the potential at the WE, which is determined relative to a reference electrode (RE). The counter electrode (CE) is an auxiliary electrode through which the current from and to the WE flows (see figure 2.1b). The potential of the CE is not controlled. Since in this setup the pathway between WE and RE remains practically free of current, the RE represents an ideal nonpolarizable electrode. Consequently, the measured change in potential between the working and the reference electrode is equal to the actual change in potential at the working electrode. By producing an adequate current flow in the circuit containing the WE and the CE, the potentiostat adjusts the potential at the WE (relative to the RE). More detailed information about cyclic voltammetry is given in the literature [16, 17, 18].

2.2 Electrochemical Reactions

An electrochemical reaction is characterized by the transfer of electrons from an electrochemical active species to an electrode or vice versa. Its direction depends on the energetic level of the electrons in the electrode and the molecular orbitals (especially the highest occupied (HOMO) and lowest unoccupied (LUMO) molecular orbitals) of the active species. Hence, an oxidation or reduction of the active species occurs:



The main driving force of an electrochemical reaction is the electrode potential in contrast to pressure and temperature in conventional chemical reactions.

For a redox reaction, the equilibrium potential E is given by the Nernst equation

$$E = E_0 + \frac{RT}{nF} \ln \frac{c_{Ox}}{c_{Red}} \quad (2.3)$$

which describes E as a function of the actual concentrations c_{Ox} and c_{Red} of the involved redox species [17]. R and F represent the gas and the Faraday constants, respectively, T is the temperature, n the number of transferred electrons and E_0 the standard electrode potential.

The Gibbs free energy ΔG , representing the net available electrical energy from a reaction in a cell, can then be obtained by [16]

$$\Delta G = -nFE \quad (2.4)$$

2.3 Electrocatalysis and Kinetics

In addition to the thermodynamic view of an electrochemical reaction, which considers the energetic levels of the initial and final state of the involved species, the rate of the reaction - determined by the kinetics - plays an important role. According to Arrhenius the rate constant k is given by [16]

$$k = A' e^{-\frac{E_A}{RT}} \quad (2.5)$$

where A' is the pre-exponential factor (also called frequency factor), T is the temperature and E_A is the activation energy of the reaction. Hence, in order to increase the rate of a reaction either the temperature has to be increased or the activation energy decreased. The latter can be achieved by catalysts.

A catalyst is defined as a substance which enhances the rate of a chemical reaction without being either consumed or generated in the process. By providing a lower activation energy and a different transition state, catalysts are able to offer alternative reaction pathways [19]. Electrocatalysis specifies a heterogeneous catalysis process including one or more electrochemical reactions. Therefore, in all cases an electron transfer will occur through the interface between the electrode and the electrolyte. In general, heterogeneous catalysis at a porous catalyst proceeds via the following seven steps [19]:

1. Mass transfer of the educts through the outer boundary layer (film diffusion)
2. Diffusion of the reactants within the pores of the catalyst (pore diffusion)
3. Adsorption of the educts at the catalyst surface
4. Chemical reaction at the interface

5. Desorption of the products from the catalyst surface
6. Diffusion of the products out of the catalyst particle (pore diffusion)
7. Mass transfer of the products through the boundary layer into the bulk solution (film diffusion)

For a heterogeneously catalyzed reaction at a bulk surface the two steps involving pore diffusion (steps 2 and 6) are skipped. The research on electrocatalysis focuses on steps 3 to 5. However, for catalytic investigations, diffusion effects always have to be either eliminated or taken into account.

The rate constant of an electrocatalytic reaction is a function of the applied potential. The overpotential η depicts the additional potential beyond the thermodynamically required potential E_{eq} needed to drive a reaction at a certain rate [16].

$$\eta = E - E_{eq} \quad (2.6)$$

This effect is also called polarization with the overpotential η depicting the extent of polarization. Basically, three different kinds of polarization have to be considered [20]: activation polarization arises from kinetic hindrances of the charge-transfer reaction taking place at the electrode/electrolyte interface. Concentration polarization originates from concentration differences of reactants or products at the electrode surface and in the bulk as a result of limited mass transfer. Additionally, ohmic polarization appears upon current flow and is connected with the resistance of the whole cell, especially of the electrolyte.

In order to investigate the kinetics of the charge-transfer reaction all polarization effects have to be considered. An enhancement of the mass transfer can be accomplished by using a well-defined convective system like a rotating disc electrode (see section 2.4). The cell resistance R , which appears upon current flow i following Ohm's law $\eta_{cr} = iR$, has to be eliminated. For this purpose, the resistance between the reference and counter electrode should be minimized, for example by using a Luggin-capillary. The residual inner resistance should then be taken into account during the measurement by using iR-correction of the potentiostat.

For the charge-transfer reaction the kinetic current density $j_k = i_k/A$ (with the active surface area A), which represents the reaction rate, is given by the Butler-Volmer equation

$$j_k = j_{k,0} \left[e^{-\frac{\alpha\eta F}{RT}} - e^{-\frac{(1-\alpha)\eta F}{RT}} \right] = j_k^+ + j_k^- \quad (2.7)$$

with the symmetry factor α of the energy barrier and the exchange current density

$j_{k,0}$, which is determined by [17]

$$j_{k,0} = nFk_0c_{Ox}^\alpha c_{Red}^{1-\alpha}. \quad (2.8)$$

k_0 is the standard rate constant and describes the facility of a reaction. The net current is the algebraic sum of the anodic j_k^+ and cathodic j_k^- current densities of which the absolute values both equal the exchange current density $j_{k,0}$ in the case of equilibrium. [16]

If an overpotential is applied to the electrode, either the anodic reaction rate will be accelerated while the cathodic reaction rate is slowed down or vice versa, depending on the sign. For high enough overpotentials, one of the two current densities contributing to the kinetic current can be neglected. For practical reasons, the equation is often presented in a semilogarithmic form, the Tafel equation [17]:

$$\eta_{ct} = a + b \cdot \log i_k \quad (2.9)$$

This equation depicts the linear relationship between the kinetic overpotential and the logarithm of the kinetic current involving two constants a and b . The constant b represents the so-called "Tafel-slope" which is a function of the number of transferred electrons n and the symmetry factor α ,

$$b = \frac{RT}{\alpha nF} \quad (2.10)$$

and can therefore contribute to the determination of reaction mechanisms [17].

2.4 Rotating Disc Electrode

According to the proceeding steps of heterogeneous catalysis shown in the last section, mass transport is a critical part of electrocatalytic processes. In order to study the electron transfer kinetics, convective electrode systems like the rotating disc electrode (RDE) are used, which allow for an enhanced and defined mass transport.

The RDE consists of a conductive disc embedded in a rod made of an insulating material like Teflon (see figure 2.2). The disk itself is generally made of a noble metal or glassy carbon and its rotation frequency can be finely adjusted by the attached motor. The rotating disc drags the electrolyte at its surface along with it and the centrifugal force propels the solution outwards from the center in a radial direction, as it is shown schematically in figure 2.2.

An induced flow normal to the surface replenishes the fluid at the disc surface. The sum result is a laminar flow of solution towards and across the electrode of which the

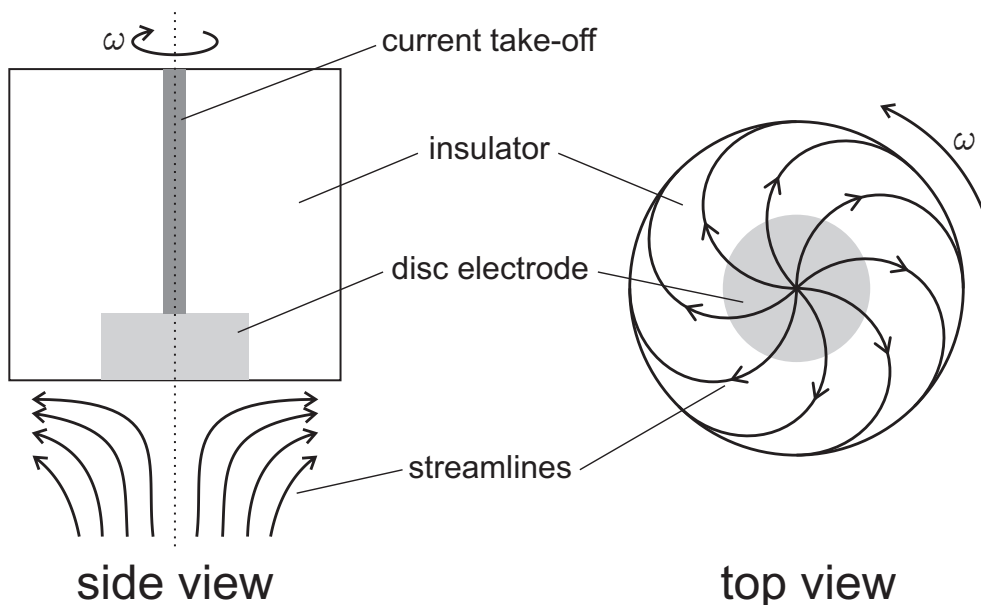


Figure 2.2: Schematic drawing of a rotating disc electrode and the radial flow of liquid (indicated by the streamlines) during rotation in side and top view, respectively.

rate can be controlled by adjusting the rotation speed. Convective mass transport is particularly important if the concentration of the involved species is low. This is the case, when dissolved gases are used as reactants, such as in the oxygen reduction reaction, due to their low solubility. For processes where the kinetic reaction is faster than the mass transfer to the active site, the reaction rate is limited by diffusion. As a consequence, each species, which arrives at the surface, is immediately converted by the reaction leading to a surface concentration c^* equal to zero. The equation for the current density j measured at the electrode surface according to Fick's law [16]

$$j = nF \frac{D}{\delta} (c_0 - c^*) \quad (2.11)$$

with the diffusion constant D , the concentration of the reactive species in the bulk c_0 and the thickness δ of the diffusion boundary layer, can then be simplified to

$$j = nF \frac{D}{\delta} c_0. \quad (2.12)$$

Levich deduced an equation relating the thickness of the diffusion layer to the rotation speed ω of the electrode, the diffusion constant D and the kinematic viscosity ν of the electrolyte [17]:

$$\delta = 1.61 D^{\frac{1}{3}} \nu^{\frac{1}{6}} \omega^{-\frac{1}{2}} \quad (2.13)$$

By combination of equations 2.12 and 2.13, the Levich equation for the diffusion

limited current density using an RDE setup is obtained:

$$j_d = 0.62 n F c_0 D^{\frac{2}{3}} \nu^{-\frac{1}{6}} \omega^{\frac{1}{2}} \quad (2.14)$$

The potential range, where the reaction is exclusively dominated by the kinetics, is narrow and its currents are low. Therefore, in order to analyze the kinetics, the steep part of the polarization curve, which is a mixed region and neither dominated by diffusion limitation nor by the kinetics, is taken into account. In this region the following equation is valid [13]:

$$\frac{1}{i} = \frac{1}{i_k} + \frac{1}{i_d} \quad (2.15)$$

By means of this relation, the kinetic current i_k is obtained by correcting the measured current i for limitations due to mass transport processes, which are represented by the diffusion limited current i_d . The diffusion limited current can easily be determined from the level of the horizontal part of the polarization curve at high overpotentials. Finally, the catalytic activity of the electrode represented by i_k can be quantified using equation 2.15. This equation was used in the presented results in order to determine the kinetic current.

2.5 Determination of the Electrochemical Active Surface Area

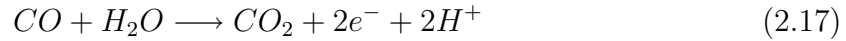
In heterogeneous catalysis the number of active sites is one of the most important properties of the catalyst. For its determination typically adsorption techniques are applied. Thereby, suitable probe molecules, which adsorb exclusively on the active surface sites and from which the adsorption mechanism is known, are adsorbed and quantified. By means of this quantification, the number of active sites can be calculated. For the electrochemical active surface area determination of platinum, hydrogen atoms and carbon monoxide molecules are commonly used as adsorbates. Both are assumed to bind as single atoms and molecules, respectively, on top of each platinum atom which constitutes the active site [21, 22]. The value of the active surface area is then determined by the measured current during desorption or oxidation of one monolayer, respectively. Hence, there are two ways to obtain the electrochemical active surface area: by using the H_{upd} region or by conducting a CO stripping measurement. The electro-adsorption of H_{upd} is referred to as under-potential deposition because on a negative scale, the process takes place at a potential that is lower than the potential required to generate $H_2(\text{g})$ [23]. For this method, a usual CV is recorded and the area of the H_{upd} adsorption or desorption is integrated properly as described in [13]. However, this technique is very sensitive

to impurities adsorbing at the metal surface. Furthermore, its value depends on the lower potential limit of the integration and it is questionable, if for each catalyst a full H_{upd} layer can be achieved before the onset of hydrogen evolution [24]. Thus, this method is not comparable between different catalysts. It should therefore only be used within one measurement series of a certain catalyst for comparisons of the ECA under equal conditions.

In order to obtain significant and reproducible values for the ECA of platinum catalysts, CO stripping is the method of choice. After adsorbing CO at a low potential until the saturation coverage is reached, the electrolyte is saturated with argon and the CO stripping behavior of the catalyst is studied in a CO-free environment. The oxidation of the adsorbed CO molecules gives rise to a distinctive feature in the recorded CV. After correcting the CV against the background from the subsequent CV to account for adsorption and oxidation processes occurring at the surface the peak is integrated. In this way, the charge Q_{CO} can be determined [13]

$$Q_{CO} = \frac{\int idE}{2\nu} \quad (2.16)$$

from the measured current i , the potential E and the scan rate ν . The factor 2 takes into account that the oxidation of CO is a two-electron process:



Q_H is the corresponding charge resulting from the analysis of the H_{upd} region [13]:

$$Q_H = \frac{\int idE}{\nu} \quad (2.18)$$

The roughness factor r_f , which denotes the ratio between the real active surface area A_{real} and the geometric area of the electrode A_{geo} , can then be determined by

$$r_f = \frac{A_{\text{real}}}{A_{\text{geo}}} = \frac{Q_H \text{ or } Q_{CO}/0.196\text{cm}^2}{195\mu\text{Ccm}^{-2}} \quad (2.19)$$

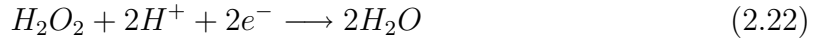
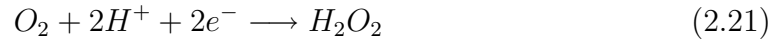
taking the geometric electrode area of 0.196cm^2 and the experimentally determined charge of polycrystalline platinum prepared by flame annealing ($195\mu\text{Ccm}^{-2}$) into account. The ECA value (in $\text{m}^2\text{g}_{\text{Pt}}^{-1}$) is most accurately obtained by the slope in a plot of measured r_f values against the applied platinum loadings. [13]

2.6 Catalytic Activity towards the ORR

In acid environment, the cathodic reaction proceeding in a fuel cell, the oxygen reduction reaction, is given by



The reaction mechanism is not understood in detail and many mechanisms involving a large number of intermediates and rate-determining steps have been proposed [25]. In general it is distinguished between the so-called four electron pathway, where all electrons are transferred in one step and a mechanism consisting of two two-electron transfers with hydrogen peroxide being an intermediate product:



The activity of a platinum electrocatalyst for the ORR is generally represented by the kinetic current obtained at a certain potential, typically at $0.9 V_{\text{RHE}}$. From RDE measurements, the kinetic current is determined using equation 2.15. Since different catalysts have to be compared this kinetic current value has to be normalized either by the active surface area to obtain the specific current density j_k or by the platinum mass resulting in the mass activity j_{mass} [13].

$$j_k = \frac{i_k}{A_{\text{real}}} = \frac{i_d \cdot i}{i_d - i} \cdot \frac{1}{r_f \cdot A_{\text{geo}}} \quad (2.23)$$

$$j_{\text{mass}} = \frac{i_k}{m_{\text{Pt}}} = j_k \frac{r_f}{L_{\text{Pt}}} \quad (2.24)$$

A_{real} is the electrochemical surface area, A_{geo} is the geometrical electrode surface area, i_d the diffusion limited current, m_{Pt} is the platinum mass and r_f is the roughness factor (see last section). Another possibility for the specification of activity is the introduction of the turnover frequency (TOF) which is commonly used in heterogeneous gas phase catalysis. According to IUPAC, it is defined as "molecules reacting per active site in unit time" [26]. The number of reacting molecules is reflected by the kinetic current i_k divided by the number of electrons n transferred in the reaction of interest. The number of electrochemical active sites is determined as discussed above as charge Q_{CO} (or Q_{H}). Therefore, the TOF is specified by

$$\text{TOF} = \frac{i_k}{n \cdot Q_{\text{CO}}}. \quad (2.25)$$

2.7 Reversible Hydrogen Electrode

Electrochemical potentials are always measured relative to a reference electrode and not on an absolute scale. In order to form a basis for their comparison, the standard hydrogen electrode (SHE) potential is defined to be zero under standard conditions (proton activity of 1 and hydrogen partial pressure of 1013 mbar) for all temperatures. The proceeding reaction is the evolution and oxidation of hydrogen, respectively:



Since the fuel cell relevant reactions like the oxygen reduction and hydrogen oxidation reaction are pH-dependent, it is more convenient to use a reference which exhibits the same pH-dependence, the reversible hydrogen electrode (RHE):

$$E_{RHE} = 0V - 0.059V \cdot pH \text{ vs. SHE} \quad (2.27)$$

The RHE potential relative to the applied reference electrode is experimentally defined as the potential value between the hydrogen evolution and hydrogen oxidation reaction (HER/HOR) with zero net current.

2.8 Differential Electrochemical Mass Spectrometry

The combination of half-cell measurements in an electrochemical cell with mass spectrometry is called Differential Electrochemical Mass Spectrometry (DEMS). This analytical method allows to in-situ quantitatively detect gaseous and volatile species available in the electrolyte. These species can be reactants, reaction intermediates as well as products. The two latter ones are in particular of interest and can be detected with short time delay. Therefore, after being formed at the working electrode, they are sucked through a porous membrane into the ion source of the mass spectrometer. The determined mass intensity can be correlated to the corresponding faradaic current obtained by electrochemical measurements and in this way, electrochemical reactions can be investigated in detail. The instrument consists of three main components: the electrochemical cell, the membrane interface and the vacuum chamber with a quadrupole mass spectrometer. The porous membrane typically consists of Teflon which due to its hydrophobic nature prevents the passage of aqueous electrolyte into the differentially pumped vacuum system. For more detailed information, see reference [27].

2.9 Identical Location Transmission Electron Microscopy

Especially due to the development of nanoscience, microscopic imaging reaching atomic resolution has become indispensable. In transmission electron microscopy (TEM), a thin specimen is irradiated with an electron beam of uniform current density. From the transmitted electrons, after interaction with the specimen, an image is formed, giving an insight into the microscopic nature of the sample.

An electron source at the top of the microscope emits the electrons, which are accelerated with about 100 – 200 kV. In the condensor system consisting of electromagnetic lenses and apertures, the electrons are focused into a thin collimated beam. Then, the beam passes the specimen where the electrons interact with the material. In this regard, the electrons can be transmitted, diffracted, backscattered or they induce the emission of photoelectrons, x-ray fluorescence or Auger electrons. The electron intensity distribution behind the specimen is imaged and magnified by a lens system onto a fluorescent screen or CCD camera. The resulting image is a two-dimensional projection of the illuminated part of the specimen. The variation in brightness can be related to the electron density of the existent atoms and the thickness of the sample. Regions where fewer electrons are able to pass through the specimen appear darker. Without much effort, the magnetic lenses can be adjusted such that the back focal plane of the lens is placed on the screen producing a diffraction pattern. This diffraction image characterizes the crystal structure of the chosen microscopic region of the specimen. Furthermore the detection of emitted x-rays can provide information about the elemental composition of the sample. This technique is called energy dispersive x-ray spectroscopy (EDX). [28, 29]

Conventional TEM analysis of high surface area catalysts is specified to be destructive, as the catalyst has to be removed from the electrode after the electrochemical measurement [30]. In investigations of the degradation of electrocatalysts, images taken from the degraded sample are compared with images from the pristine catalyst powder. Thus, in order to draw significant conclusions about occurring changes an extensive statistical analysis is indispensable. Therefore, in our group a new TEM technique dubbed identical location transmission electron microscopy (IL-TEM) was developed, which circumvents the catalyst removal from the electrode and facilitates the comparison of identical microscopic regions of the catalyst before and after a degradation treatment [15].

For this method, the TEM grid itself is used as a working electrode for the accelerated stress tests in the electrochemical cell. In order to be able to find the same location before and after the stress test, a finder grid is used which is decorated with letters and numbers. Its material is gold, because it has to be stable in the electrolyte, and it is coated by a thin amorphous carbon film. A photograph of such a TEM grid is shown in figure 2.4a.

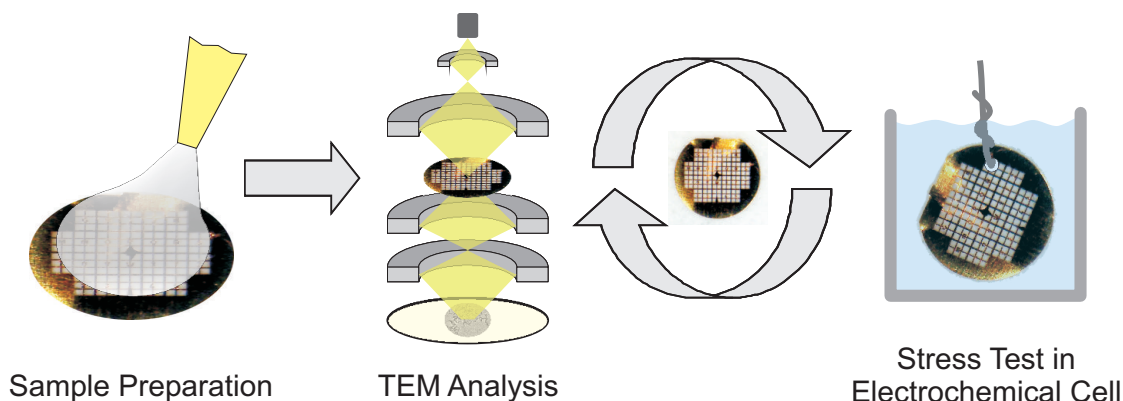


Figure 2.3: Procedure of IL-TEM: first, the sample is prepared by pipetting the diluted catalyst suspension onto the carbon coated TEM grid. Then, it is inserted into the TEM, where several regions are recorded. Afterwards, the sample is transferred to the electrochemical cell, where it is exposed to accelerated stress tests. Subsequently, the sample is dried and transferred again into the TEM. There, the identical regions as before the stress test are relocated. The cycle consisting of the TEM analysis and the electrochemical treatment can be repeated.

The measurement procedure of IL-TEM is schematically shown in figure 2.3. It consists of the following steps:

1. Preparation of the catalyst sample on the gold finder grid
2. TEM investigation of pristine sample
3. Treatment in the electrochemical cell
4. TEM investigation of degraded sample at the identical locations

The last two steps can thereby be repeated several times.

The amorphous carbon film is prepared in a high vacuum evaporator by evaporation of carbon onto a mica substrate using a carbon thread. By floating the carbon film onto water (off the supporting mica substrate) and drawing the grid through the carbon covered surface, the carbon film is finally placed onto the gold finder grid. In order to receive a uniform distribution of the catalyst particles, an adequate wetting of the aqueous catalyst suspension has to be ensured. Therefore, the carbon film (on the grid) is exposed to oxygen plasma created by a glow discharge which leads to an increased hydrophilicity. Afterwards, the catalyst suspension is applied leading to a low catalyst loading in order to avoid overlapping of catalyst particles. For that purpose, low concentrations are used and/or the residual droplet is carefully removed after a few seconds using filter paper. After drying, the TEM grid can be inserted into the TEM, where step two is carried out.

The procedure of IL-TEM is described in the following by a specific example illustrated in figure 2.4. For the TEM analysis, a TEM equipped with a CCD camera

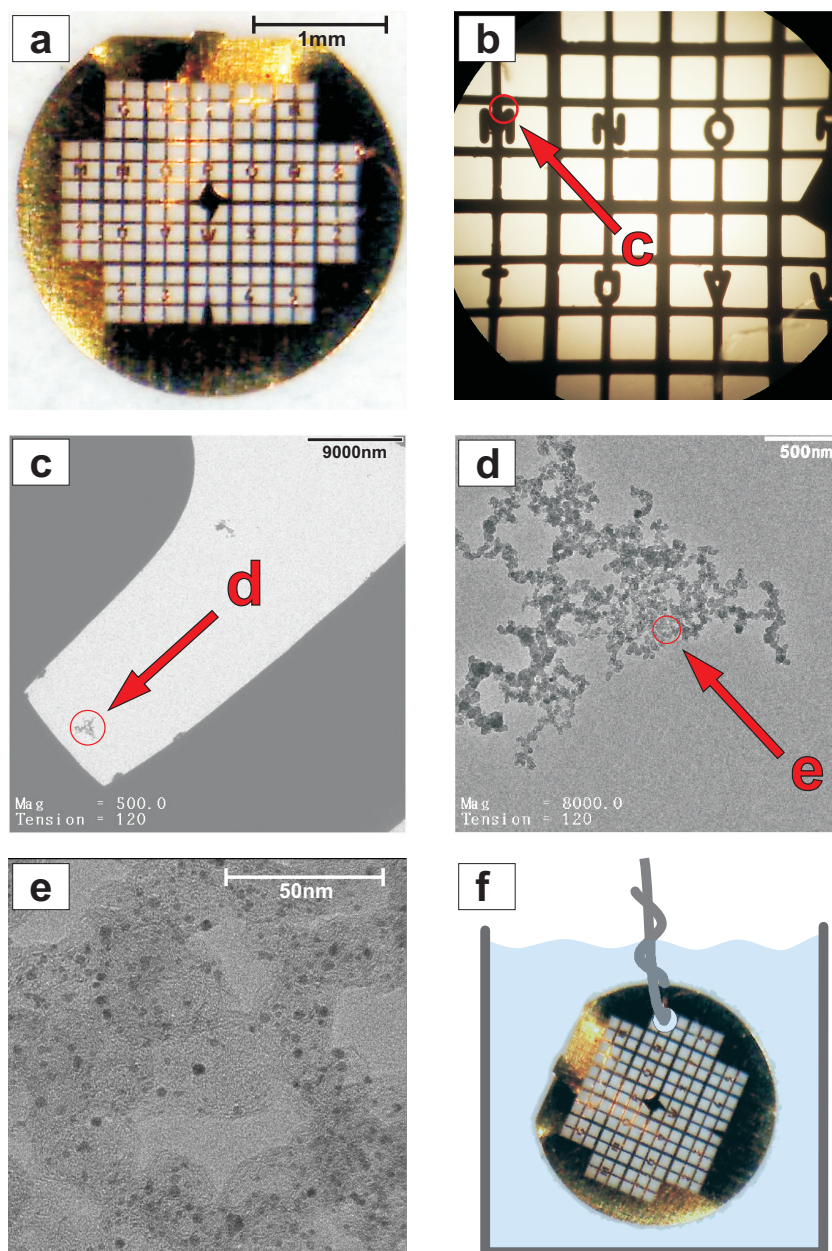


Figure 2.4: Procedure of relocation in IL-TEM demonstrated for Pt/C 2-3 nm: figure (a) shows a photograph of a TEM gold finder grid. In the TEM, a part of the grid close to the letter "M" is chosen and highlighted (b). Then this part is magnified and one of the catalyst agglomerates is chosen (c). After zooming in, a flat part of the agglomerate is selected (d), where a high resolution image at high magnification (150k) is taken (e). Then the TEM grid is transferred to the electrochemical cell and applied as working electrode by drilling a hole through it and connecting it to a wire as shown in figure (f). Afterwards the identical locations have to be retrieved by means of the recorded intermediate steps (b-d).

for the relocation steps and the possibility to record negatives for the final images is of advantage. After gaining an overview of the sample, especially about the homogeneity of the catalyst, different regions of the catalyst film are chosen for IL-TEM. For every location, the position on the grid has to be marked in an overview as shown in figure 2.4b (in this example, the position would be close to the letter M). Then the magnification is increased to about 500 to get an overview of the square hole next to the M where bigger catalyst agglomerates can be distinguished. After taking an image and highlighting the selected particle agglomerate (see figure 2.4c), the magnification can be further increased and again, one or two suitable parts of the agglomerate are chosen and well adjusted images are recorded. Usually, one additional magnification is sufficient for retrieving the same location again. Nevertheless, it is of course possible to include more intermediate steps, simplifying the relocation afterwards. Typically, five to ten different locations in various parts of the grid are recorded in such a way. Each quadratic hole of the grid should contain only one or two locations because as the thin carbon film is sensitive to drying processes, cracking and vanishing of the film together with the catalyst particles can occur in some square holes.

Afterwards, step three can be carried out. For this purpose, the TEM grid is transferred to the electrochemical cell. In order to use the grid as working electrode, a hole is penetrated through the grid in the outer rim using a sharp needle or wire. Then, the grid is threaded by a platinum or gold wire and connected to it, as schematically shown in figure 2.4f. In this way, the grid is immersed into the electrolyte and applied as a working electrode. In order to stabilize the setup, the wire can be stiffened by inserting it into a Teflon tube and fixing it to the cover plate of the cell. By this means, the signal of the wire in the CV is reduced. For the material of the wire, there are two suitable options for the investigation of Pt-based catalysts: gold and platinum. The gold wire is very resistant to acid and high potentials, only traces of silver have to be avoided by boiling it in concentrated nitric acid. Furthermore it is guaranteed that all platinum ions in the system originate from the catalyst sample. However, the big advantage of using a platinum wire is the possibility to monitor the electrical connection between the wire and the grid by conducting a CV and recognizing the characteristic gold features. Unfortunately, it is not possible to distinguish features of the catalyst itself due to its low concentration.

After assembling the electrochemical cell with the TEM grid as working electrode, the accelerated stress test, i.e. an electrochemical treatment, can be conducted. The measurement of the decrease in surface area during the treatment can optionally be monitored by installing a "normal" working electrode and connecting it in parallel to the grid. After the measurement, the TEM grid is dipped into ultrapure water to get rid of electrolyte salts and subsequently dried in a nitrogen stream or at ambient

conditions.

The fourth step again takes place at the TEM where the grid is inserted into the sample holder in the same direction as in step two to simplify the relocation process. For that purpose, the wedge-shaped mark pointing to the center of the grid (in figure 2.4a in the lower part) is convenient to use for the positioning as it is visible to the naked eye. After the insertion, each location has to be retrieved on the basis of the records from step two. The corresponding TEM images can then be compared to each other allowing for scrutinizing changes of single particles or carbon structures. Consequently, this method is suitable to get an insight into microscopic processes occurring during the treatment or, in other words, into the degradation mechanism.

Chapter 3

Experimental Details

In the following, the experimental details for the conducted measurements are given. First, the preparation of the working electrode including the catalyst film is described. Then, the experimental setup with all components is presented before the procedures of the most important measurements are specified.

3.1 Working Electrode Preparation

For the rotating disc electrode measurements (*Radiometer Analytical, France*) home-made electrode tips were used. They consist of a cylindrical Teflon® body (about 11 mm × 20 mm) with a tight opening for the glassy carbon disc (5 mm × 3 mm) and a thread on the opposite side which fits onto the RDE instrument [31]. In between, there is a small hole which provides space for the electrical connection of the electrode. For the preparation, the Teflon body is heated up in a drying cabinet to about 420K leading to an extension and softening which enables the glassy carbon disc to be carefully pressed into the hole. In order to ensure a leak-proof enclosure of the disc it is possible to coat the edges of the glassy carbon with Teflon-spray. After cooling down, the tip can be polished in order to get a smooth planar surface.

Before the application of the catalyst, the glassy carbon surface was cleaned in an ultrasonic bath for one minute to remove old catalyst remains as well as in concentrated perchloric acid for one minute to get rid of other impurities. After rinsing the tip with Millipore Milli-Q® water ($> 18.3 \text{ M}\Omega \text{ cm}$, $\text{TOC} < 5 \text{ ppb}$) and drying under ambient conditions the catalyst film was prepared. In figure 3.1, the procedure of electrode preparation is shown schematically. The catalyst powder was dispersed ultrasonically in ultrapure water to a concentration of $0.14 \text{ mg}_{\text{Pt}}\text{mL}^{-1}$ for at least ten minutes. Before each preparation, the catalyst suspension was again put into the ultrasonic bath for approximately three minutes. During ultrasonic agitation, $20 \mu\text{L}$ of the suspension was pipetted onto the clean glassy carbon disc (5 mm diameter,

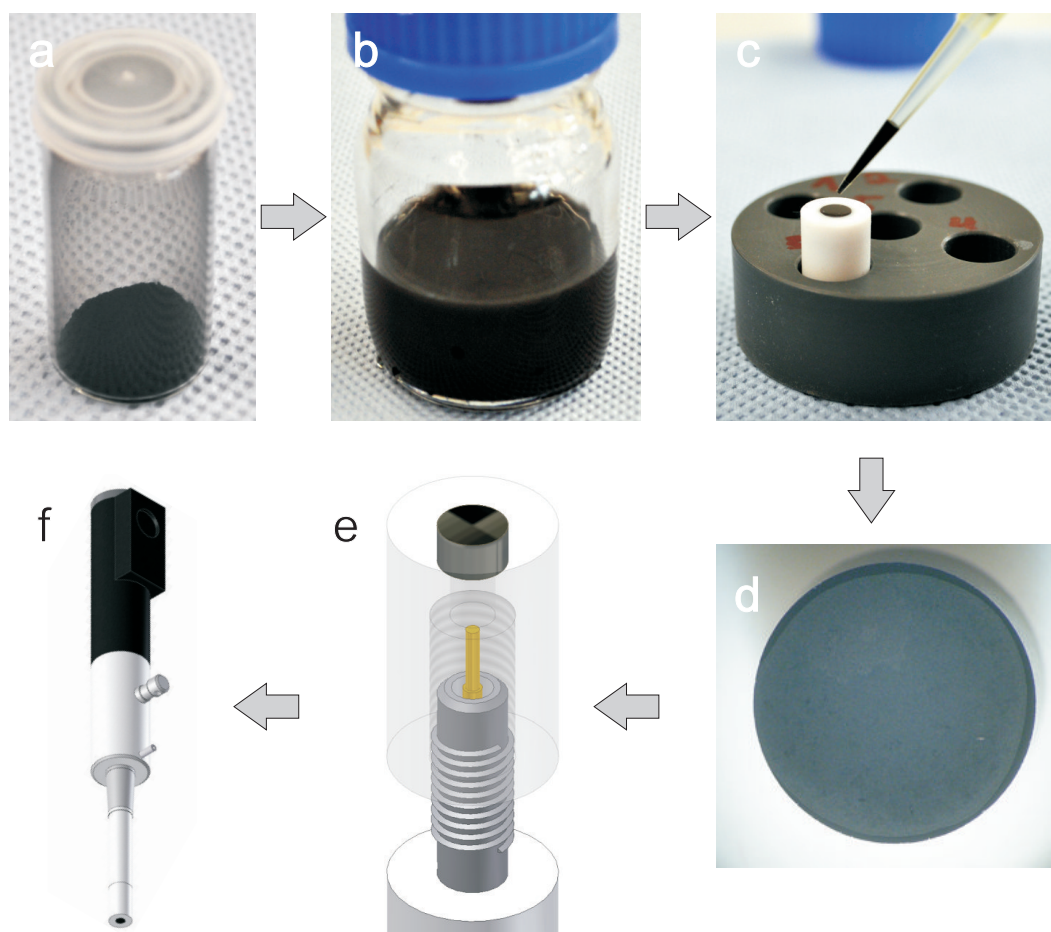


Figure 3.1: Preparation procedure of the catalyst film on the working electrode: the catalyst is provided as dry black powder (a) of which an aqueous suspension is prepared (b). A small amount of this suspension is pipetted onto the glassy carbon surface of the electrode tip (c) and dried to receive a homogeneously distributed catalyst film which covers the whole glassy carbon surface (d). After ensuring an electrical contact from the glassy carbon to the rotating shaft using a gold plated pin (e) the electrode is fixed through the thread and the rotating disc electrode is ready for use (f).

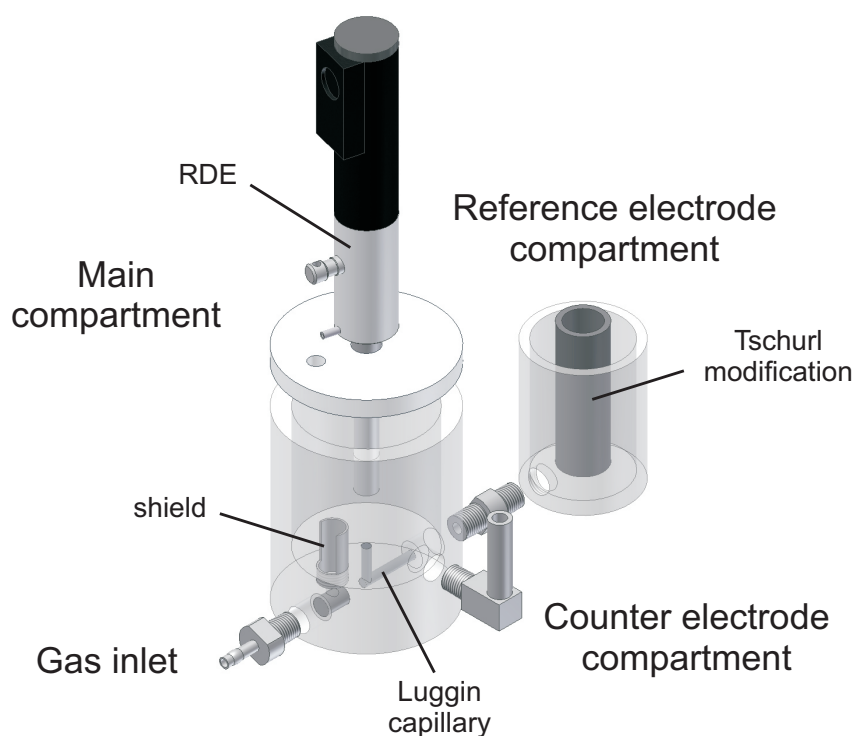


Figure 3.2: Schematic drawing of the applied electrochemical Teflon cell with its components. It is divided into the three indicated compartments, one for each of the three electrodes.

0.196 cm² geometrical surface area) leading to a platinum loading of 14 $\mu\text{g}_{\text{Pt}}\text{cm}^{-2}$ (if not noted otherwise this loading was used in all presented measurements). The catalyst suspension was dried in a nitrogen stream in order to receive a homogeneously distributed catalyst film covering the whole glassy carbon surface (see figure 3.1d). Afterwards, the electrode tip was attached to the RDE, where gold plated pins which exhibit a spring, ensured the electrical contact to the electrode.

3.2 Electrochemical Cell Design

The electrochemical measurements were conducted in a homemade three-compartment electrochemical Teflon-cell (see figure 3.2), using a rotating disc electrode setup. Teflon® was used for the cell instead of the commonly used glass because glass has shown to be unstable in alkaline solution [32], which was used as electrolyte for some measurements. The cell is divided into three compartments, one for each electrode. The electrolyte was added into the cell in a way that every compartment has a sufficient level of solution and electrical contact is ensured. For saturation of the electrolyte with gas, the gas flowed through the gas inlet into the cell passing a porous Teflon cylinder, which tightens the cell and minimizes the size of the gas bubbles. Inside the cell, a Teflon shield is located close to the gas

inlet in order to avoid gas bubbles reaching the working electrode surface. The RDE or another working electrode was guided through a hole of the cover plate from above into the main chamber. The compartment for the counter electrode is directly attached to the main chamber while the reference electrode compartment is connected by a Luggin capillary. There, the reference electrode was inserted into a Tschurl modification [33], in which a Nafion® membrane at the bottom inhibits chloride impurities from the reference electrode to reach the main chamber.

All three electrodes were connected to a potentiostat while the gas inlet was connected to a gas changer which allowed switching between argon (purity 5.0), oxygen (purity 4.8), hydrogen (purity 5.0) and carbon monoxide (purity 3.0) gas (all *Air liquide* or *Westfalen*). The potentiostat, the RDE and the gas changer were controlled by a LabView program.

3.3 Procedure of Experimental Measurements

Before each measurement, the electrochemical cell was boiled out twice in deionized water to remove impurities. Additionally it was regularly cleaned in both an alkaline bath consisting of KOH dissolved in isopropanol and an acid bath consisting of a mixture of sulfuric and nitric acid.

The electrolyte was prepared using Millipore Milli-Q® water and perchloric acid (*Suprapure; Merck, Germany*), sulfuric acid (*Normatom; Merck, Germany*) or KOH pellets (*Suprapure; Merck, Germany*) in order to obtain a concentration of 0.1 mol L^{-1} .

During the preparation of an electrochemical measurement the cell was set up, the rotating disc electrode with the catalyst film was immersed into the electrolyte and the necessary connections for the gas, the electrodes and the RDE were carried out. Then cyclic voltammetry measurements were started. In-situ iR-correction was applied for all measurements.

Electrochemical Cleaning

Before activity or degradation measurements, the potential was cycled for 50 to 100 cycles to high oxidative potentials (about $1.4 V_{\text{RHE}}$) in order to get rid of organic impurities. This procedure is called "electrochemical cleaning". Afterwards, a stable cyclovoltammogram in the range between 0.05 and $1.0 V_{\text{RHE}}$ was recorded.

Reversible Hydrogen Electrode

Although a SCE was used as a reference electrode, all potentials are given with respect to the reversible hydrogen electrode (RHE), which was measured for every

experiment. For this, the electrolyte was saturated with hydrogen. During rotation (1600 rpm), the potential value between the hydrogen evolution and hydrogen oxidation reaction (HER/HOR) with zero current was determined as RHE potential with respect to the SCE.

ECA Determination

The ECA was mainly determined in CO stripping measurements. After adsorbing CO at a potential of $0.05 V_{\text{RHE}}$ until the saturation coverage was reached, the electrolyte was purged with argon for 20 minutes before the CO was oxidized in a CO-free environment. The resulting peak was integrated after correction for the adsorption behavior by subtracting the subsequent CV. The surface charge and the roughness factor were then determined as described before in chapter 2. Within one measurement process, in some cases the ECA was determined using the area of H_{upd} of a CV.

Catalytic Activity towards the ORR

Polarization curves of the catalysts were determined by cycling the potential during rotation of the electrode (1600 rpm) in oxygen saturated electrolyte. For the evaluation of the ORR activity the polarization curves were corrected from capacitive currents by subtraction of a blank CV in argon purged electrolyte which was conducted with the same scan rate (50 mVs^{-1}). For the analysis, the steep part of the polarization curve around $0.9 V_{\text{RHE}}$, the so-called "mixed region", was taken into account to determine the specific kinetic current (for details see chapter 2).

Degradation Measurements

In order to evaluate the stability of electrocatalysts accelerated stress tests upon potentiodynamic as well as potentiostatic conditions were conducted. The loss of active surface area due to induced degradation processes was followed by determining the ECA at least before and after the electrochemical treatment, and often additionally in between in order to study the characteristic trend. For measurements at elevated temperatures, the electrolyte temperature was adjusted by an automatic temperature control using a heating coil inserted into a Teflon tube and a Teflon coated Pt100 thermo couple placed in the working compartment of the electrochemical cell.

Differential Electrochemical Mass Spectrometry

For further investigations of the total oxidation of the carbon support, DEMS measurements were conducted. In order to increase the conductivity of the electrolyte, a

higher concentration (0.5 M H₂SO₄) was used. The catalyst loading was 50 μg cm⁻² and a porous Teflon membrane with a pore size of 0.03 μm, a porosity of 50% and a thickness of 124 μm (*Gore, USA*) was used as an interface. The proportionality factor between the faradaic current and the mass ion current was determined by evaluating at least three CO stripping experiments for each degradation measurement. Further experimental details are given in reference [27].

Identical Location TEM Procedure

For the IL-TEM investigations a gold finder grid (400 mesh; Plano, Germany) was coated with an amorphous carbon film. The hydrophilicity of the carbon film, which was necessary for a uniform distribution of the catalyst particles, developed during a glow discharge exposure to oxygen plasma. After this pretreatment, 5 μL of a tenfold diluted catalyst suspension were pipetted onto the gold finder grid. In order to keep the catalyst loading as low as possible (to avoid overlapping of catalyst particles), the drop was delicately absorbed off the grid after approximately 10 seconds, using filter paper. The grid was dried, and then investigated using a JEM 2010 microscope (JEOL, Japan) with an accelerating voltage of 120 kV and a magnification of 100k and 150k, respectively. TEM micrographs were recorded before and after the treatment procedures, on identical locations of the catalyst.

Chapter 4

Potential Cycling Degradation Measurements

In fuel cell research much effort is made to improve the cathode catalyst. Different concepts for catalysts with higher performance have been developed, of which the most important ones are discussed in the following chapters. A crucial requirement in respect of catalyst development is the ability to compare and evaluate existing and newly developed catalysts. Since investigations of fuel cell stacks are very time-consuming and complex, an alternative method which focuses on the catalyst itself is the operation of accelerated stress tests in an electrochemical cell. Although these investigations distinguish themselves as being much less complex, there are still several parameters which influence the experimental results. A fact that is reflected in the high variation of activity values for standard catalysts in the literature [4]. For example, the obtained activities strongly depend on the reagents and the measurement procedures. Regarding degradation experiments, the results vary even more because there is no generally accepted standard accelerated stress test for electrocatalysts, though several suggestions have been made [34]. The common attempt is to imitate the conditions of the electrode in a fuel cell during operation with the main focus being start/stop-cycles, automotive operation or steady-state conditions. One degradation treatment which is often applied is potential cycling. However, there is still the question of suitable potential limits, which scan rate should be applied, which electrolyte should be chosen etc. Even more important than the comparability between different research groups is reproducibility of the chosen degradation procedure within a test series. In the following, by means of a commercial Pt/C electrocatalyst (4-5 nm, *Tanaka Kikinzoku Kogyo K. K., Japan*) some of the most important parameters which have an influence on potential cycling treatments using a RDE setup are presented and shortly discussed.

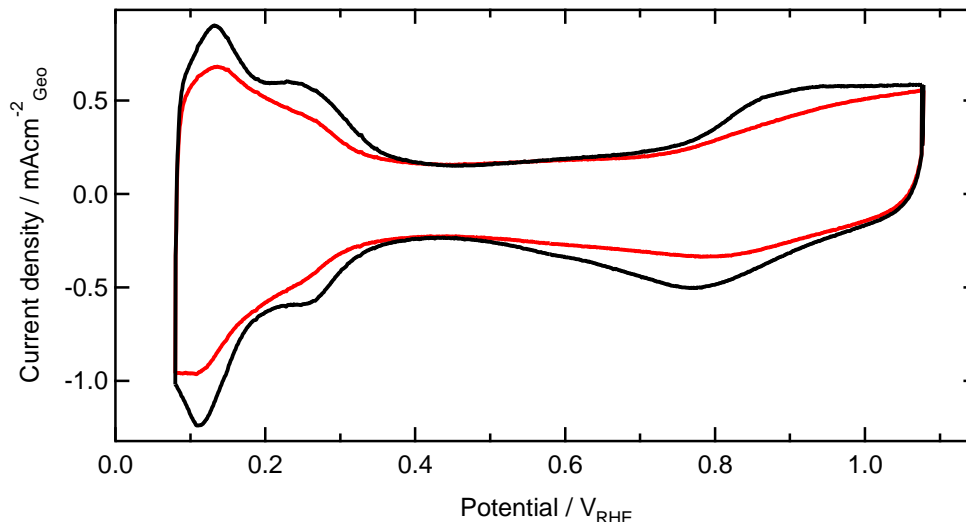


Figure 4.1: CVs of Pt/C 4-5 nm before (red) and after (black) an electrochemical cleaning procedure, i.e. continuous potential cycling from 0.05 to 1.305 V_{RHE} with 1 Vs^{-1} for 50 cycles.

4.1 Removing Impurities of Industrial Electrocatalysts

The standard cathode electrocatalyst for PEM fuel cells consists of platinum nanoparticles supported on a high surface area carbon like carbon black. The synthesis of carbon black is carried out by thermal cracking or partial oxidation of natural gas, oil or other hydrocarbons [35]. Depending on the feedstock there are always different amounts of impurities left in the carbon powder which can later be found in the catalyst.

Additionally, during the precipitation process of platinum ions onto the carbon support different reagents are used, for example reducing agents or other solvents than water, which can lead to organic contamination. Inorganic impurities can originate from incomplete removal of the counterion of the platinum salt, for example.

In electrochemistry the influence of organic impurities can clearly be seen during the first CVs of Pt/C as it is shown in figure 4.1. At potentials above $0.7 V_{\text{RHE}}$ there is a distinctive difference between the initial CV and one obtained after a continuous cycling procedure. In the initial CV, the platinum oxidation peak is suppressed while there is a continuous increase in current caused by the oxidation of organic impurities. Additionally, the H_{upd} region consists of a smaller area and the specific features are less pronounced. During potential cycling to high potentials applying a high scan rate (0.05 to $1.35 V_{\text{RHE}}$ with 1 Vs^{-1}), the organic impurities are oxidized. Afterwards the adsorption of hydrogen and oxygen species on the platinum surface is not suppressed anymore which is important for the function of the catalyst.

This just described cleaning effect leads to a growth of the area in the H_{upd} region during the first CVs of potential cycling, which can easily be mistaken for the growth

of the platinum surface area due to unidentified processes. However, since this effect can also be shown for polycrystalline Pt, not the platinum surface area itself but the accessible active surface area increases due to the removal of organic impurities. Therefore one should always conduct an electrochemical cleaning procedure before each measurement. The suitable amount of cleaning cycles, the scan rate and the potential limits have to be chosen in order to obtain a clean active surface without influencing the catalyst too much, e.g. by inducing particle agglomeration. Additionally, CO stripping experiments should be used in order to determine the active surface area since this method is less sensitive to impurities. CO displaces most molecules from the platinum surface due to its high bond strength.

4.2 Degradation Behavior changes with Scan Rate

One of the most commonly used procedures for accelerated stress tests is potential cycling. In these tests, suitable potential limits and a scan rate have to be chosen. The fact that variation of the potential limits changes the degradation behavior is well-known [11]. However, the dependency on the applied scan rate of the potential cycling treatment has to the best of the author's knowledge not been studied in detail. Therefore several degradation treatments have been conducted applying 1800 cycles each, but varying the applied scan rate. The results are shown in figure 4.2. From chart (a) of figure 4.2 one can clearly see that the loss in active surface area per cycle is enhanced for slower scan rates. However, chart (b) indicates that with respect to time the loss in active surface area is higher for faster scan rates. Consequently, the frequency of changing between an oxidized and reduced surface is important, but also the time staying in the oxidizing and reducing potentials, respectively, is not negligible. Although the curve for 250 Vs^{-1} does not exactly fit into this order, a trend can be identified. Treatments conducted with scan rates between 500 and 1000 Vs^{-1} show an almost identical behavior with respect to time. Thus, above a certain threshold for the scan rate, only the amount of cycles and not the time is dominating the loss in active surface area. This finding was also confirmed by measurements using square wave potentials with frequencies between 1 and 13 Hz . In this frequency range the number of cycles was crucial for the loss in active surface area while the treatment time played a minor role [36, 37].

4.3 The Choice of Electrolyte influences Catalyst Stability

Accelerated stress tests conducted in RDE setups require the use of a liquid electrolyte with perchloric acid and sulfuric acid being the most common ones. On the one hand, activity measurements in perchloric acid provide higher activity values

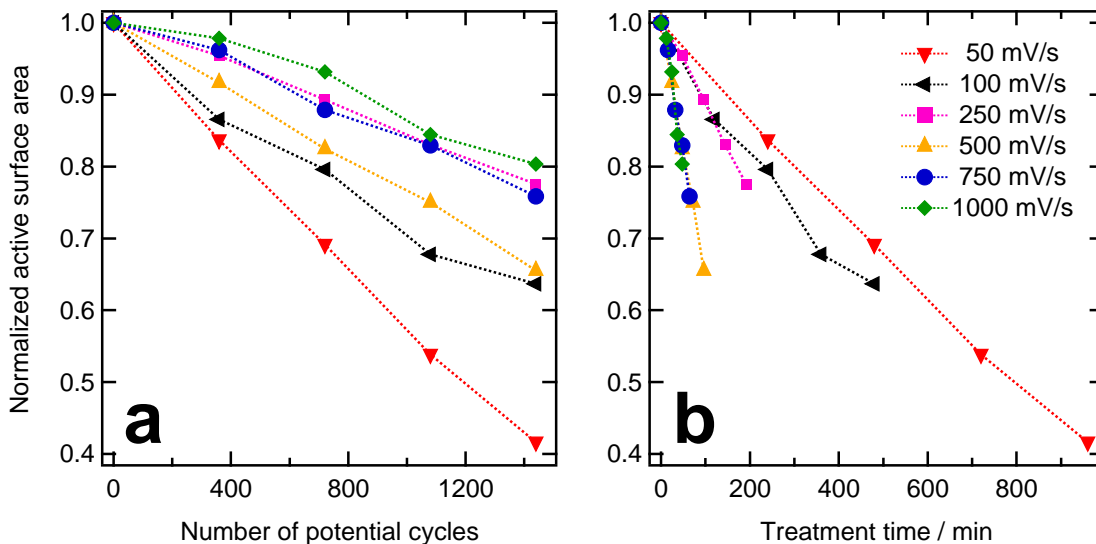


Figure 4.2: Decrease in active surface area (determined using H_{upd}) with the number of cycles (a) and time (b) during a potential cycling treatment between 0.4 and 1.4 V_{RHE} for 1800 cycles with the indicated scan rates.

than in sulfuric acid because the adsorption of the perchlorate anion to the platinum surface is much weaker than the one of the sulfate anion [38]. The kinetics of the reactions can therefore be measured without disturbing blocking effects. On the other hand, the Nafion® membrane used in a PEM fuel cell exhibits sulfonic acid groups which are chemically closer to sulfuric acid. Hence, it is important to know if the choice of electrolyte has a significant influence on the experimental results. Therefore, degradation measurements were conducted in both 0.1 M HClO_4 and 0.1 M H_2SO_4 , which are compared in figure 4.3.

It can clearly be seen that there is a significant difference in the loss of active surface area for the use of sulfuric and perchloric acid, respectively. That is, the loss in active surface area is increased for the use of sulfuric acid compared to perchloric acid as electrolyte. However, both electrolytes exhibit the same trend of an increased loss for higher upper potential limits and the enhancement effect is in both cases approximately a factor of three. This effect can have several reasons: the properties of the particular anions, different trace impurities in the employed suprapure acids or the difference in acid strength. The latter is not large, but sulfuric acid is a diprotic acid which leads to a decreased pH value. For both acids the first ionization step can be assumed as complete dissociation due to their high dissociation constants. The

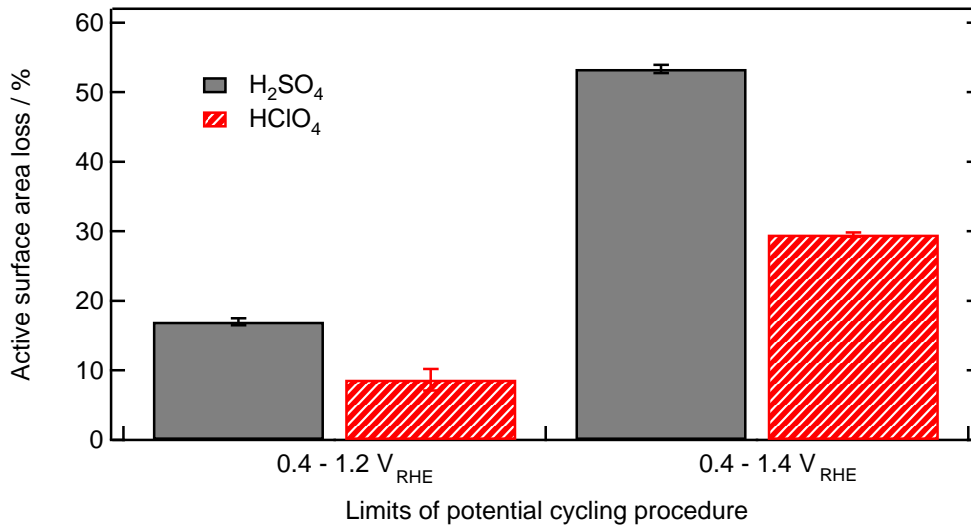


Figure 4.3: Comparison of the loss of active surface area determined by CO stripping in 0.1 M sulfuric acid and 0.1 M perchloric acid as electrolyte, respectively, of Pt/C 4-5 nm induced by a potential cycling treatment for 3600 cycles with given potential limits.

second dissociation process, which is only possible for sulfuric acid, has a dissociation constant of about $K_a = 0.01$ ($pK_a = 1.99$ [39]) which leads to a decrease in the total pH from 1 to 0.96.

It is not clear what exactly causes the difference in loss of the observed active surface area. Further studies using different pH values of the electrolytes should be conducted to verify the pH influence. For the comparability of degradation measurements, it should be ensured that the mechanism is identical. If this is the case, i.e. only the amount of ECA loss varies, qualitative trends can still be compared.

4.4 Traces of Chlorides cause increased Degradation

Ionic contaminants like chlorides play an important role in the application of fuel cells because they can interfere significantly with the occurring electrochemical processes [40]. Chloride anions can originate from the manufacturing process of the catalyst because often chloride salts of platinum are used. But chloride contaminants can also simply arise from the cooling water, from airborne salts during the intake of air or from other components [41]. Considering the average concentration of chlorides in U.S. public water supplies of 11.5 mg L^{-1} [42] ($3.2 \times 10^{-4} \text{ mol L}^{-1}$) or in Europe of even 52 mg L^{-1} [43] ($1.5 \times 10^{-3} \text{ mol L}^{-1}$), a great effort is needed to avoid trace amounts of chlorides in the fuel cell system.

Regarding electrochemical measurements in test cells, chlorides can be released from reference electrodes containing chloride solutions (like the Saturated Calomel Elec-

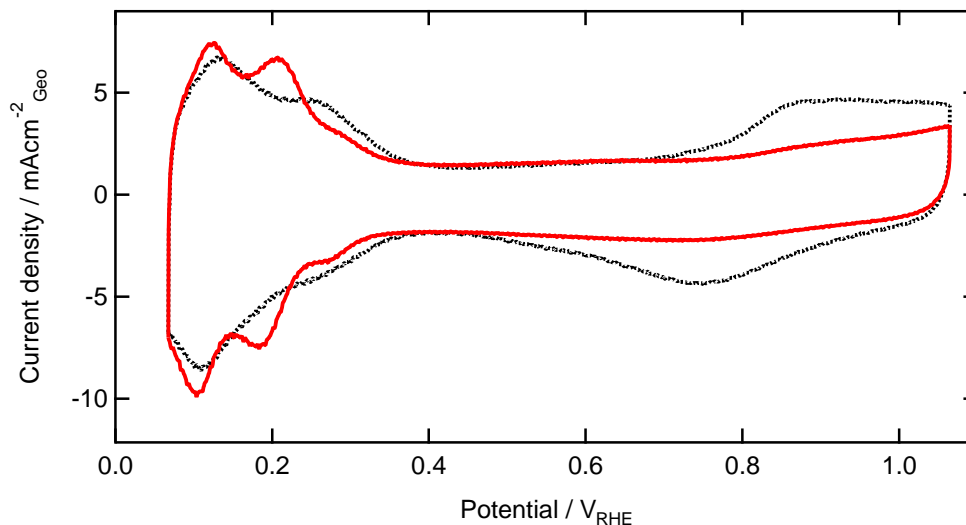


Figure 4.4: Comparison of the CVs of Pt/C 4-5 nm with (red line) and without (black dashed line) added chlorides (1×10^{-3} M KCl in 0.1 M HClO_4) (both 1 Vs^{-1}). The H_{upd} features change clearly and the oxidation is inhibited by the ions.

trode (SCE) or the Ag/AgCl electrode) which are most commonly used. This effect has been shown together with the induced decrease in activity of polycrystalline platinum for chloride concentrations above $1 \times 10^{-6} \text{ mol L}^{-1}$ [33]. Stamenkovic *et al.* studied the kinetics of the oxygen reduction reaction in an aqueous sulfuric acid solution containing chlorides and reported a strong inhibition of the ORR especially on the Pt(100) surface modified by adsorbed chloride anions [40]. It is also known that the dissolution of platinum in an aqueous environment is significantly enhanced by adding chlorides due to the formation of tetra- or hexachloro complexes [44, 41]. Furthermore, the influence of chlorides in a single cell test of a PEM fuel cell showed an increased loss of electrochemical surface area [45]. Consequently the influence of trace amounts of chlorides on the degradation of Pt/C electrocatalysts is important to study.

The adsorption of chlorides on the Pt/C electrocatalyst can be detected by cyclic voltammetry. In figure 4.4, the measured CVs with and without added chlorides are shown and the features change in agreement with the literature [38]: the H_{upd} region is narrowed in the presence of chlorides together with a small change of the characteristic features, whereas the double-layer region is widened due to a strong retardation effect of oxide formation by adsorbed chloride ions.

Figure 4.5 shows the dependency of loss in active surface area on the concentration of chlorides in the electrolyte. There is a pronounced enhancement of degradation with increasing chloride concentration. Even at concentration levels far below the ones in drinking water, the degradation is significantly accelerated. Consequently, this study underlines the necessity of chloride free environments in PEM fuel cells and in

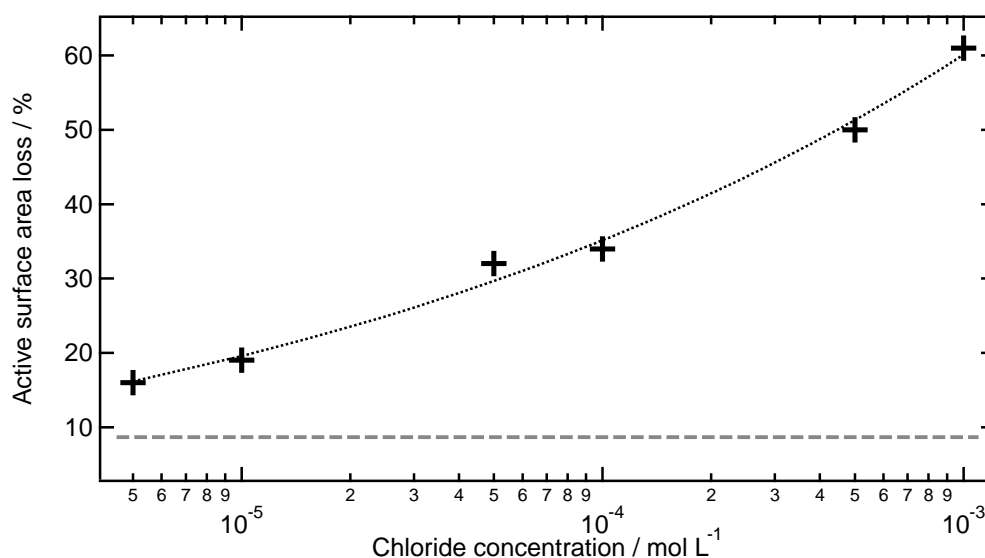


Figure 4.5: The loss of active surface area caused by a potential cycling treatment (0.4 - 1.2 V_{RHE}, 1 Vs⁻¹, 3600 cycles) with different chloride concentrations in the electrolyte (0.1 M HClO₄). The dotted line is a power function fit and serves as a guide to the eye. The grey dashed line shows the measured loss for the identical treatment without added chlorides.

this context also in half-cell measurements in order to guarantee the transferability of the results.

4.5 Degradation Behavior depends on Convection and Catalyst Loading

An important aspect in heterogeneous catalysis is the occurrence of mass transport limitations which inhibit high reaction rates. The reaction rate is thereby limited by diffusion and not by the kinetics of the reaction. This situation can be changed by inducing convection in order to enhance the mass transport from and to the surface. At the surface, there always remains the so-called "diffusion boundary layer" which is a thin layer with laminar flow where mass transport can only take place by diffusion. The diffusion limitation of oxygen during the ORR is well-known and in order to be able to study the reaction rate, for example a RDE is used where controlled mass transport conditions are ensured due to the rotation of the electrode. For many degradation mechanisms mass transport of species like platinum ions, platinum particles, and adsorbates is relevant as well. Thus, the influence of convection induced by rotation of the electrode during a degradation treatment was analyzed.

As can be seen in figure 4.6a, rotation during stress tests unambiguously leads to an enhanced degradation. In the specific example, the loss in active surface area is almost doubled when rotation is applied. The influence of rotation is independent of the scan rate as well as of other upper potential limits within the oxidative region.

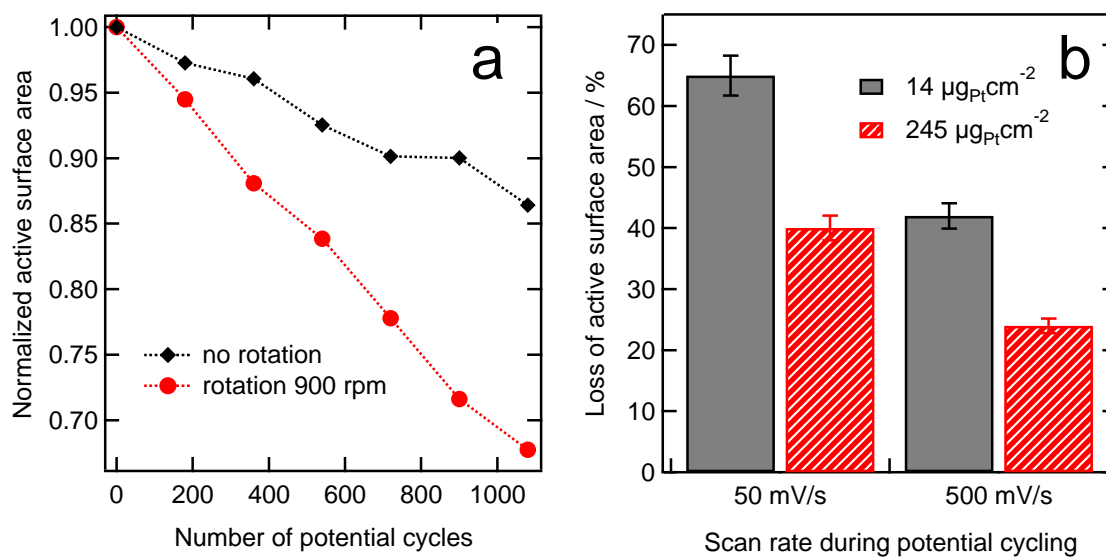


Figure 4.6: (a) Decrease in active surface area with the number of potential cycles with 1 Vs^{-1} from 0.4 to $1.4 \text{ V}_{\text{RHE}}$ with and without rotation at 900 rpm . (b) Comparison of the loss of active surface area for the same potential cycling treatment ($0.4 - 1.4 \text{ V}_{\text{RHE}}$, 1 Vs^{-1} , 1800 cycles) with different catalyst loadings (see legend) for two different scan rates (in both cases, 0.1 M HClO_4 was used as electrolyte).

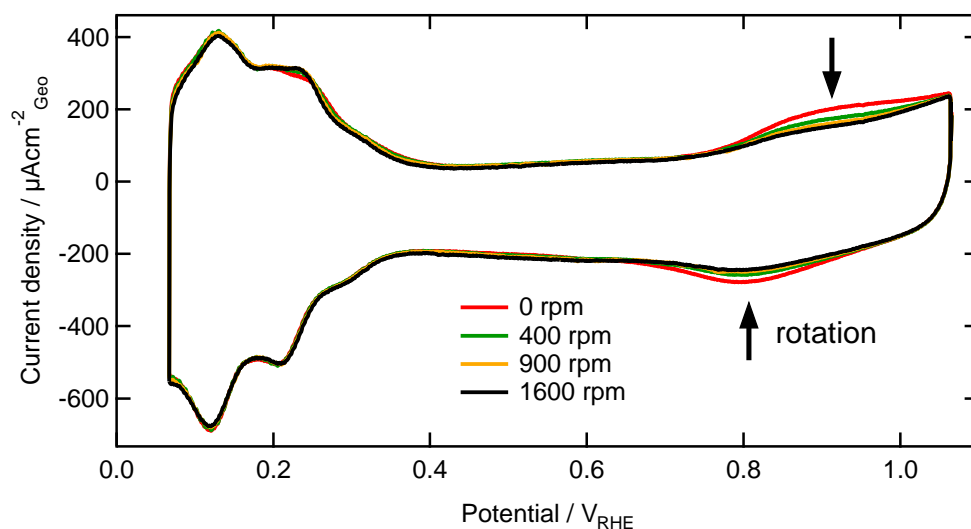


Figure 4.7: Change of voltammetric features (50 mVs^{-1}) of Pt/C 4-5 nm in the presence of $5 \times 10^{-5} \text{ molL}^{-1}$ chlorides (in 0.1 M HClO_4) due to rotation of the electrode. The arrows indicate the damping of the oxidation and reduction peak of platinum due to the adsorption of chlorides.

For the identical treatment at 100 mVs^{-1} as well as for the identical treatment with $1.2 V_{\text{RHE}}$ as upper potential limit comparable results were obtained. A possible explanation of this effect is that the convection reduces the thickness of the diffusion layer, which means that species from the bulk can easier reach the surface. In the same way, intermediates and products can go away from the surface to the bulk more easily. Consequently, these findings indicate that mass transport processes are involved in the degradation process. This is in line with the observation that the catalyst loading also has an effect on the rate of loss of active surface area because in the dense layer the diffusion of species is reduced. Hence, the comparison of the degradation for different loadings during identical treatments reveals a big variation in the loss of active surface area (see figure 4.6b). Consequently, this finding is another implication for the involvement of mass transport processes during the degradation.

Regarding section 4.4, one possible reason for the increase in the loss in active surface area of the electrocatalyst by inducing convection are impurities like, for example, chlorides, which enhance the degradation processes. Since rotation increases the effective concentration of contaminants at the platinum surface, the occurring electrochemical processes are being affected. This accumulation effect can be visualized by adding a small amount of chlorides to the electrolyte and monitoring the changes of the CV of a standard electrocatalyst upon rotation (see figure 4.7). The same effect is also observable comparing the CVs of two different catalyst loadings using the identical electrolyte containing chlorides. The lower the loading

the more pronounced are the characteristic changes in the voltammetric features due to adsorption of chlorides. Hence, these observations show that for the utilized chloride concentrations the absolute number of adsorption sites for chloride ions on the platinum surface of the catalyst is higher than the number of chloride ions in the accessible volume at the surface.

Considering possible degradation mechanisms suggested in the literature there are processes discussed which involve mass transport of catalyst species, i.e. platinum dissolution and particle detachment. For both processes redeposition can take place with a certain probability which depends on the thickness of the diffusion layer. From former studies it is known that the amount of platinum lost from the electrocatalyst due to a degradation treatment can be found in the electrolyte using ICP-OES [46]. But unfortunately, until now it was not possible to distinguish between platinum ions and platinum nanoparticles. Although an extensive analytical study is required due to the very low concentrations in order to solve this problem, it would enable one to distinguish between these degradation mechanisms. Therefore, a project with an analytical laboratory is planned for the investigation of platinum species in the electrolyte after accelerated stress tests.

4.6 Conclusion

It was shown, that for degradation tests using an RDE setup it is crucial to keep the experimental procedure within a test series as constant as possible. Only one parameter should be changed at a time, including the catalyst itself as a parameter. Impurities of any kind have to be avoided because they can interfere with the electrochemical processes and lead to misinterpretations. In order to guarantee the best possible reproducibility using industrial catalysts, before each degradation measurement an electrochemical cleaning procedure has to be conducted and the active surface area should be determined by CO stripping measurements instead of using the H_{upd} region. In this way, within one series of measurements reliable values for the degradation and trends can be obtained.

Furthermore, these investigations give interesting insights into occurring degradation processes. The significant influence of mass transport indicates a dissolution or particle detachment process. Furthermore, the dependence of the degradation on the kind of electrolyte, the chloride concentration and the scan rate gives additional hints for the interpretation of degradation processes. Extensive analytical studies are planned in order to distinguish between Pt ions and nanoparticles diffusing into the electrolyte.

Chapter 5

IL-TEM Investigation of the Degradation of Standard Electrocatalysts

The long term performance of fuel cells is a fundamental criterion for their commercial viability. In this respect, the degradation of the electrocatalyst accompanied by a loss of active surface area is of major relevance. Much effort is spent on quantifying and elucidating the degradation mechanisms of electrocatalysts [11]. Instead of investigations in a highly complex fuel cell stack, half-cell measurements using accelerated stress tests are advantageous for these studies.

Typically, degradation is characterized by the decrease in electrochemically active surface area. In this way, catalysts can be compared regarding their stability from a quantitative point of view. However, if further improvements of the electrocatalysts shall be achieved, it is essential to get an insight into the mechanistic processes occurring during degradation.

One possibility in this respect is the application of transmission electron microscopy, which provides a microscopic insight into the structure of the catalyst. TEM is often used in combination with X-ray diffraction (XRD) in order to obtain the particle size distribution and the corresponding average crystallite size, respectively. These methods can be applied to a degraded sample, i.e. a catalyst sample which was exposed to a stress test. Conclusions about occurred changes due to degradation, like particle growth, can be drawn by comparing the results obtained by this investigation with the ones obtained for the pristine sample. Such a characterization exhibits two major disadvantages: first, for the analysis the catalyst has to be removed from the electrode after the treatment which characterizes the method as being destructive and therefore not suitable for following changes with time [30]. Secondly, in TEM single microscopic regions are visualized which not necessarily represent the whole sample. Hence, for common TEM degradation analysis a large number of

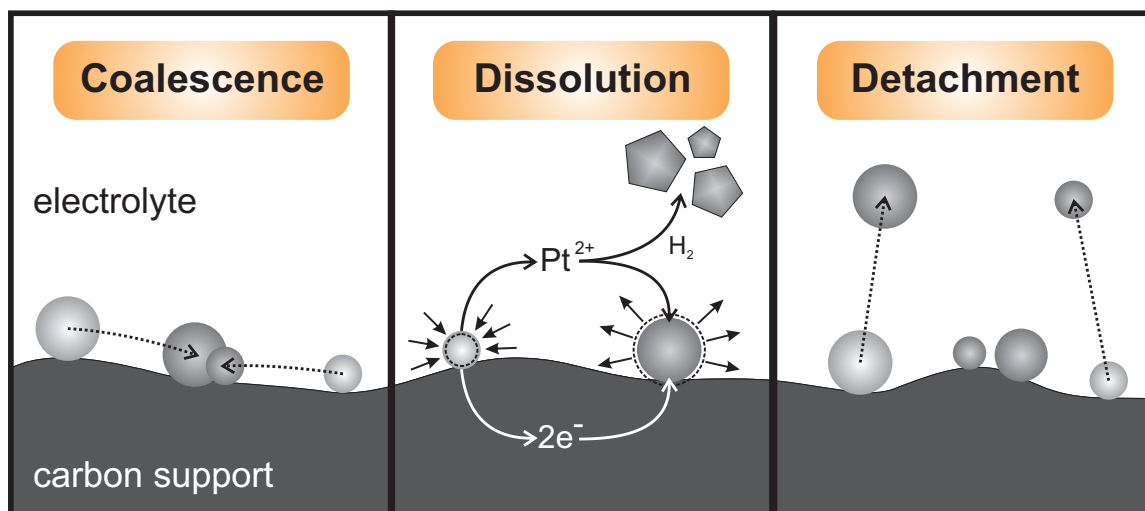


Figure 5.1: Schematic illustration of the different degradation mechanisms occurring in a fuel cell: the coalescence via particle migration, the dissolution of platinum with subsequent redeposition onto larger particles (electrochemical Ostwald ripening) or precipitation in the membrane after reduction by hydrogen, and the detachment of whole particles from the carbon support.

images has to be taken into account and good statistics have to be made in order to be able to draw significant conclusions about degradation processes. Therefore, a TEM technique was developed by our group which distinguishes itself as being non-destructive and allows the comparison of identical regions of the catalyst before and after a treatment: identical location transmission electron microscopy (IL-TEM) [15]. Details about this technique are given in section 2.9.

In this chapter, after introducing the different degradation mechanisms for Pt/C electrocatalysts, the results of the application of the IL-TEM technique in combination with ECA measurements for the investigation of the degradation behavior of standard electrocatalysts are presented. In this respect, the commonly used potential cycling as well as potentiostatic treatments at elevated temperatures were conducted.

5.1 Degradation Mechanisms of Platinum Nanoparticles in Fuel Cells

In general, three different degradation mechanisms are distinguished (see figure 5.1): (i) the migration and concomitant coalescence of the nanoparticles on the support, (ii) the detachment of whole nanoparticles from the support, and (iii) metal dissolution [47, 11]. The latter results either in re-deposition on larger particles, the so-called electrochemical "Ostwald ripening", or in precipitation in the membrane electrolyte [48].

Coalescence involves the migration of platinum nanoparticles on the carbon support together with subsequent merging of aggregated particles. Thus, particle growth is induced. The driving force for this process is the minimization of the total surface energy with rising diameter. Coalescence goes along with a characteristic change of the particle size distribution. The initial size distribution originates from the synthesis process and does not have to be Gaussian. However, since larger particles are formed at the expense of merging particles with no preference for a specific particle size, the resulting size distribution will be differing from the initial one as follows: the side towards large particles rises while the intensity (number of particles) for the rest of the size distribution decreases without other significant changes in the shape. The resulting size distribution is then characterized by a tail towards large particles [49].

Another mechanism inducing particle growth is **platinum dissolution** and redeposition. For the latter process, two possibilities exist: according to an electrochemical **Ostwald ripening**, larger particles grow at the expense of small ones. Due to their higher solution pressure (analog to the increased vapor pressure), smaller particles dissolve preferentially. The dissolved platinum species then are able to move through the electrolyte to a larger particle, where they are precipitated. In the end, small particles dissolve while larger ones grow leading to a decrease in total surface energy. The maximum of the particle size distribution is thereby shifted to higher values, while a tail remains towards small particle sizes [49]. By this means, Ostwald ripening can be distinguished from particle growth induced by coalescence. In addition to Ostwald ripening, dissolved platinum ions can also diffuse into the membrane electrolyte, where they are chemically reduced by hydrogen permeating from the anode. This **precipitation of Pt ions in the membrane** leads to a platinum band or large particles [48]. In a half-cell, the latter process leads to an increased concentration of platinum ions in the aqueous electrolyte with a concomitant shrinking and vanishing of small particles.

Particle detachment is characterized by whole particles dropping off the carbon support. Detached particles can either be released into the electrolyte or redeposited at another location of the catalyst. This mechanism is often related to oxidation of the underlying carbon support [48, 14]. Particle detachment was shown in our group to be the dominant mechanism upon potential cycling of a Pt/C 4-5 nm electrocatalyst [46]. In this case, no carbon corrosion was visible.

Additionally, the carbon itself can be completely oxidized to carbon dioxide, which in extreme cases leads to a structural collapse of the whole electrode [50]. In a PEM fuel cell, system start/stop and local hydrogen starvation are two major contributions to carbon corrosion due to the thereby induced high potentials [51].

The degradation of fuel cell catalysts is a complex superposition of several mech-

anisms. In order to improve the catalyst durability, these processes have to be identified and the dependence of individual mechanisms on the system parameters has to be determined. Based on these findings, new concepts can be developed.

5.2 Degradation Behavior of Standard Electrocatalysts

In the literature, various possible degradation mechanisms for Pt/C electrocatalysts are suggested (see figure 5.1) and for each mechanism examples are given [11]. The presented results vary a lot, even if standard Pt/C or Pt-alloy/C electrocatalysts are used. Hence, the degradation mechanism seems to be very sensitive to the testing procedure and in particular to the type of catalyst. However, no systematic study regarding the correlation between the specific synthesis procedure steps and the resulting degradation mechanism at otherwise fixed conditions has been conducted. Only with regard to different kinds of carbon supports, the durability in respect of its total oxidation has been studied in more detail (see for example [51]). The influence of the carbon support on the degradation mechanism of the nanoparticles, however, has not been specified. A possible reason for this might be the reluctance to disclose details of the synthesis procedure, particularly in the case of industrial involvement. Thus, the synthesis procedure of commercially available industrial catalysts is often not available. Additionally, as the synthesis is very complex all parameters have to be accurately controlled to obtain a significant reproducibility.

In the present investigation, for the first time the degradation mechanisms of five electrocatalysts were compared on a microscopic level. This was accomplished by using IL-TEM in combination with RDE measurements in order to evaluate the degradation behavior of the catalysts during a potential cycling treatment. The potential limits thereby were $0.4 V_{\text{RHE}}$ and $1.4 V_{\text{RHE}}$, respectively and the applied scan rate was 1 Vs^{-1} . The electrolyte (0.1 M HClO_4) was constantly purged with argon during the measurements. More detailed information about the measurement procedure is given in section 3.

The five different electrocatalysts used for these experiments are specified as follows (see table 5.1):

All catalysts are high surface area catalysts with carbon black as support. The latter is the same carbon black with a BET surface area of about $700 \text{ m}^2 \text{ g}^{-1}$ for all catalysts except for the one with the graphitized carbon (*Ptgraph*). The particle size is 2-3 nm for *Pt3nm*, *Pt20%* and *Ptgraph* and 4-5 nm for *Pt5nm* and *Pt₃Co*, respectively. Furthermore, it is noteworthy to point out that the catalyst *Pt5nm* was fabricated by a heat treatment of *Pt3nm*. More details about the synthesis of these commercial catalysts are not available.

In figure 5.2, the loss of active surface area for the five applied electrocatalysts upon

Table 5.1: Characterization of the applied electrocatalysts (catalysts supplied by *Tanaka Kikinzoku Kogyo K. K., Japan*). The amorphous high surface area carbons all consist of the same carbon black with a BET surface area of approximately $700 \text{ m}^2 \text{ g}^{-1}$.

Notation	Particle Composition	Particle Size	Carbon Support	Pt Loading
Pt5nm	Pt	4-5 nm	amorphous	50.6%
Pt3nm	Pt	2-3 nm	amorphous	46%
Pt20%	Pt	2-3 nm	amorphous	20%
Ptgraph	Pt	2-3 nm	graphitized	46.5%
Pt ₃ Co	Pt ₃ Co	4-5 nm	amorphous	48.3% (4.1% Co)

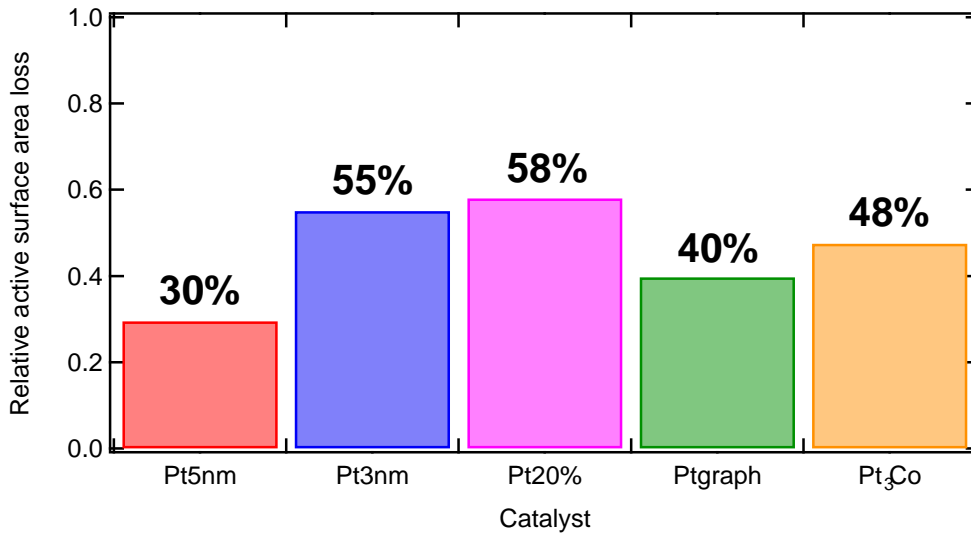


Figure 5.2: Total relative loss of active surface area (determined by CO stripping) of the different electrocatalysts upon potential cycling for two hours ($0.4-1.4 \text{ V}_{\text{RHE}}$, 1 Vs^{-1} , 0.1 M HClO_4).

an identical potential cycling treatment is displayed. In this way, the particular catalysts can be put in order in terms of their durability (according to the measured total ECA loss) as follows:

$$Pt5nm > Ptgraph > Pt_3Co > Pt3nm \geq Pt20\%$$

Apparently, either the particle size or the high temperature treatment are responsible for an enhanced durability of the catalyst *Pt5nm*. The alloy catalyst *Pt₃Co*, which exhibits the same particle size as *Pt5nm*, loses considerably more active surface area upon the stress test. Hence, a stabilizing effect through alloying, which is described in the literature [52], cannot be confirmed for this catalyst. Furthermore, the graphitization of the carbon support has a beneficial effect on the stability of the whole catalyst. The Pt loading does not seem to have a detectable influence on the degradation of the catalyst, as the ECA loss of *Pt3nm* and *Pt20%* are almost equal.

However, the significance of the value for the loss of active surface area is limited

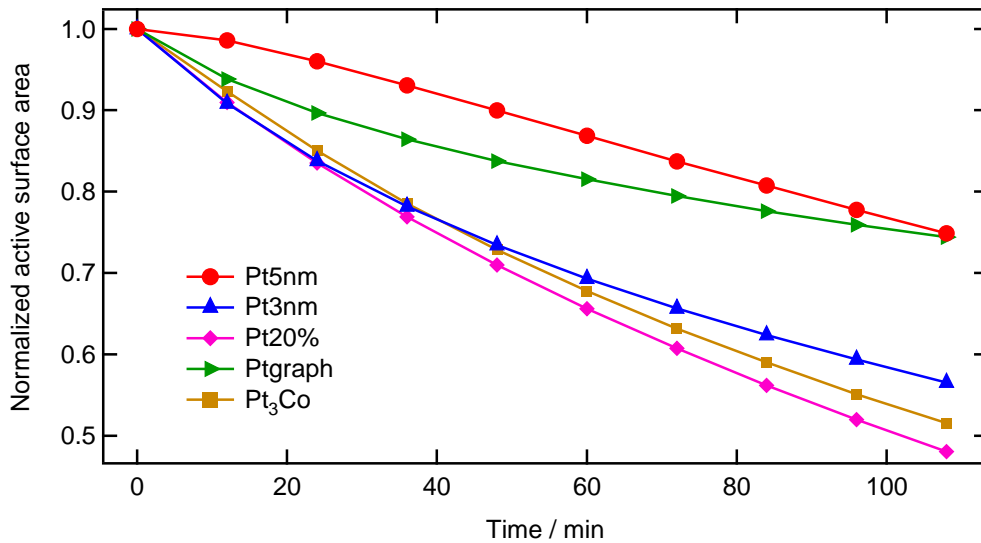


Figure 5.3: Time-dependent decrease of active surface area for the different electrocatalysts during the degradation treatment. The values were obtained using H_{upd} and were evaluated in a limited time interval. Therefore, the absolute values differ from the ones determined by CO stripping (see figure 5.2).

and should only serve as a rough indication for the durability of the catalyst. All of these values exhibit a large standard deviation between 10% and 20%. Additionally, the starting point of the measurement, for example, can have a great influence on the exact value depending on the course of surface area loss.

More information about the degradation behavior is obtained by analyzing the characteristic time-dependent decrease of ECA during the stress test. Therefore, for each catalyst the same period of the stress test was evaluated by determining the active surface area using the H_{upd} region (see 5.3). As shown earlier (see section 4) this method can be influenced by existent contaminations leading to a pseudo-increase of ECA in the beginning. Consequently, for all catalysts the ECA values starting not until 12 minutes after the first CO stripping are shown and the absolute values can not be directly compared to the ones determined by CO stripping from figure 5.2. The observed trends can be used as indication for the underlying degradation mechanisms. At first glance, especially the trend for *Pt5nm* stands out from the ones of the other catalysts. The latter ones are all dominated by an almost exponential behavior while the decrease in ECA of *Pt5nm* approximately corresponds to a linear decay. Having a closer look at the degradation progressions of the catalysts besides *Pt5nm*, they mainly show a steep initial decay and flatten out with time. This behavior is less pronounced for *Pt₃Co* where the trend is more continuous. Additionally, the trend for *Ptgraph* stands out because the catalyst seems to be stabilized after an initial rapid loss of active surface area in a much more pronounced manner than the other catalysts.

A qualitative mechanistic interpretation for the observed trends could be that *Pt5nm* is dominated by a different degradation mechanism than the others. The most similar behavior is found for *Pt₃Co* which is characterized by only a slight curvature in the corresponding curve. The trends additionally indicate a difference in the involved degradation mechanisms of *Ptgraph* and the other two catalysts with particle diameters of 2-3 nm. The latter ones show a very similar behavior which is a sign for similar mechanistic degradation processes. In contrast, *Ptgraph* is more stable and the decrease rapidly flattens out. This can be a sign for either a completely different degradation mechanism or that the superposition of existent processes is different. In order to get a more accurate insight into the degradation mechanisms, the degradation behavior has to be studied on a microscopic level. Therefore, IL-TEM was conducted for all of the mentioned electrocatalysts.

In the following, the influence of various parameters concerning the degradation behavior is discussed in separate sections. In order to be able to compare such complex catalyst systems, comparisons are preferentially made by changing only one specific parameter at a time. By means of the five applied electrocatalysts, the influence of particle size and heat treatment, loading, support properties and kind of metal of the nanoparticles are investigated.

5.2.1 Dependence of Catalyst Loading

Ostwald ripening as well as coalescence requires the interaction between particles. This interaction is limited to an effective range the particles have to be located in. As a consequence, the platinum loading on a catalyst, which determines the distance between particles for a given particle size, might affect the degradation mechanism. In order to study the influence of catalyst loading on the degradation process, two Pt/C catalysts with comparable particle size and the same carbon support were compared. As mentioned before, the total surface area loss and the characteristic decrease of ECA with time are similar for these two catalysts. IL-TEM was used to investigate and compare the degradation mechanisms of the catalysts.

In figures 5.4 and 5.5 the catalysts *Pt3nm* and *Pt20%* are illustrated before and after the accelerated stress test, respectively. For both samples, the Pt nanoparticles are basically homogeneously distributed on the high surface area carbon. The particle density is thereby clearly higher for *Pt3nm* compared to *Pt20%*, in agreement with its higher platinum loading.

After the treatment, in both cases the density of particles decreases and larger particles, mostly spherically shaped, have been formed. It seems that in parts with higher particle density the particles somehow melted together to form a large platinum structure. No changes can be observed for the carbon support upon this treatment except for small distortions as it was also shown for *Pt5nm* [15]. In

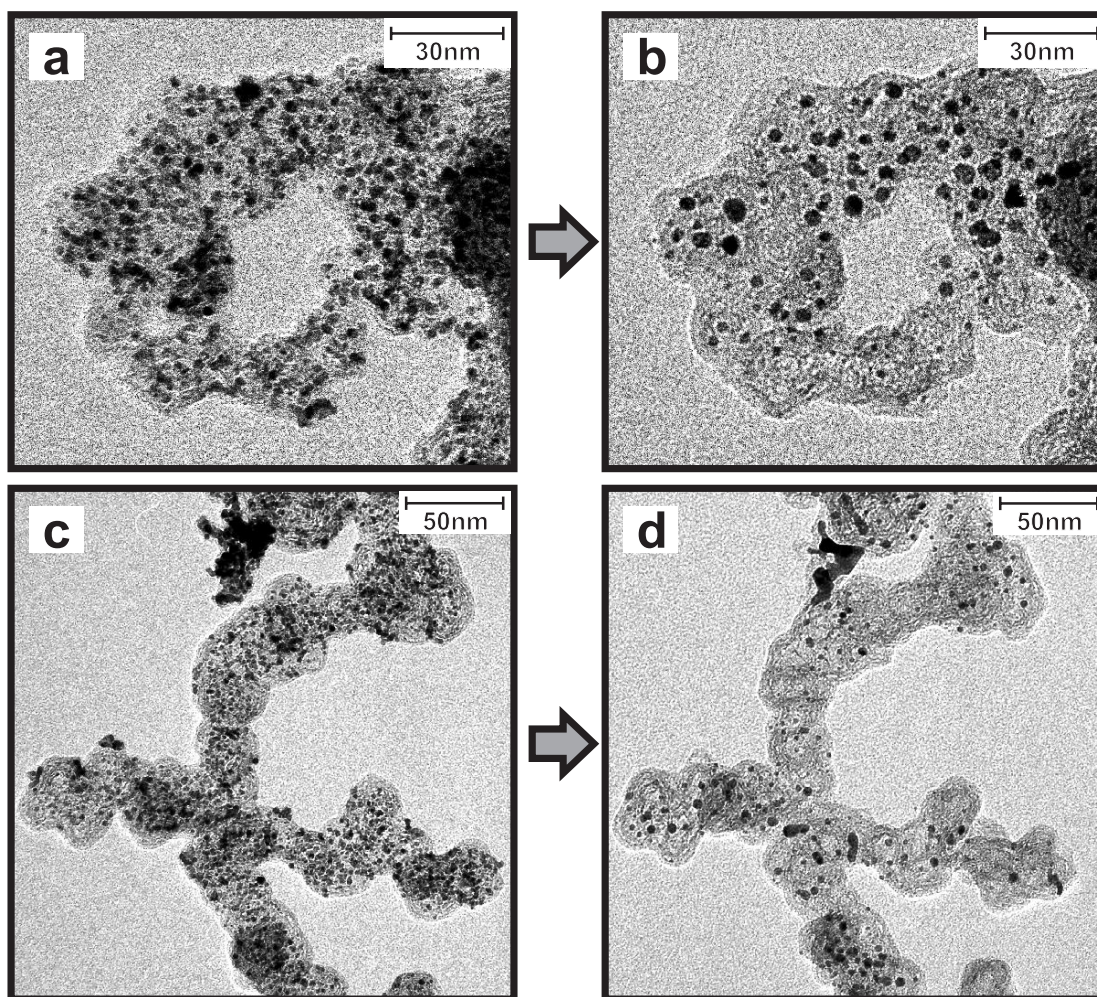


Figure 5.4: IL-TEM images (magnification 100k) of the catalyst *Pt_{3nm}* before (a,c) and after (b,d) the potential cycling treatment (2h, 0.4-1.4 V_{RHE}, 1 V s⁻¹, 0.1 M HClO₄). While the carbon support does not change significantly, particle growth can clearly be identified.

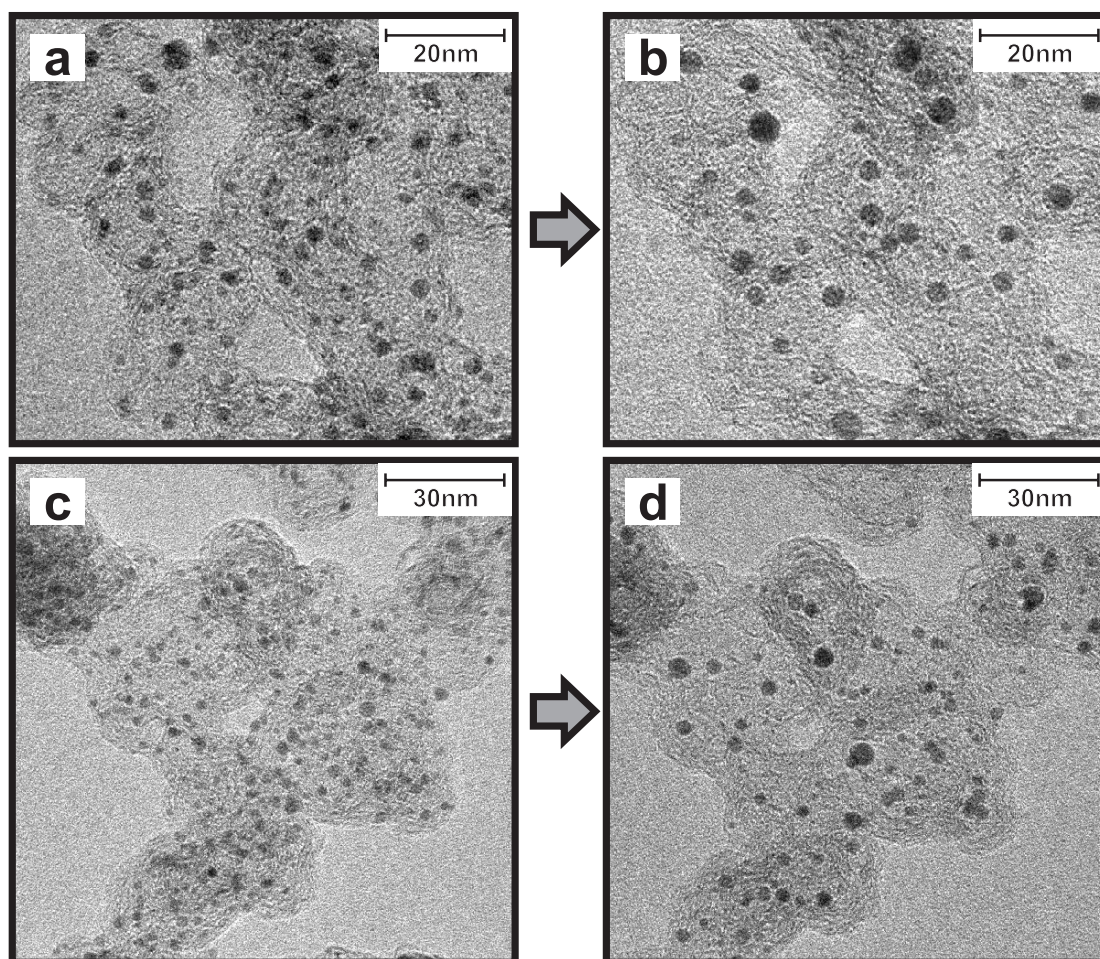


Figure 5.5: IL-TEM images (magnification 150k) of the catalyst *Pt20%* before (a,c) and after (b,d) the potential cycling treatment (2h, 0.4-1.4 V_{RHE}, 1 V s⁻¹, 0.1 M HClO₄). The carbon support does not change, while particle growth occurs.

both cases, after the stress test a few isolated particles located next to catalyst agglomerates on the thin carbon film of the grid can be found (not shown), which can be assigned to redeposited detached particles [15].

For specific areas within the images, a statistical evaluation of the particle size distribution was made. As identical regions before and after the treatment are considered, the number of particles does not have to be large in order to obtain significant information. The results of the analysis are given in figure 5.6. It is noteworthy that for the catalyst *Pt20%*, particles with diameters below 1 nm could not unambiguously be distinguished from structures of the carbon support. Therefore, the size distribution was cut at low diameters. The corresponding statistical results are given in table 5.2.

Table 5.2: Statistical evaluation of the changes in number of particles and particle diameters for *Pt3nm* and *Pt20%* upon the degradation treatment from identical regions using the images of IL-TEM. The corresponding particle size distributions are shown in figure 5.6.

Catalyst	Before/After Treatment	Number of Particles	Average Particle Diameter	Standard Deviation
Pt3nm	before	240	2.4	1.1
Pt3nm	after	93	3.0	1.1
Pt20%	before	158	2.3	0.8
Pt20%	after	50	3.1	0.9

In both cases, the total loss of surface area (see figure 5.2) as well as the initial particle size distribution are comparable. Furthermore, the resulting change is similar. The size distributions of both catalysts are displaced to approximately the same extent to higher particle sizes and consist of a lower number of particles, but in each case without a significant change in standard deviation.

As discussed, particle growth can originate from an electrochemical Ostwald process or from coalescence of migrating particles. In this case no tail towards small diameters develops during the treatment and small particles are not exclusively missing. Therefore, it can be proposed that coalescence is the main degradation mechanism. In order to check if additional processes might be involved, a rough estimation can be made. Assuming the particles (definite numbers of the statistics are given in table 5.2) as spheres, the change in number of particles and particle size account for 39% and 41% in ECA loss instead of the measured 55% and 58% (see figure 5.2) for *Pt3nm* and *Pt20%*, respectively. This indicates that an additional degradation mechanism is involved. The possible processes are Pt dissolution and particle detachment. Considering dissolution of platinum, there should be a preferred disappearance of small particles. Such an observation could not unambiguously be confirmed. Instead, the appearance of single particles on the carbon film of the grid indicates particle detachment. Therefore, this mechanism is most probable to cause the additional

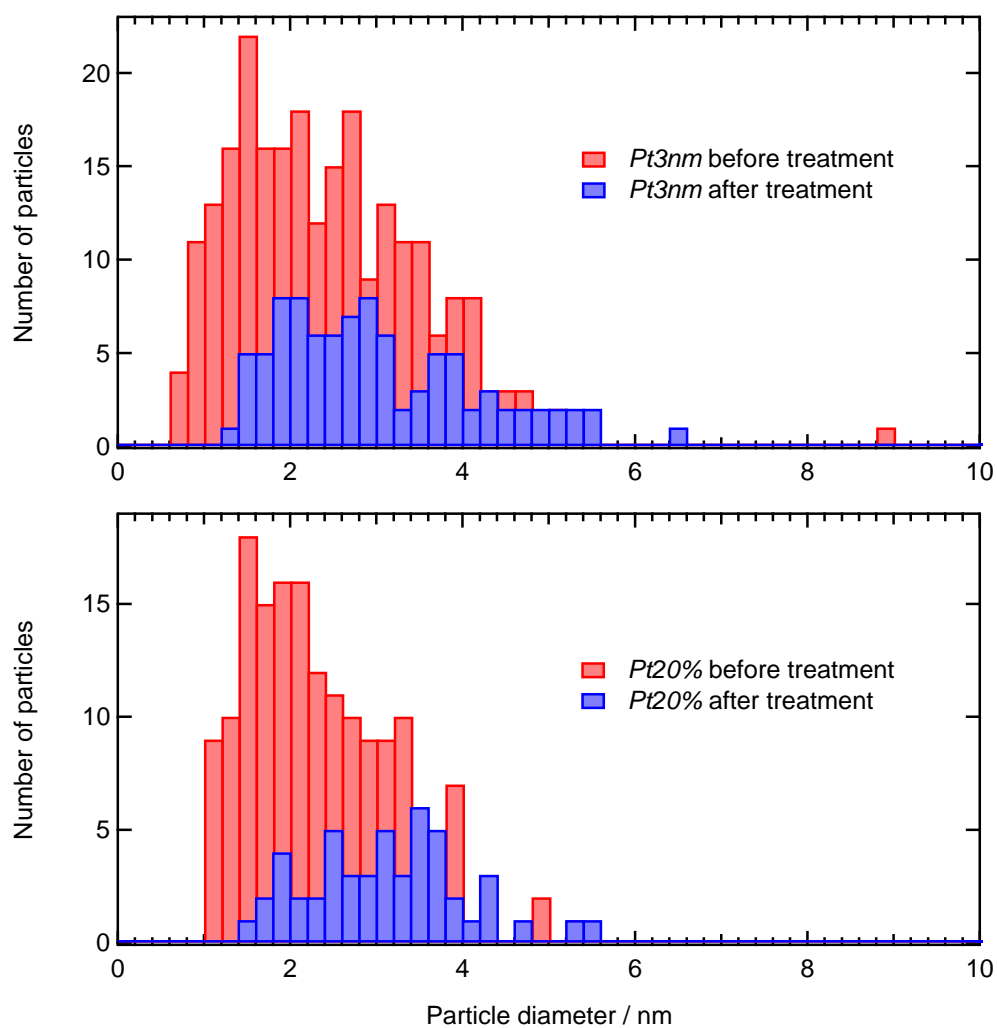


Figure 5.6: Particle size distributions for (a) *Pt3nm* and (b) *Pt20%* in each case before and after the degradation treatment (2h, 0.4-1.4 V_{RHE}, 1 Vs⁻¹, 0.1 M HClO₄) with 55% and 58% ECA loss, respectively. The corresponding statistical values are given in table 5.2.

loss of ECA.

As a conclusion, a change in the platinum loading of the catalyst from 20% to about 50% has no significant effect on both the durability and the degradation mechanism. Upon the applied conditions, the predominant degradation process is migration and concomitant coalescence in combination with detachment of whole particles from the carbon support.

5.2.2 Influence of Support Properties

The nature of the support can profoundly influence the degradation processes because the interaction between the particles and the support is crucial for particle migration and detachment.

The catalysts dubbed *Pt3nm* and *Ptgraph* exhibit approximately the same particle size and loading, but an amorphous and a graphitized carbon support, respectively. Therefore, these catalysts are suitable in order to study the influence of the carbon support on the degradation mechanism. From the total loss of ECA shown in 5.2, it is known that the graphitized catalyst *Ptgraph* is more stable than the one with the amorphous carbon support *Pt3nm*. The loss in ECA decreases 55% for *Pt3nm* compared to 40% for *Ptgraph*. The time dependence of degradation during potential cycling shown in figure 5.3 indicates an early stabilization of *Ptgraph* after an initial decay, whereas *Pt3nm* continues to degrade.

The images of *Ptgraph* received by IL-TEM (see figure 5.7) show the characteristic carbon structure for graphitized carbon with its graphitic planes especially at the edges of the primary particles [35]. No distinguishable change of the carbon support upon the potential cycling treatment can be observed. The platinum particles seem to be evenly distributed with a slight preference for the positions at the graphitic planes. During degradation, particle growth occurs leading to large particles which are preferably located at the previously denser parts of the sample. The particles seem to undergo the same process as the catalyst *Pt3nm* (see figure 5.4), but without losing as much metal. The shape of the formed large particles developed on the graphitized carbon seems to be not as uniform and spherical as the one from *Pt3nm*. Although a reason for this difference is not clear, a possible explanation is a retardation of migration on graphitized carbon due to an enhanced interaction with the support. Other mechanisms like particle detachment seem to play a minor role on the graphitized support. The characteristic trend in degradation for the catalyst *Ptgraph* (see figure 5.3) can most likely be ascribed to an initial rapid decrease in active surface area due to coalescence which leads to a concomitant stabilization of the catalyst. The catalyst with the coalesced particles seems to be more durable under the applied conditions. A statistical evaluation of the images of *Ptgraph* was not possible as the particles could not be clearly distinguished from the underlying

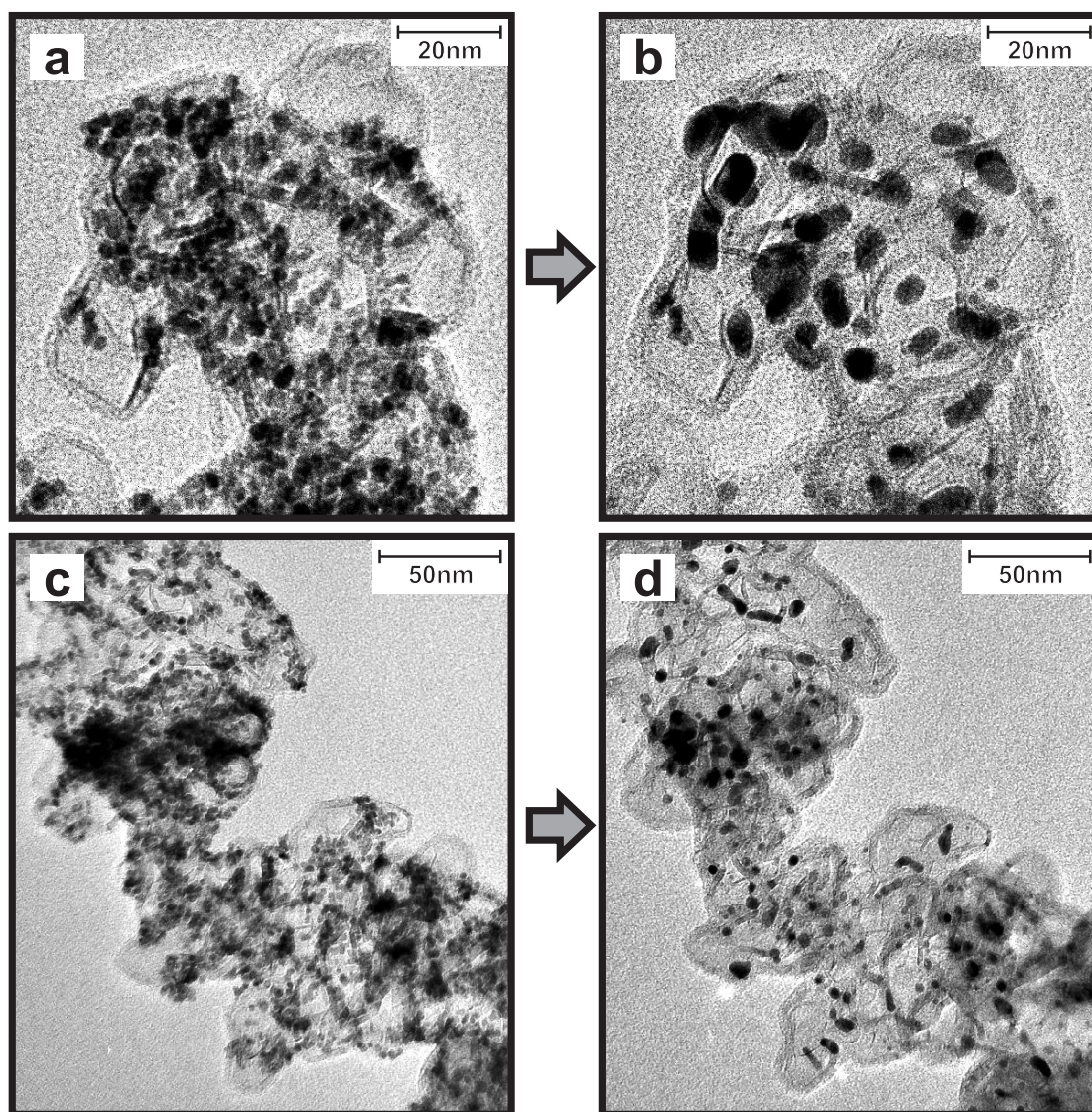


Figure 5.7: IL-TEM images (magnification 150k) of the catalyst *Ptgraph* before (a,c) and after (b,d) the potential cycling treatment (2h, 0.4-1.4 V_{RHE}, 1 Vs⁻¹, 0.1 M HClO₄). The carbon support with its graphitic planes can be observed unchanged before and after the treatment. The platinum particles undergo coalescence to non-spherical larger particles.

carbon support. However, for this catalyst, dissolution as well as Ostwald ripening seems to be less significant since several small particles stay unaltered in size.

Concluding the findings, the degradation behavior is strongly influenced by the nature of carbon support and thereby affects the loss in active surface area. The detachment of whole particles is more pronounced for *Pt3nm* than for *Ptgraph*. However, in both cases particle coalescence is the predominant degradation mechanism.

5.2.3 Impact of Temperature Pre-Treatment and Particle Size

In terms of the activity of standard electrocatalysts towards the oxygen reduction reaction, a particle size effect is reported [4]. With respect to degradation, the influence of the particle size is even more obvious: firstly, the solubility of small particles rises with decreasing diameter and secondly, the anchoring of a particle is dependent on its size and shape. Consequently, the question arises in what way the particle size affects the durability of the catalyst as well as the degradation mechanism.

To investigate this question, two electrocatalysts *Pt5nm* and *Pt3nm* (see table 5.1) were compared regarding their degradation behavior upon potential cycling. The catalysts exhibit an identical carbon support and a comparable platinum loading but different particle sizes with 4-5 nm and 2-3 nm, respectively. As mentioned before, the catalyst *Pt5nm* was synthesized from the catalyst *Pt3nm* by performing thermal annealing. Therefore, potential influences resulting from the heat treatment cannot be neglected. As discussed before, the degradation behavior with time (shown in figure 5.3) shows different trends for these two catalysts, indicating different degradation mechanisms.

The degradation behavior of *Pt5nm* upon fast potential cycling (see IL-TEM in figure 5.8) had already been verified [46]. The degradation proceeds via a single degradation mechanism: particle detachment. This behavior is demonstrated in detail in figure 5.9, where the identical region of the catalyst is shown before and after the electrochemical treatment. Several particles are highlighted with circles and the carbon support is enframed with lines. In figure 5.9e, the selected particles and the borders of the carbon support are superimposed. Apparently, the shape of the carbon support does not change significantly upon the treatment and all particles highlighted with green circles stay approximately at the identical position and keep their size. The particles highlighted by red circles vanish. The latter observation can be related to the detachment of these particles. Since the size of the particles does not change and the vanishing particles exhibit random particle sizes, dissolution of platinum and Ostwald ripening can be neglected. Additionally, the occurrence of particle migration, which is involved in the coalescence mechanism, is negligible because the particles remain at their position and no particle growth is

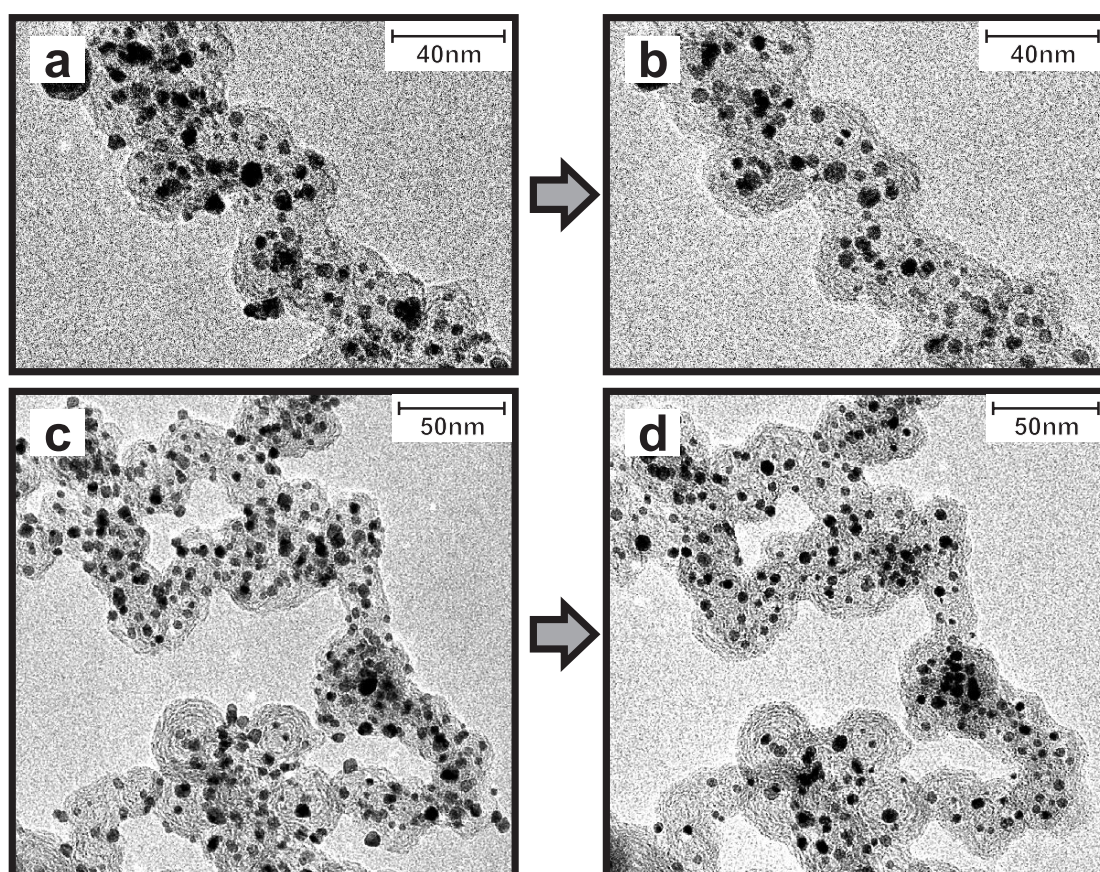


Figure 5.8: IL-TEM images (magnification 100k) of the catalyst *Pt5nm* before (a,c) and after (b,d) the potential cycling treatment (2h, 0.4-1.4 V_{RHE}, 1 Vs⁻¹, 0.1 M HClO₄). The number of nanoparticles decreases while no change in particle size or in the support is observed.

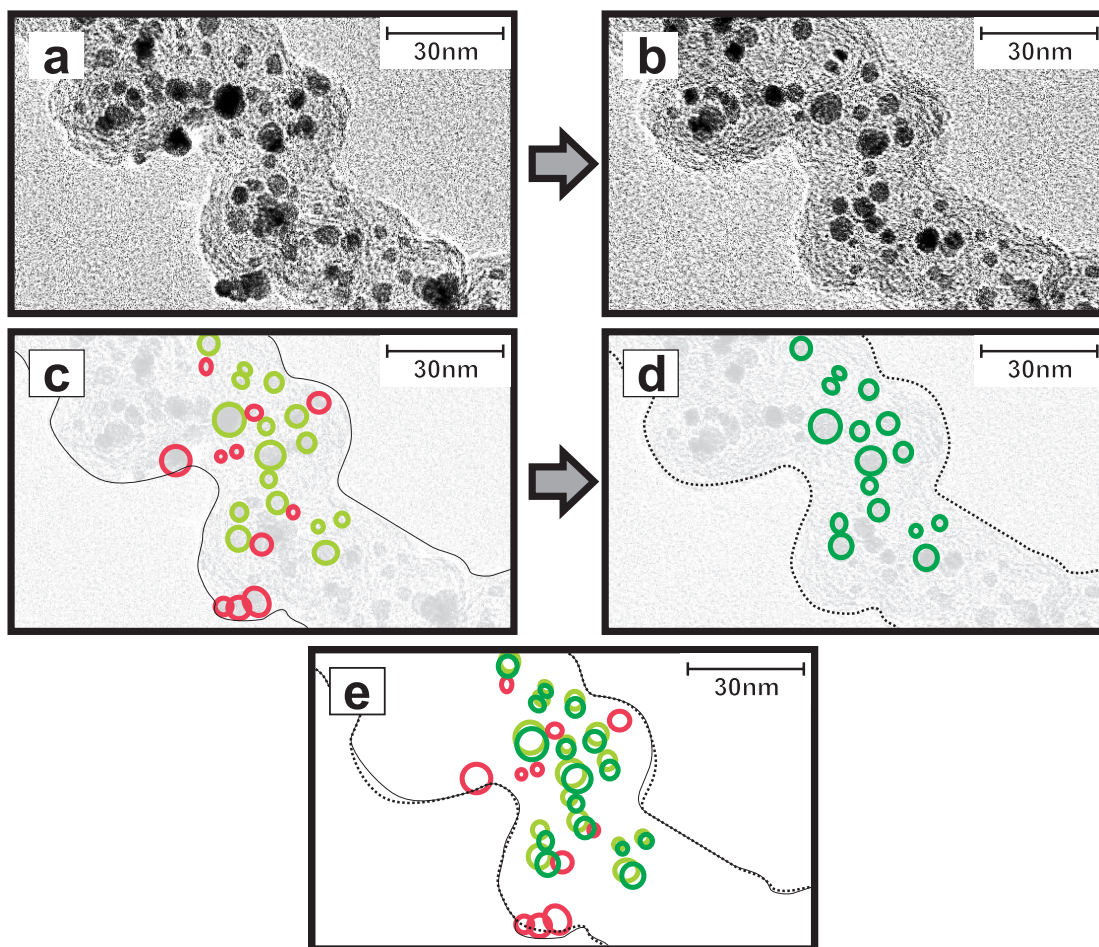


Figure 5.9: Analysis of IL-TEM images of the catalyst *Pt5nm* (before (a) and after (b) the treatment) considering one exemplary region of figure 5.8. Figures (c) and (d) show the enframed support and several particles from the images (a) and (b) highlighted with circles. Part (e) shows the overlay of (c) and (d). Particles with green labels stay unaltered in position and size whereas red labeled particles disappear.

detected. Consequently, for *Pt5nm* only particle detachment is observed while for *Pt3nm* coalescence is dominating the degradation process.

Considering the preparation procedure of the two catalysts, i.e. the fact that *Pt5nm* was synthesized by thermal annealing of *Pt3nm*, some further assumptions can be made about the processes: the heat treatment of the catalyst *Pt3nm* apparently leads to the migration and concomitant coalescence of the particles resulting in an increased particle size. The latter mechanism is similar to the degradation mechanism induced by the electrochemical treatment for this catalyst. So it can be assumed that *Pt5nm* does not undergo particle coalescence because this process was induced beforehand during the heat treatment leading to stabilized particles. Thus, for *Pt5nm* coalescence is completed after its synthesis and only particle detachment takes place during the stress test leading to an approximately linear decrease in active surface area. For *Pt3nm*, both mechanisms occur simultaneously resulting in an increased initial loss due to coalescence with a superimposed linear loss of ECA caused by particle detachment.

Thermal annealing of a carbon supported electrocatalyst not only leads to particle growth, but can also influence the carbon support. Apparently, total oxidation of the carbon occurred to a small extent during the heat treatment as can be seen in the slight increase of Pt loading from 46% to 50.6%. Further modifications of the carbon support cannot be excluded. The total oxidation of the carbon support during the electrochemical treatment was investigated by DEMS measurements.

In order to obtain an adequate current signal for the detection of CO₂ by the mass spectrometer and making the H_{upd}-region available for ECA measurements, the potential range of treatment was expanded to 0.05 - 1.7 V_{RHE}. Figure 5.10 shows the comparison of the amount of CO₂ produced by total oxidation of carbon between the two catalysts during identical potential scans.

Although the signal is quite noisy, a clear trend can be observed. The CO₂ production with time is comparable for *Pt5nm* and *Pt3nm*. In both cases the amount of produced CO₂ decreases with time. Apparently, the heat treatment did not considerably stabilize the carbon support against total oxidation. In order to characterize the different behavior of the two catalysts in more detail, the relation between the loss in ECA and the loss of carbon due to CO₂ production is shown in figure 5.11.

It can clearly be seen that in both cases the relationship between the decrease of ECA and loss of carbon is approximately linear. The ECA loss per produced CO₂ is higher for *Pt3nm* compared to *Pt5nm*. The larger particles from catalyst *Pt5nm* are thus more stable in comparison with their underlying support than it is the case for *Pt3nm*. This behavior is consistent with the observation that for *Pt3nm*, coalescence occurs in addition to particle detachment.

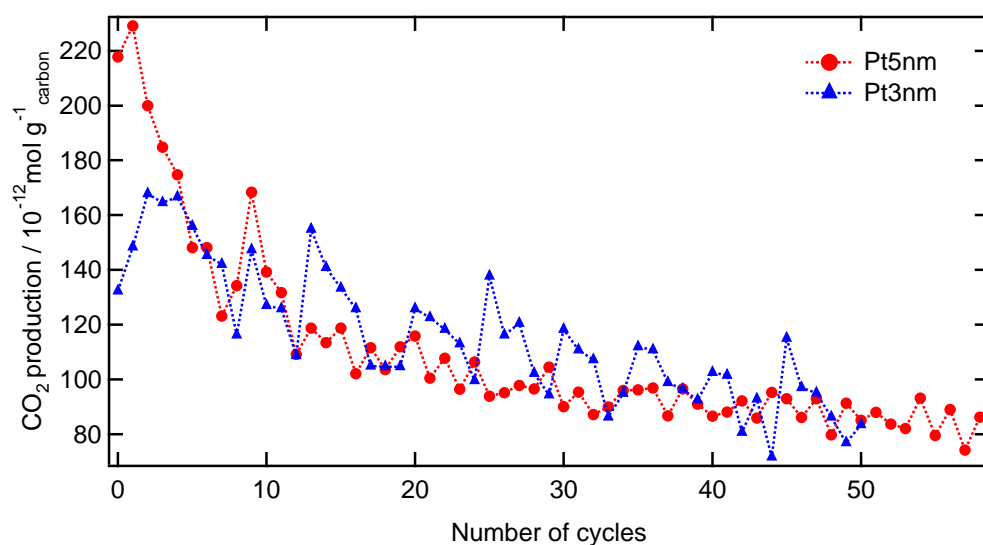


Figure 5.10: DEMS investigation: amount of produced CO₂ of *Pt5nm* and *Pt3nm* during potential cycling from 0.05 to 1.7 V_{RHE} (50 mVs⁻¹, 0.5 M H₂SO₄) per initially applied carbon mass measured by DEMS.

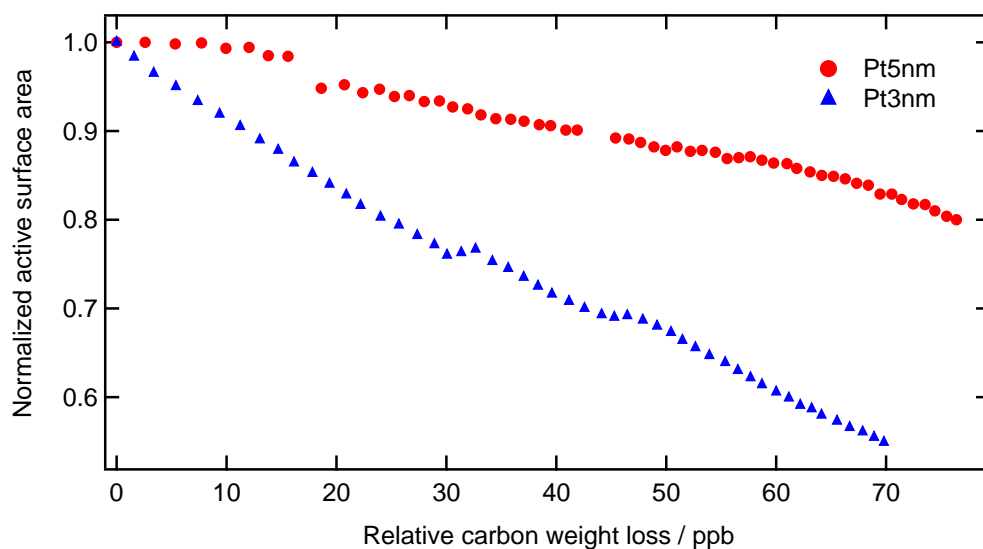


Figure 5.11: ECA determined by H_{upd} against the corresponding carbon loss measured by DEMS (calculated from the produced CO₂) during potential cycling from 0.05 to 1.7 V_{RHE} (50 mVs⁻¹, 0.5 M H₂SO₄).

From this graph, it can be concluded that total oxidation cannot be the only cause for the observed loss in active surface area. In the literature, particle detachment and in some cases also coalescence of particles are described to be caused by corrosion of the underlying carbon [11, 48]. If this assumption was true then the curves of the two catalysts in the graph would be on top of each other. Since this is not the case, it can be assumed that total oxidation of the carbon support is not the only reason for the degradation of these two catalysts. However, total oxidation of carbon could still be crucial for one of the two occurring processes, i.e. coalescence or particle detachment. In order to answer this question, further DEMS measurements in combination with IL-TEM are necessary.

Consequently, a possible explanation for the modified behavior of the two similar catalysts during degradation is the anticipation of particle growth induced by coalescence for the catalyst *Pt5nm* upon the heat treatment procedure during its fabrication.

5.2.4 Effect of Alloying Platinum with Cobalt

It is known that alloying platinum with other transition metals has a beneficial effect on its catalytic activity for the oxygen reduction reaction [6, 7, 8, 9]. However, it is not clear, how the durability of the catalyst is affected by alloying [11]. There are reports about problems with leaching of cobalt from the particles into the membrane [4] as well as reports about the stability of bimetallic nanoparticles being superior to the one of plain platinum nanoparticles [52].

As shown above, the stability of the applied bimetallic catalyst *Pt₃Co* is lower than the Pt catalyst with the comparable particle size, *Pt5nm*. However, the time-dependent ECA loss of *Pt₃Co* exhibits a trend similar to *Pt5nm*, i.e. an almost linear decay, whereas all other catalysts show a more pronounced curvature. This similar trend indicates an analogical degradation mechanism. The corresponding TEM images before and after the accelerated stress test are shown in figures 5.8 and 5.12.

Again, no change in the carbon support upon the stress test is observable. The amount of metal particles decreases whereby especially larger particles disappear. In order to further analyze this phenomenon, the images (a) and (b) from figure 5.12 are reproduced in figure 5.13. The red arrows highlight several positions where upon cycling larger particles disappear from the support. The green arrow indicates a particle which has not been there before the treatment which is a sign for the particle detachment mechanism. Furthermore, the images (c) and (d) (see figure 5.12) show one magnified part of the images 5.12 (c,d). There, a decrease in particle size unambiguously takes place. This phenomenon might be related with dissolution although this process would typically lead to a preferred dissolution of smaller

particles. A possible explanation is that the larger particles exhibit a higher amount of cobalt which is leached out during the electrochemical treatment. This process causes a collapse of the particle itself or a destabilization leading to a complete disappearance. From these images, coalescence and Ostwald ripening can be excluded due to the absence of particle growth while two degradation mechanisms seem to be predominant: cobalt leaching and particle detachment.

Consequently, the durability of the applied $\text{Pt}_3\text{Co}/\text{C}$ electrocatalyst is inferior to plain platinum in the same particle size range. The degradation mechanism has an additional contribution due to leaching of cobalt from the particles besides particle detachment. No other degradation process could be detected.

5.2.5 Summary

In summary, the degradation of standard carbon supported Pt-based electrocatalysts is a complex process which is considerably influenced by parameters like support properties, alloying and particle size or heat treatment of the catalyst, respectively. For larger particles like in *Pt5nm* and *Pt₃Co*, no coalescence was observed in contrast to all other catalysts which exhibit smaller particle sizes. This finding can originate from a stabilization effect due to the preceding temperature-induced coalescence during the preparation procedure. The bimetallic catalyst exhibits an additional degradation mechanism: the leaching of the non-noble transition metal from the particles. In order to decrease the amount of detached particles the anchoring of the particles can be improved by using a graphitized carbon support. The loading does not have a significant effect in the range between 20% and 50%. Although the degradation mechanisms are mainly a superposition of different kinds of processes, one mechanism can often be distinguished as being predominant. An overview of the verified degradation mechanisms for the five applied electrocatalysts upon the potential cycling treatment is given in table 5.3.

Table 5.3: Attribution of the degradation mechanisms verified in the conducted investigation to the electrocatalysts. The processes are classified from being dominant (+++) to occurring to a small extent (+). Some processes could not be verified and are therefore not relevant for the degradation mechanism (-). * The dissolution process is in this case related to leaching of the alloy particles.

Notation	Particle Detachment	Coalescence	Dissolution
Pt5nm	+++	-	-
Pt3nm	++	+++	-
Pt20%	++	+++	-
Ptgraph	+	+++	-
Pt-Co	+++	-	++*

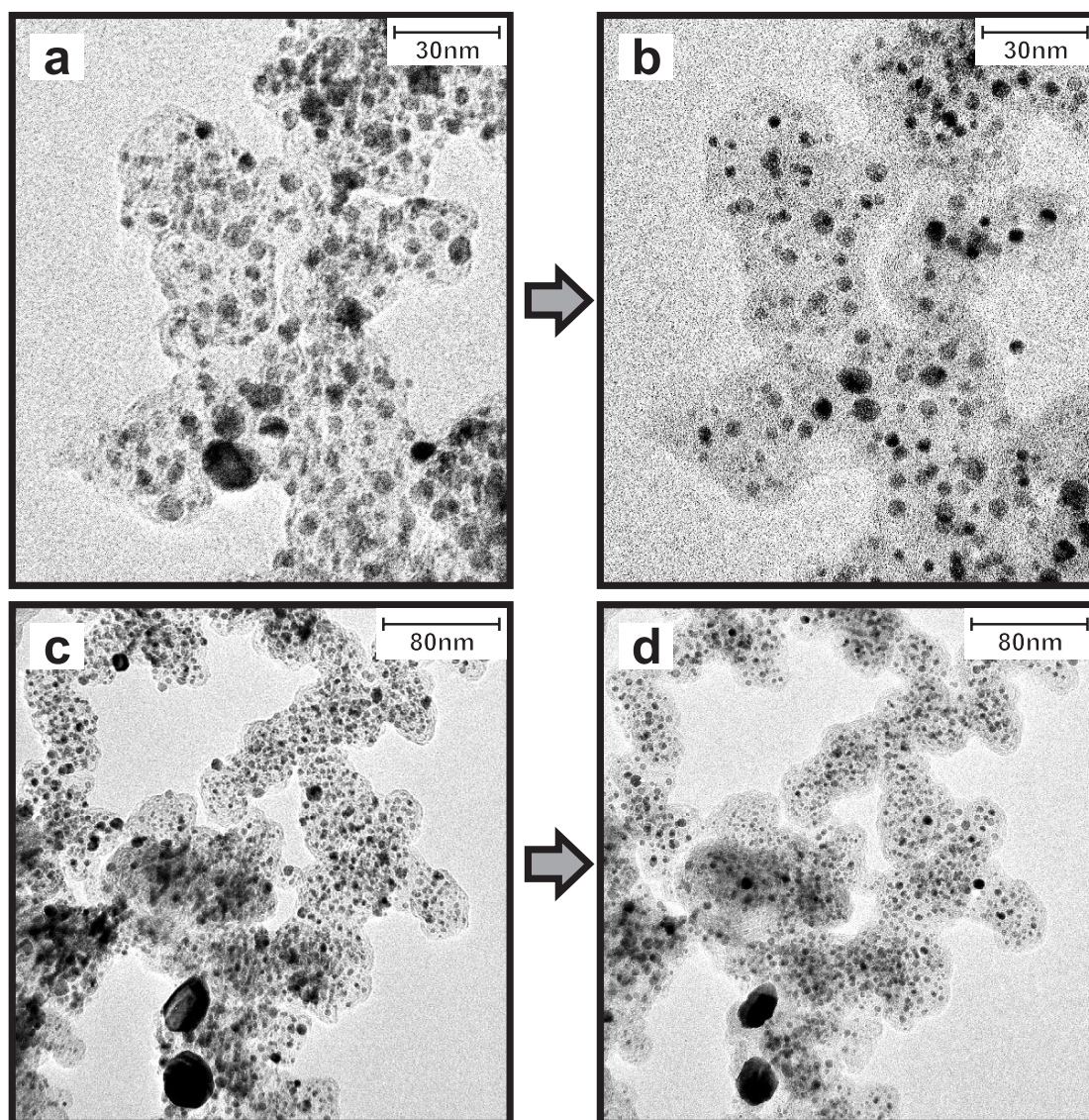


Figure 5.12: IL-TEM images (magnification 100k) of the catalyst Pt_3Co before (a,c) and after (b,d) the potential cycling treatment (2h, 0.4-1.4 V_{RHE}, 1 Vs⁻¹, 0.1 M HClO₄). While no change is observable for the carbon support, the particle density decreases.

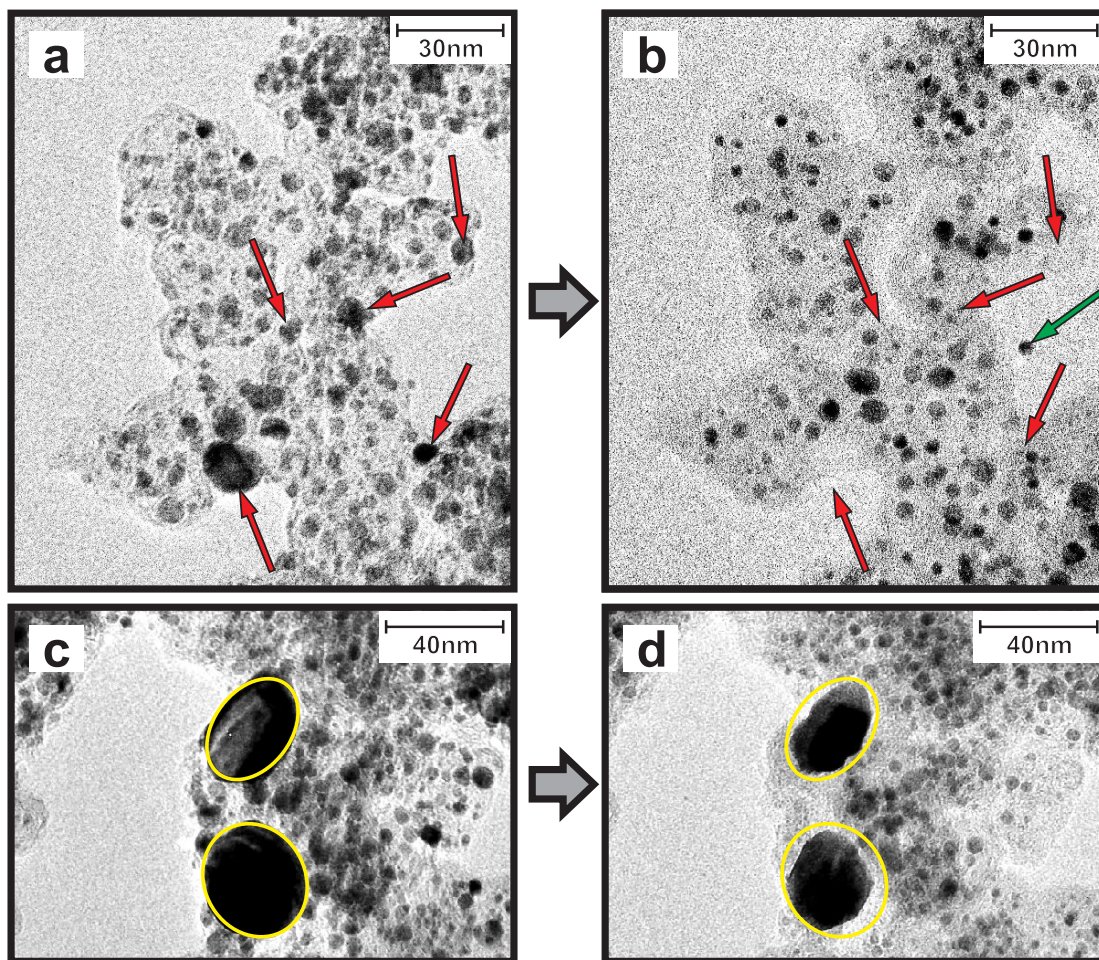


Figure 5.13: Analysis of IL-TEM of the catalyst Pt_3Co considering two parts of the images shown in 5.12. The red arrows in parts (a) and (b) indicate the loss of larger particles while the green arrow highlights a redeposited particle. In part (c) and (d), the yellow circles demonstrate the shrinking process of large particles.

5.3 Degradation Behavior at elevated Temperatures

So far, the powerful approach of IL-TEM in conjunction with RDE measurements was predominantly utilized for degradation studies of HSA catalysts at room temperature for cycling to high potentials. Upon these treatments, no visible change in the carbon support of the catalyst was observed. In the following, investigations are presented, where IL-TEM was extended to elevated electrolyte temperatures, i.e. close to operating temperatures of PEMFCs [53]. At elevated temperatures, corrosion of the carbon support has shown to occur for Pt/C electrocatalysts [54]. This process was suggested to lead to a collapse of the macroscopic catalyst layer in the MEA and thus plays an important role for the life time of PEMFCs [55, 51]. The catalyst chosen for this investigation was *Pt5nm* which has been most extensively studied in our group. Instead of potential cycling a constant electrode potential between 1.0 and 1.4 V_{RHE} was applied for 16 hours. It is noteworthy, that at room temperature no loss of ECA is observed for this Pt/C electrocatalyst under these conditions.

In a first step the catalyst stability was evaluated on the basis of the ECA loss as a function of potential under potentiostatic conditions. The electrolyte was thermostated at two different temperatures, 333 and 348K, respectively, and the ECA was determined in CO stripping experiments before and after potential holds for 16h. In figure 5.14 representative CO stripping curves are shown together with the subsequent cyclovoltammograms of the uncovered catalyst surface. Comparing the CO stripping curves before and after the degradation treatment, it is apparent that the degradation treatment not only leads to a decrease in surface area, but also to a profound change in the features of the CO stripping peak. Oxidation of the CO monolayer adsorbed on the degraded catalyst starts at lower potentials than on the pristine sample. Furthermore the stripping peak broadens and splits into two main maxima. Such peak splitting for CO monolayer oxidation on Pt HSA catalysts has been reported previously and was related to a bimodal particle size distribution caused by coalescence [56]. It should be noted, however, that a similar behavior can be observed on polycrystalline platinum as well. In figure 5.15, three different shapes of the CO stripping features are shown for the initial smooth surface and for roughened surfaces due to oxidative treatments. Especially after oxidizing the polycrystalline platinum, the shape resembles a bimodal structure and can thus also be related to structural changes on the Pt surface. Consequently, the appearance of a broader bimodal shape does not unambiguously identify particle coalescence.

A further consequence of the degradation treatment is seen in the cyclovoltammogram of the uncovered catalyst surface. Due to the degradation treatment, an additional redox-couple appears between 0.4 and 0.7 V_{RHE} , which can be assigned to a quinone/hydroquinone peak of oxidized carbon [11]. As expected, this characteristic

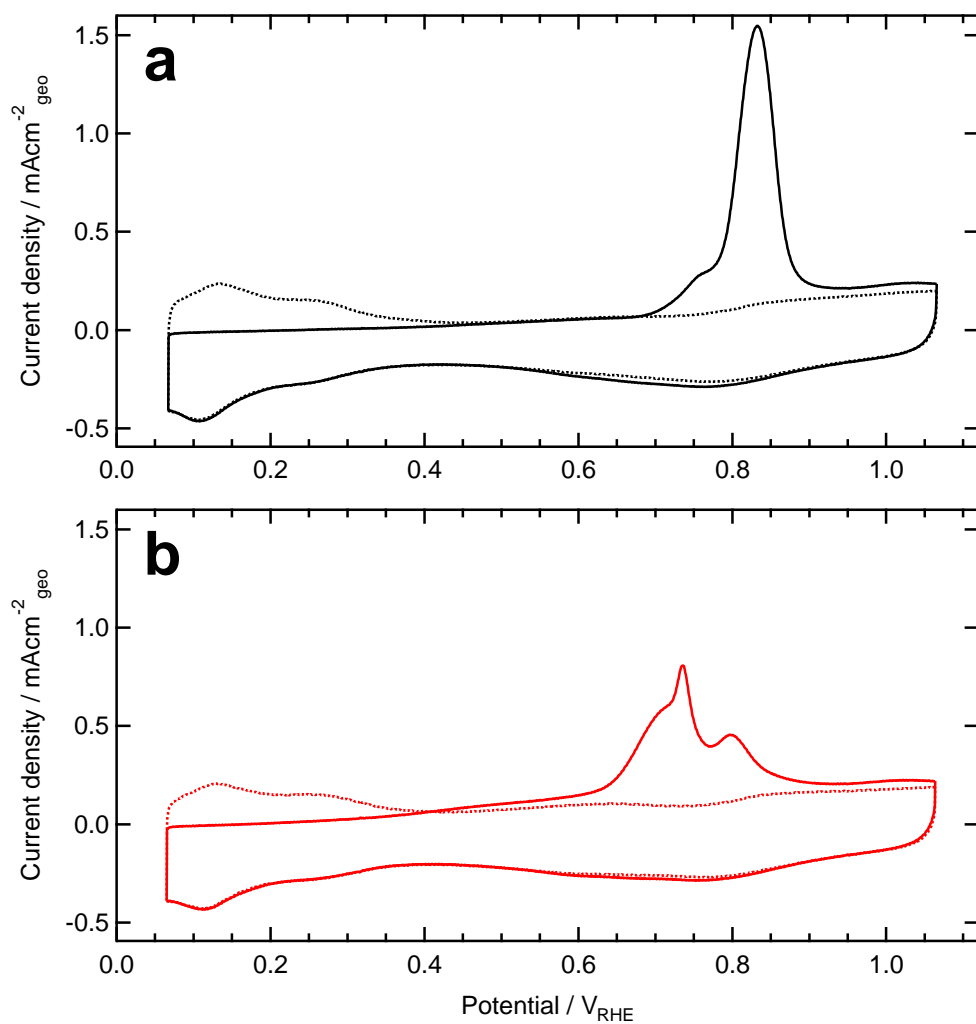


Figure 5.14: CO stripping curves and subsequent cyclic voltammograms (dotted lines) of *Pt5nm* recorded at room temperature in 0.1 M HClO₄ before (a) and after (b) a potentiostatic treatment at 1.2 V_{RHE} and 333K for 16h. The scan rate was 50 mVs⁻¹.

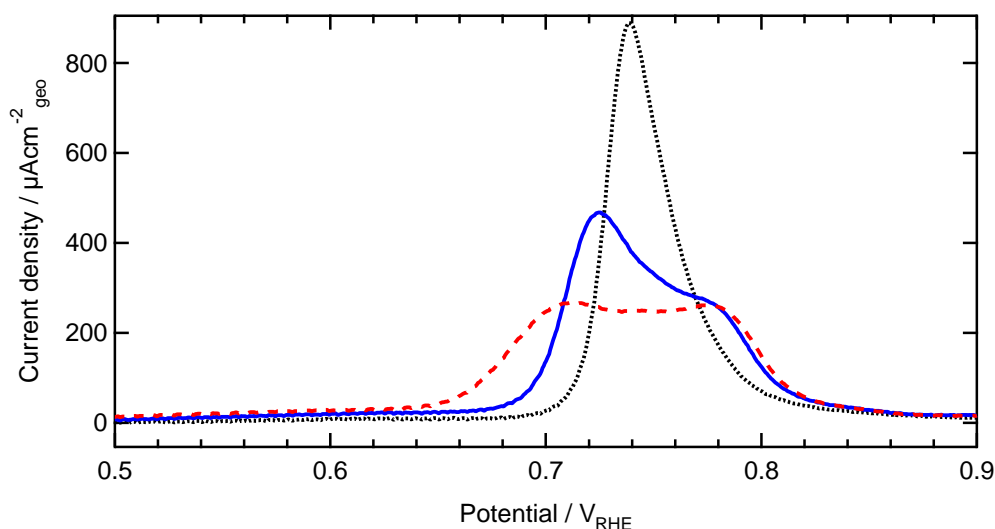


Figure 5.15: CO stripping curves of polycrystalline Pt at a scan rate of 50 mVs^{-1} in 0.1 M HClO_4 . Depending on the preceding treatment the features change dramatically: the initial curve shows a distinctive single maximum (black dotted line) whereas after an oxidative potential cycling ($0.4\text{-}1.4 \text{ V}_{\text{RHE}}$ with 1 Vs^{-1} for 5 min for the red dashed line and $0.4\text{-}1.4 \text{ V}_{\text{RHE}}$ with 1 Vs^{-1} for 60 min for the blue line) the peak broadens and splits up.

oxidation feature got more and more pronounced with increasing applied potentials during the degradation treatment. It is noteworthy, however, that the redox-couple cannot exclusively be assigned to the oxidation of the HSA carbon support, but is also correlated to the oxidation of the carbon electrode the catalyst was attached to. Indeed, the massive oxidation of the carbon electrode faces one with experimental difficulties, such as increased double layer capacitance and leaking of the Teflon sealing of the RDE tips which lead to a diminished reproducibility of the absolute ECA loss. Nevertheless, some qualitative trends can be derived from these measurements which are summarized in figure 5.16.

Under the applied degradation treatment, ECA loss starts for both temperatures, i.e. 333K and 348K, at a potential of about $1.0 \text{ V}_{\text{RHE}}$ and increases steadily with increasing the applied potential. Furthermore, as a tendency, ECA loss at 348K is higher than at 333K. This behavior was expected, since at room temperature, under none of these treatments any ECA loss was observed.

As discussed above, this standard degradation study was followed by IL-TEM in order to get a better insight into the degradation mechanisms occurring during the electrochemical treatments. Based on the data summarized in figure 5.16, several different treatment conditions (potential and temperature) for IL-TEM investigations were chosen. Studies at $1.2 \text{ V}_{\text{RHE}}$ and 333K, $1.3 \text{ V}_{\text{RHE}}$ and 348K, and $1.4 \text{ V}_{\text{RHE}}$ and 333K were conducted for each 16 hours, like in the ECA loss measurements. For the treatment at $1.2 \text{ V}_{\text{RHE}}$ and 333K no significant changes neither in the carbon support nor regarding the Pt particles could be determined in IL-TEM (see figure

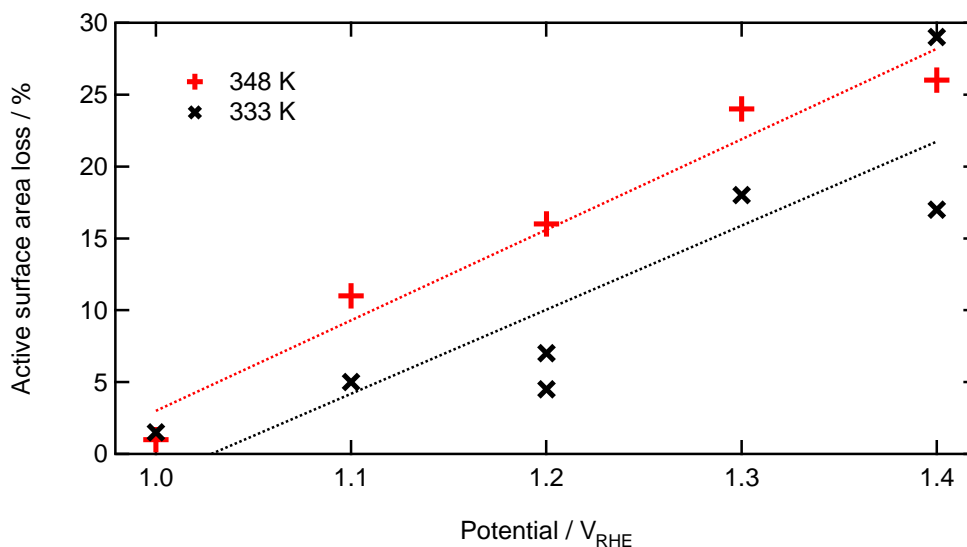


Figure 5.16: ECA loss as function of the applied potential for two different temperatures, 333K and 348K, respectively. Measurements were performed in 0.1M $HClO_4$ for 16 hours using the catalyst *Pt5nm*. The lines serve as a guide to the eye to display the trend.

5.17).

However, at increased degradation (1.3 V_{RHE} and 348K) profound changes in the HSA catalyst could be identified (see figure 5.18). In contrast to previous studies, it is observed that the increased temperature leads to severe changes in structure and shape of the HSA carbon support besides modifications of the particles as well. The amount of particles decreased and the carbon support considerably contracted. In part (c) and (d) in this figure, the shrinking of the carbon leads to agglomeration of the particles facilitating coalescence. Some parts of the catalyst layer are even missing completely after degradation, although it cannot be distinguished if in course of oxidation the carbon particles detached from the TEM grid or were completely oxidized to carbon dioxide. However, an analysis of the Pt surface area based on the parts of the catalyst layer which were present in the TEM micrographs before and after degradation leads to a value of 16% in ECA loss. This is less than the value determined in the CO stripping (24%) investigation and thus it can be speculated that some carbon particles indeed got completely oxidized and the Pt particles washed into the electrolyte solution. In figure 5.19 further examples of this IL-TEM analysis are shown and specific changes are highlighted. The green arrow in part (b) of the figure shows a redeposited particle. This incident together with the fact that there is no preferred vanishing of small particles indicates that the observed ECA loss can in part be related to a particle detachment process, which was identified as the main degradation mechanism for the same catalyst under the potential cycling treatment at room temperature (see section 5.2).

However, in contrast to these previous studies, it is further seen that the increased

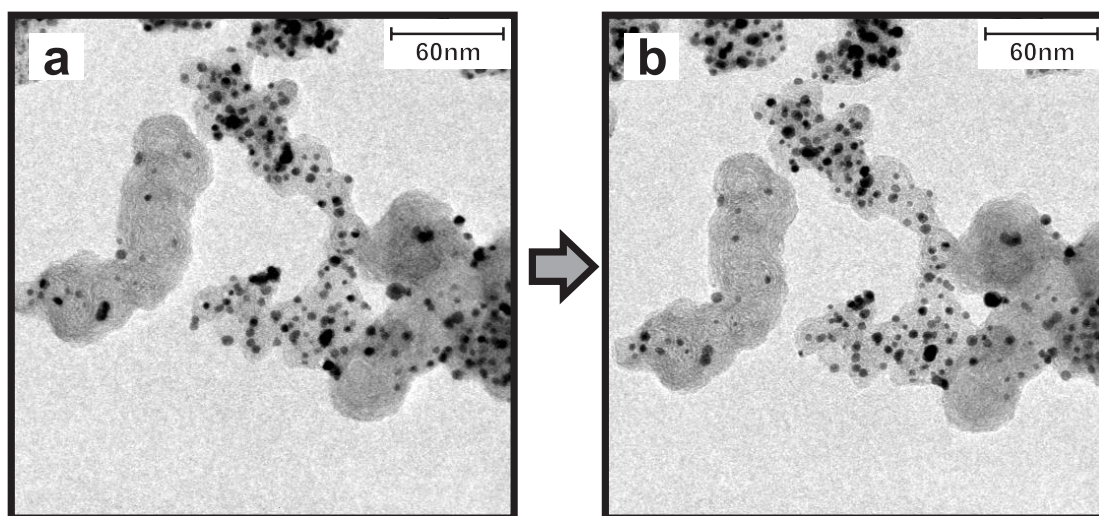


Figure 5.17: IL-TEM images (magnification 100k) of the catalyst *Pt5nm* before (a) and after (b) a potentiostatic treatment at 1.2 V_{RHE} and 333K (0.1 M HClO₄) for 16 hours. No significant change is observed.

temperature leads to severe changes in structure and shape of the HSA carbon support as well. Especially in figure 5.19a and b, it is observed that after degradation some carbon particles exhibit circular shapes with more graphitized borders and very thin centers (some of such graphitic planes are highlighted with orange arrows). This observation is in accordance with the "Cutaway" model which predicts that the corrosion of carbon particles starts in its cores and proceeds to the outer sides due to the higher density of graphitic layers in the shell region of carbon black particles [35, 57]. Hence, the corrosion of carbon leads to a hollow graphitic structure of the carbon primary particles [58].

Increasing the applied potential to 1.4 V_{RHE} (333K), IL-TEM faces clear limitations. In figure 5.20, it is shown that the applied electrochemical treatment leads to dissolution of the Au finder TEM grid itself and subsequent electrochemical deposition of large Au particles where previously less noble Pt particles were attached to the HSA carbon support. This finding was confirmed by EDX measurements where almost no platinum was observed besides a large amount of gold. Nevertheless, also in these measurements a severe oxidation of the HSA carbon support is observed.

Summary

It is demonstrated that under potentiostatic conditions at elevated temperatures Pt nanoparticle agglomeration is induced by the oxidative shrinking of the HSA carbon support. In a MEA, this process would lead to a collapse of the catalyst layer. Furthermore, indications for the oxidation of carbon particles from the centre to its borders in accordance with the "Cutaway" model are found. The severe carbon

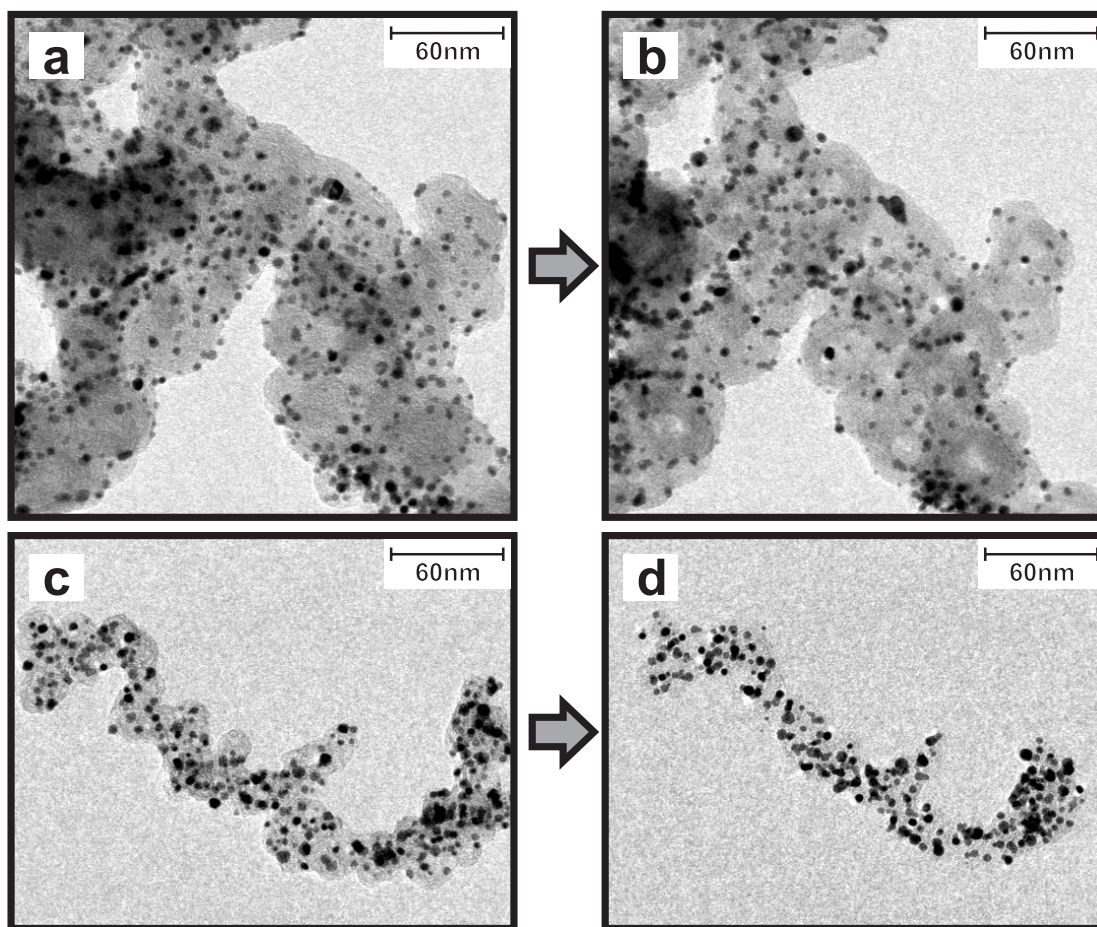


Figure 5.18: IL-TEM images (magnification 100k) of the catalyst *Pt5nm* before (a,c) and after (b,d) a potentiostatic treatment at $1.3 V_{\text{RHE}}$ and 348K (0.1 M HClO_4) for 16 hours. The carbon support changes significantly.

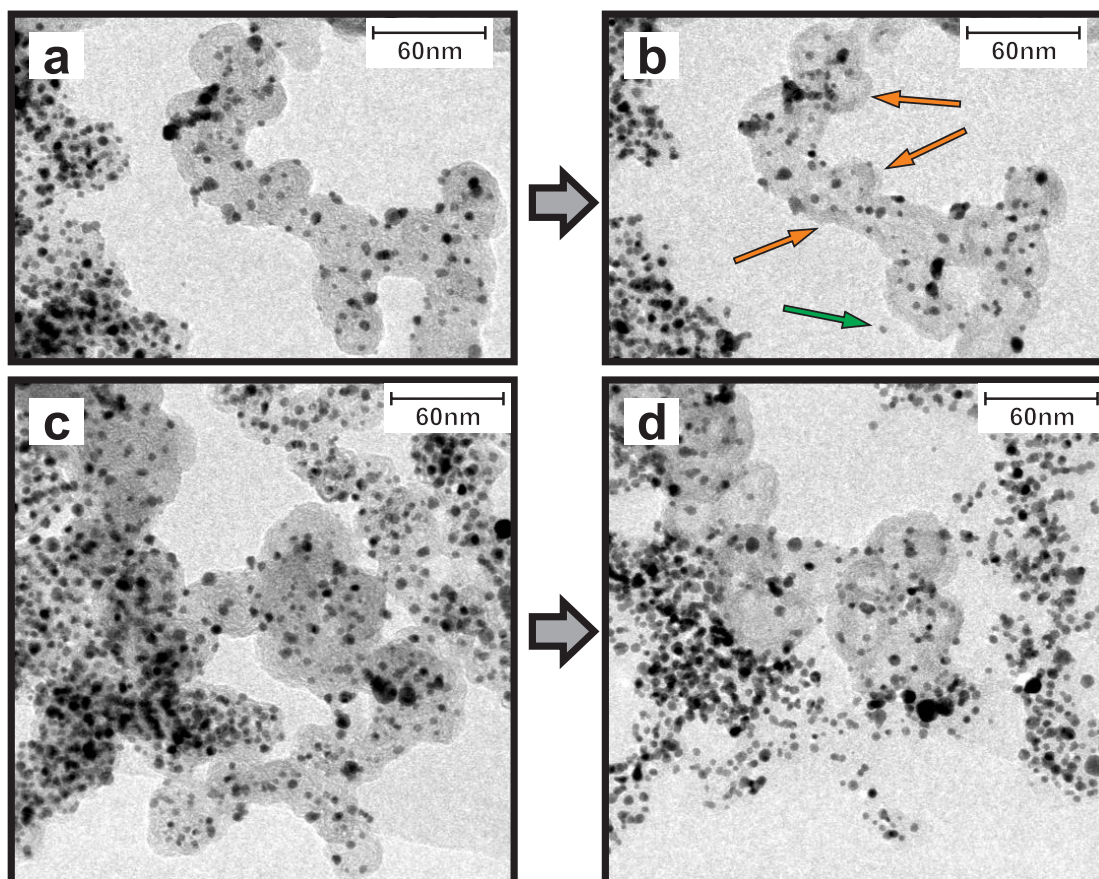


Figure 5.19: Further IL-TEM images (magnification 100k) of the catalyst *Pt5nm* before (a,c) and after (b,d) a potentiostatic treatment at 1.3 V_{RHE} and 348K (0.1 M HClO₄) for 16 hours. A thinning of the carbon support is observed leading to hollow graphitic structures (some graphitic planes are indicated by the orange arrows). Additionally, the green arrow highlights a single detached particle.

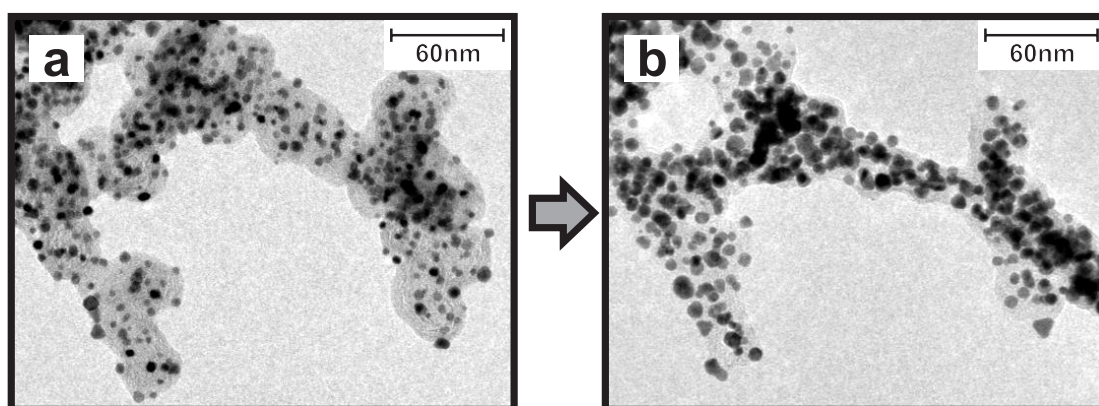


Figure 5.20: IL-TEM images (magnification 100k) of the catalyst *Pt5nm* before (a,c) and after (b,d) a potentiostatic treatment at 1.4 V_{RHE} and 348K (0.1 M HClO₄) for 16 hours. The platinum particles get replaced by gold particles due to dissolved gold from the grid.

support oxidation at rather positive potentials is a direct result of elevated temperatures. At the same time the Pt nanoparticles are affected relatively weakly and no evidence for an Ostwald ripening process, i.e. the preferential dissolution of small Pt particles and concomitant growth of larger ones, can be found. It rather seems that the impact of increased temperatures is small for the Pt nanoparticles whereas it is severe for the HSA carbon support.

5.4 Conclusion

In this chapter, the degradation behavior of standard electrocatalysts was scrutinized and related to specific properties as well as to different treatment conditions.

The investigation of the electrocatalysts on a microscopic scale using IL-TEM is an ideal method for identifying the dominating degradation mechanisms. However, by means of commercial electrocatalysts only trends concerning influencing factors can be established. For a more detailed correlation of degradation mechanisms to specific factors based on the synthesis procedure the latter has to be known and controlled in detail. As a starting point, investigations with model electrocatalysts with well-known properties were generated and investigated. First results are given in chapter 6.

Additionally, the feasibility of IL-TEM at temperatures close to PEMFC operation has been demonstrated. In this way, even more realistic fuel cell conditions can be investigated using this powerful method. Processes like the collapse of the catalyst layer due to carbon corrosion can be studied using IL-TEM.

Consequently, a new technique has been found which facilitates a reliable ex-situ characterization of the durability of fuel cell catalysts. IL-TEM in combination with ECA measurements is suitable to predict the life-time of an electrocatalyst under operation and facilitates the elucidation of degradation mechanisms representing a starting point to develop highly durable catalysts.

Chapter 6

Different Concepts towards High-Performance Catalysts

The main challenge in the development of proton exchange membrane fuel cells is the design of cheap and stable electrocatalysts for the oxygen reduction reaction [59]. In order to meet the requirements for large-scale applications, the catalytic activity per mass of platinum has to be increased by a factor of >4 [4]. In this respect, the amount of expensive platinum has to be reduced by either going to smaller particle sizes or by using bimetallic particles, for example. Alloys of platinum with non-noble transition metals like cobalt, nickel or copper additionally increase the specific activity towards the oxygen reduction reaction [6, 7, 8, 9].

In addition to its activity, the long term stability is crucial for the applicability of an electrocatalyst in a fuel cell [10, 11]. In this regard, the metal particles as well as the support have to be optimized.

In this chapter, some promising approaches for the improvement of the performance and durability of oxygen reduction catalysts are presented and explained in more detail using published papers concerning the particular concept. First, well-defined electrocatalysts consisting of small platinum clusters on a carbon substrate are discussed regarding their production and characterization including activity and stability aspects. Their applicability as model catalysts for the investigation of particle size effects, reaction mechanisms, and especially of degradation mechanisms is demonstrated. Afterwards, the possibility of modifying the catalyst support using transition metals in order to enhance its durability is analyzed on a microscopic scale. Finally, the concept of using bimetallic nanoparticles is demonstrated by means of a Au-Pt core-shell catalyst and a Pt-Co alloy catalyst, respectively.

6.1 Supported Platinum Clusters as Model Electrocatalyst

Optimizing the usage of precious materials is of great importance for many catalytic processes. For that purpose, the active surface area exposed to the reactants can be maximized by reducing the particle size of the noble metal. Indeed, in this way, the amount of precious metal and thus the costs for the catalyst are minimized, but by entering the nanoscale, additional effects have to be considered. It is well-known that the properties of nanoparticles and clusters differ from the ones of the bulk material. For the size range above approximately 1 nm these properties can often be explained theoretically by including additional boundary conditions into the equations available for the bulk material (from solid state physics). A vivid example for this change of properties is the fact that gold particles in the nanometer scale exhibit a shiny red color (instead of the characteristic golden appearance), which was used to color glasses in former times. The absorption behavior can thereby be explained by the Mie theory [60, 61]. Of course, the change of the electronic and geometric properties also have a great influence on the catalytic activity due to changed adsorption sites, modified heats of adsorption etc. [62]. For example, gold clusters with small particle sizes lose their inert character known from the bulk and catalyze the oxidation of carbon monoxide [63, 64]. Consequently, the catalytic activity can be modified by adjusting the particle size of the active material.

However, for standard platinum oxygen reduction catalysts, an unfavorable particle size effect is described leading to a decrease in specific activity with smaller diameters. The corresponding mass activity is reported to show a maximum at around 3.5 nm [4]. This effect is typically ascribed to the inhibitive specific adsorption of electrolyte anions on different crystal facets, the fraction of which changes with particle size [65]. For non-adsorbing electrolytes like perchloric acid, a similar behavior is suggested and attributed to the change in potentials for the adsorption of oxygen-containing species [4, 66].

In order to study the influence of the particle size on the catalyst performance and durability, a preparation procedure for suitable model electrocatalysts was developed. In the following, two papers are presented describing the preparation procedure together with first characterizations and stability investigations in different electrochemical environments.

6.1.1 Size-selected clusters as heterogeneous model catalysts under applied reaction conditions

The main motivation for the generation of size-selected supported platinum clusters is the creation of a powerful model system facilitating diverse fundamental studies. Until now, model electrocatalysts were mainly represented by single crystals or

polycrystalline materials which differ a lot from supported particles. The developed system resembles the commercially applied catalysts, but it is less complex and exhibits a defined nature. That is, the particle size, the particle density and the kind of substrate can be adjusted. By this means, the controversial particle size effect, the impact of the distances between single particles and the influence of different supports can be studied in detail. Furthermore, information about reaction and especially about degradation mechanisms can be obtained.

The following paper presents a detailed description of the preparation of the model catalyst and a first electrochemical characterization. The clusters were generated in a laser ablation source equipped with guiding ion optics and a mass spectrometer and subsequently landed onto the support, in this case either a carbon coated TEM grid or a glassy carbon electrode. By means of a transfer chamber, the sample was transferred from ultra high vacuum to ambient conditions, where the transfer to the TEM and electrochemical measurements were conducted. The TEM images demonstrate that no agglomeration due to surface mobility of the particles occurs. From a statistical analysis, the particle diameter of the clusters was determined and the effect of deposition time on the density was visualized. For the electrochemical investigation, cyclic voltammetry as well as the CO stripping behavior showed to be characteristic for platinum and the obtained active surface area could be directly related to the corresponding deposition current. This finding validates the possibility of the method to adjust the density of particles on the support and correctly determine its surface area by CO stripping. The relevance of this model system for catalysis is shown by the measurement of the electrocatalytic activity towards the oxygen reduction reaction indicating a particle size effect. Further studies using model electrocatalysts with several different particle sizes and narrower particle size distributions are in preparation.

Size-selected clusters as heterogeneous model catalysts under applied reaction conditions

S. Kunz, K. Hartl, M. Nesselberger, F.F. Schweinberger, G. Kwon, M. Hanzlik,
K.J.J. Mayrhofer, U. Heiz and M. Arenz

Physical Chemistry Chemical Physics, 2010, Volume 12, Issue 35, Pages
10288 - 10291

Permanent weblink:

<http://dx.doi.org/10.1039/C0CP00288G>

Reproduced by permission of the PCCP Owner Societies.

Size-selected clusters as heterogeneous model catalysts under applied reaction conditions

Sebastian Kunz,^a Katrin Hartl,^a Markus Nesselberger,^b Florian F. Schweinberger,^a GiHan Kwon,^a Marianne Hanzlik,^c Karl J. J. Mayrhofer,^d Ueli Heiz^a and Matthias Arenz^{*b}

Received 20th April 2010, Accepted 28th June 2010

DOI: 10.1039/c0cp00288g

First results of investigations are presented, where size-selected metal clusters generated in ultra high vacuum (UHV) are transferred to ambient conditions and tested for suitable electrochemical applications. As demonstrated, the transfer allows for the characterization of clusters by transmission electron microscopy (TEM) as well as catalytic measurements, which is exemplified by the application of electrochemical measurements. It is demonstrated that well known electrochemical processes on the carbon supported Pt clusters are detected, and thus Pt clusters can be characterized with respect to their accessible surface area, an essential requirement for the study of catalytic processes. Furthermore, as an example for an important electrocatalytic process, it is shown that the oxygen reduction reaction can be probed on the cluster samples featuring a detrimental particle size effect, previously reported for industrial catalysts as well.

Studies of noble metal model systems have a long history and play a decisive role in the understanding of heterogeneous catalysis. Over the last decades experimental investigations under ultra high vacuum (UHV) conditions as well as theoretical work have provided significant insight into the relationship between the electronic and geometric surface structure of bulk materials and their catalytic activity. A detailed understanding of the reaction mechanism of important processes has been established, and even improvements for applied catalysis have been deduced. In addition, various studies on metal nanoparticles have been performed, with the trend towards investigating the catalysts under more realistic reaction conditions. For an overview see ref. 1–3

Size-selected clusters have been successfully trapped and investigated in UHV demonstrating unique electronic and geometric properties depending on the exact number of atoms in the cluster. Furthermore, size-selected clusters deposited onto planar supports were utilized as heterogeneous catalysts under UHV conditions and in high pressure cells.^{4–6} Due to the independent control of cluster size, size distribution and coverage on the support, these systems are well-suited as model systems for experimental studies of catalytic reactions

and mesoscopic phenomena that influence reaction rates and mechanisms, such as spill-over and reverse spill-over effects. Most recent studies on the epoxidation and oxidative dehydrogenation of hydrocarbons already anticipate their outstanding potential for the research of industrial relevant catalytic reactions.⁷

In the present study, size-selected platinum clusters were prepared under UHV conditions using a laser ablation source.⁵ Focusing the second harmonic of a 100 Hz Nd:YAG laser along with a pulse of compressed He onto a rotating metal disc, neutral and charged metal clusters of various sizes are generated upon supersonic expansion through a nozzle into a differentially pumped vacuum system. The cluster beam is guided through the UHV apparatus by an octopole ion guide and electrostatic ion optics towards the bender, which consists of an electrostatic quadrupole that separates positively charged clusters from non-charged and negatively charged ones, respectively. In addition, the cluster beam is size-selected at the bender since only positively charged clusters with a certain mass-to-charge ratio can exit the bender on an appropriate trajectory through the exit hole into the following ion optics.⁷ The size-selected cluster beam is subsequently guided into a quadrupole mass-spectrometer (QMS), which can either be operated in an ion-guide or in a mass resolving mode. The latter mode provides a second highly accurate mass selection so that even clusters with an exact number of atoms can be selected. The maximum cluster mass of the current QMS setup is limited to 9000 amu. In the presented work the mass spectrometer was mainly operated in the ion-guide mode and size-selection was achieved by means of the bender system. This allowed the preparation of clusters that are large enough in size to enable the use of TEM as a characterization method.

After passing the mass spectrometer, the clusters are deposited onto different substrates that are mounted on a sample holder of a manipulator. In this initial study standard TEM grids covered with a thin amorphous carbon film and glassy carbon (GC) substrates were used as support materials. After cluster deposition the samples are transferred out of UHV *via* a vacuum load lock with an automatic pneumatic gate, without breaking the vacuum in the main chamber. By optimizing the setup, the duration and the complexity of the sample transfer procedure has been significantly reduced.

In Fig. 1 the control of the cluster size *via* the electrostatic bender is shown based on two examples. Relatively high cluster coverages, suitable to perform catalytic measurements, were applied. For the first sample (Fig. 1a and b) the average cluster size determined from several TEM micrographs is 1.34 nm with a standard deviation of about 12%. The predominant

^a Lehrstuhl Physikalische Chemie, Technische Universität München, Lichtenbergstr. 4, 85748 Garching, Germany

^b Department of Chemistry, University of Copenhagen, Universitetsparken 5, DK-2100 Copenhagen Ø, Denmark. E-mail: m.arenz@kemi.ku.dk

^c Institut für Elektronenmikroskopie, Technische Universität München, Lichtenbergstr. 4, 85748 Garching, Germany

^d Abt. Grenzflächenchemie und Oberflächentechnik, Max Planck Institut für Eisenforschung, Max-Planck-Str. 1, 40237 Düsseldorf, Germany

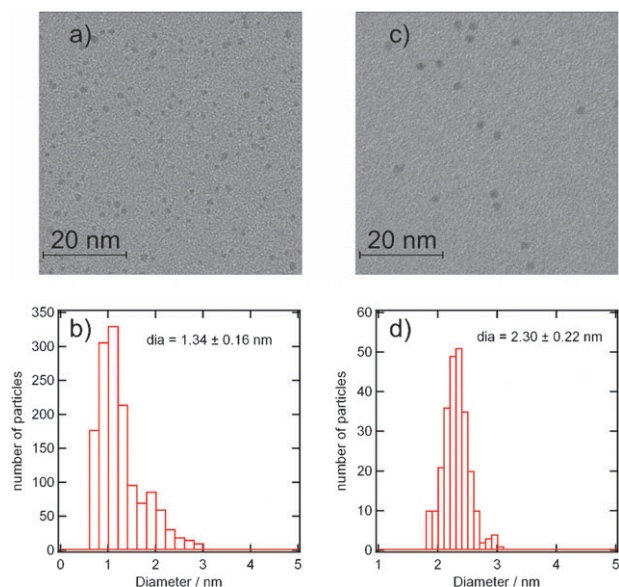


Fig. 1 TEM micrographs demonstrating size control of the Pt cluster. (a) Size selection *via* electrostatic bender and QMS at lowest resolution; (b) corresponding histogram of the cluster size obtained from the analysis of several TEM micrographs. The larger sizes are due to agglomerates; (c) size selection *via* the electrostatic bender with QMS in transmission mode; (d) corresponding histogram of the cluster size obtained from the analysis of several TEM micrographs.

factor for the calculated standard deviation of the size histogram is the shoulder towards larger cluster diameters indicating to some degree the formation of coalesced clusters at the chosen coverage. By changing the electrostatic settings of the bender, the average cluster size was changed to 2.3 nm with a standard deviation of less than 10% (Fig. 1c and d). In both cases, the Pt clusters appear to be randomly distributed on the support and the observed agglomeration can be attributed to the statistical likelihood of an incoming cluster to impinge on a previously deposited one. Pronounced agglomeration due to cluster migration on the carbon support is not discernable, *i.e.* no agglomerates larger than 4 nm are formed. Furthermore, in contrast to the previous reports of close-packed arrays of Pt clusters supported on amorphous carbon, no ordering of the as-deposited clusters on the support has been observed.⁸ In order to test the stability of UHV-prepared Pt clusters on the carbon support the clusters were analyzed after prolonged subjection to ambient (air) and liquid (water and diluted acid solutions) conditions. No changes could be detected by TEM; consequently the samples can easily be transported and shipped without specific precautions. In Fig. 2 a series of different Pt cluster samples is presented, which were prepared with the same settings at the bender and mass spectrometer, but increasing coverage. The required deposition time varies depending on the achieved optimization of the cluster current. For the highest coverage shown (Fig. 2c), the deposition time was 1 h with cluster currents varying between 0.7 and 1.5 nA. At low coverage (0.004 cluster per nm²) the clusters are isolated from each other, exhibiting a size of 2.3 nm with an extremely small size distribution (Fig. 2a and d). With increasing coverage (0.02 cluster per nm²; Fig. 2b and e) a few agglomerated clusters appear amongst still mostly well-separated clusters.

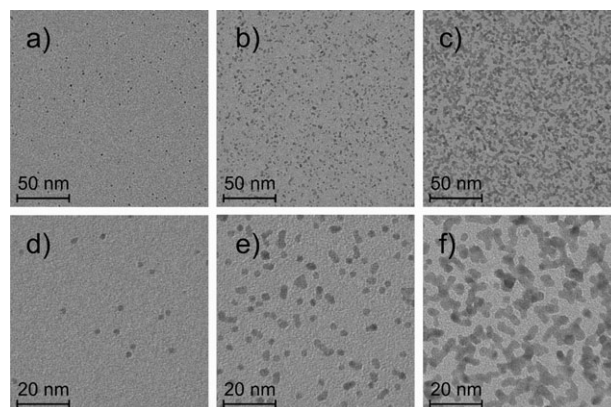


Fig. 2 TEM micrographs demonstrating the variation of the Pt cluster coverage. Clusters of same size have been deposited onto a carbon film with increasing coverage. The size selection was obtained *via* the electrostatic bender with the QMS in transmission mode. The coverage estimated by analyzing the TEM micrographs is 0.004 (a, d), 0.02 (b, e), and 0.05 (e, f) cluster per nm². Due to agglomeration, the latter determination exhibits a higher uncertainty. The deposition times depend on the achieved optimization of the cluster current; for the presented micrographs they were 1.5 h at 10–80 pA cluster current (a, d), 0.5 h at 500–1000 pA (b, e) and 1 h at 700–1500 pA.

Finally, on the sample with high loading (~ 0.05 cluster per nm²) almost no isolated clusters can be observed anymore (micrographs Fig. 2c and f) and the Pt clusters form branched structures that cover most of the carbon substrate.

Alternatively to depositing clusters on a TEM grid, a glassy carbon (GC) substrate can be used, which enables electrocatalytic measurements of the Pt clusters in a rotating disk electrode setup. In Fig. 3 the results of such measurements are shown for a Pt cluster sample prepared under the same preparation conditions as the one shown in Fig. 2b and e. Measurements on a polycrystalline Pt disk are included for comparison. The cyclic voltammogram of the cluster sample in Fig. 3a clearly exhibits the typical features of Pt, *i.e.* the adsorption/desorption of hydrogen at low potentials and oxygenated species at high potentials. The observed voltammogram was stable, indicating the absence of dissolution of the Pt clusters within the measurement time. The electrochemically active surface area (ECSA) of the Pt cluster can be determined utilizing the oxidation of a pre-adsorbed CO monolayer, *i.e.* so-called CO stripping experiments (Fig. 3b). Note that the peak potential of the stripping curve is shifted towards higher potentials as compared to polycrystalline bulk Pt. This finding is in line with an inhibited reactivity for CO oxidation previously observed on carbon supported high surface area Pt catalysts and Pt nanoparticles deposited on gold substrates as well.^{9,10} Furthermore, it was seen that at high cluster coverage with pronounced cluster agglomeration the CO oxidation curve splits into two peaks (not shown), similar to previous work which reported a splitting in the CO stripping peak as evidence for nanoparticle agglomeration.¹¹

An alternative possibility to determine the cluster coverage is to measure and integrate the neutralization current during cluster deposition. Both approaches (cluster current integration and CO-stripping) have been applied to two different

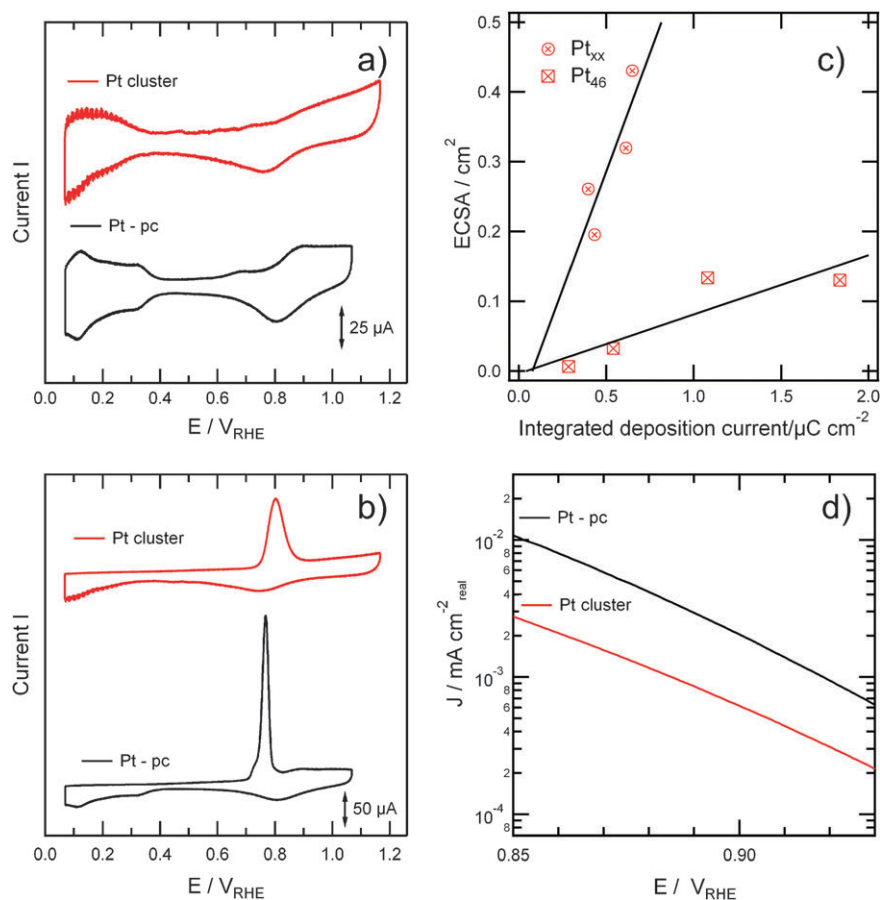


Fig. 3 Comparison of electrochemical measurements utilizing a Pt-cluster sample and polycrystalline Pt. (a) Cyclic voltammetry in Ar saturated 0.1 M HClO₄ solution at 50 mV⁻¹; (b) CO stripping curves recorded at 50 mV⁻¹ (leading to an ECSA of 0.32 cm²); (c) electrochemical surface area determined from CO stripping measurements as a function of the integrated cluster current measured during deposition. Pt_{xx} indicates measurement series with size selection by electrostatic bender and QMS operated in an ion-guide mode, Pt₄₆ indicates measurement series with additional size selection in QMS to 8974 amu; (d) Tafel plot extracted from polarization curves recorded in oxygen saturated electrolyte (50 mV⁻¹).

cluster sizes in the present study. Fig. 3c shows the results gained for the different experimental approaches, plotted with respect to each other. In addition, linear fits are presented for both cluster sizes, illustrating the good accordance that is found for the two different methods. Furthermore, the results show that the combination of both methods allows the determination of the cluster coverage (by measuring the neutralization current) and the accessible surface area of the catalysts (by means of CO-stripping). Thus, a detailed characterization of the cluster dispersion on the model catalyst can be achieved for electrochemical studies utilizing this approach, which is an important requirement for reactivity studies in catalysis research. Utilizing the determined slope of the linear fits in Fig. 3c, the number of accessible surface atoms can be estimated for the supported Pt₄₆ and Pt_{xx} clusters leading to values of 25 ± 10 and 208 ± 88 , respectively (the error is based on the error given in the linear fit). Simply assuming cluster disks, these values correspond to cluster diameters of 0.8 ± 0.3 nm and 2.3 ± 0.9 nm and thus correspond well with the cluster diameter for Pt_{xx} determined by TEM, *i.e.* 2.3 nm without any agglomeration. It is noteworthy, however, that for a determination of the cluster geometry, further, more detailed measurements are necessary.

Rotating the working electrode, a controlled diffusion profile of species dissolved in the electrolyte is created, which allows for kinetic measurements of the oxygen reduction reaction (ORR), which is one of the most important reactions in electrocatalysis. In Fig. 3d a Tafel plot is shown, displaying the current density J of the ORR normalized to the ECSA as a function of potential. As for the CO stripping curve, the comparison to polycrystalline Pt reveals a detrimental influence of the ORR rate (normalized to the surface area) on the particle size which is also observed for industrial high surface area catalysts.^{12,13} On the Pt cluster sample the specific activity for the ORR is approximately $0.6 \text{ mA cm}^{-2}_{\text{Pt}}$ compared to $0.45 \text{ mA cm}^{-2}_{\text{Pt}}$ and $2.1 \text{ mA cm}^{-2}_{\text{Pt}}$ on a standard carbon supported Pt high surface area catalyst with an average particle size of 5 nm¹⁴ and polycrystalline Pt, respectively. With respect to previous studies on the Pt particle size effect on the ORR, it seems that the influence of the particle size on the reaction rate is most pronounced comparing polycrystalline Pt and/or unsupported Pt black particles (~ 30 nm) to carbon supported high surface area catalysts (1–5 nm). The difference in the ORR activity between supported high surface area catalysts with different mean particle sizes is comparably small and additionally might depend on the catalyst loading.^{12,13}

Further studies concerning the particle size effect are in preparation.

In conclusion, the presented results demonstrate that size-selected Pt cluster prepared in UHV can be transferred out of the vacuum, characterized by TEM and applied for electrocatalytic measurements. A combination of cluster current measurement during the preparation and CO-stripping experiments enables the examination of the cluster dispersion of the catalyst. Electrochemical studies, which have not been reported previously for size selected clusters, feature a detrimental effect of the particle size on the CO oxidation reaction as well as the oxygen reduction reaction, properties previously reported for industrial high surface area catalysts as well. In contrast to these catalysts, however, size-selected clusters deposited onto planar substrates are much better defined and thus suitable model systems for a large variety of studies concerning cluster stability as well as activity.

Experimental

TEM measurements are performed using a JEM 2010 microscope (JEOL, Japan) at an acceleration voltage of 120 kV. The TEM grids (Quantifoil, Germany) are coated with a holey carbon film covered with a 2 nm extra layer of amorphous carbon which serves as a support for the size selected clusters. The electrocatalytic measurements are conducted in an all-Teflon three-compartment electrochemical cell at room temperature, using a home-built potentiostat. A saturated Calomel electrode (SCE), separated by an electrolytic bridge from the main cell compartment, was used as reference electrode, however, all potentials are given with respect to the reversible hydrogen potential (RHE), which was measured with a polycrystalline Pt rotating disc electrode for every experiment. A graphite rod was used as counter electrode. The electrolyte was prepared using Millipore Milli-Q[®]-Wasser (>18.3 MΩ cm, TOC < 5 ppb) and concentrated HClO₄ (suprapure; Merck, Germany). The CO stripping measurements were recorded as follows. The potential was held at 0.05 V_{RHE} and the electrolyte was saturated first with carbon monoxide for 5 min and subsequently with argon for 20 min. CO stripping polarization

curves were then recorded by scanning the potential to positive potentials with 50 mV s⁻¹. For the oxygen reduction reaction the electrolyte was purged with oxygen for at least 5 min and the polarization curves are recorded with 50 mV s⁻¹ and a rotation rate of 1600 rpm.

Acknowledgements

This work was supported by the DFG through the Emmy-Noether project ARE852/1-1. Katrin Hartl and Sebastian Kunz acknowledge the German FCI for a chemistry funds scholarship; Karl J. J. Mayrhofer the Austrian FWF for an Erwin-Schrödinger Scholarship.

References

- 1 J. Libuda and H. J. Freund, *Surf. Sci. Rep.*, 2005, **57**, 157–298.
- 2 M. Salmeron and R. Schlogl, *Surf. Sci. Rep.*, 2008, **63**, 169–199.
- 3 G. A. Somorjai and J. Y. Park, *Chem. Soc. Rev.*, 2008, **37**, 2155–2162.
- 4 M. N. Blom, D. Schooss, J. Stairs and M. M. Kappes, *J. Chem. Phys.*, 2006, **124**.
- 5 U. Heiz, F. Vanolli, L. Trento and W. D. Schneider, *Rev. Sci. Instrum.*, 1997, **68**, 1986–1994.
- 6 Y. Watanabe and N. Isomura, *J. Vac. Sci. Technol., A*, 2009, **27**, 1153–1158.
- 7 S. Vajda, M. J. Pellin, J. P. Greeley, C. L. Marshall, L. A. Curtiss, G. A. Ballentine, J. W. Elam, S. Catillon-Mucherie, P. C. Redfern, F. Mehmood and P. Zapol, *Nat. Mater.*, 2009, **8**, 213–216.
- 8 R. Alayan, L. Arnaud, M. Broyer, E. Cottancin, J. Lerme, S. Marhaba, J. L. Vialle and M. Pellarin, *Phys. Rev. B: Condens. Matter Mater. Phys.*, 2007, **76**.
- 9 M. Arenz, K. J. J. Mayrhofer, V. Stamenkovic, B. B. Blizanac, T. Tomoyuki, P. N. Ross and N. M. Markovic, *J. Am. Chem. Soc.*, 2005, **127**, 6819–6829.
- 10 K. A. Friedrich, F. Henglein, U. Stimming and W. Unkauf, *Colloids Surf., A*, 1998, **134**, 193.
- 11 F. Maillard, S. Schreier, M. Hanzlik, E. R. Savinova, S. Weinkauff and U. Stimming, *Phys. Chem. Chem. Phys.*, 2005, **7**, 385–393.
- 12 H. A. Gasteiger, S. S. Kocha, B. Sompalli and F. T. Wagner, *Appl. Catal., B*, 2005, **56**, 9–35.
- 13 K. J. J. Mayrhofer, B. B. Blizanac, M. Arenz, V. R. Stamenkovic, P. N. Ross and N. M. Markovic, *J. Phys. Chem. B*, 2005, **109**, 14433–14440.
- 14 K. J. J. Mayrhofer, V. Juhart, K. Hartl, M. Hanzlik and M. Arenz, *Angew. Chem., Int. Ed.*, 2009, **48**, 3529–3531.

6.1.2 Electrochemically induced nanocluster migration

In addition to the activity of a catalyst, its long term stability is of great importance in catalysis research. On the way of developing new catalysts with an improved durability, the knowledge about mechanisms occurring during degradation as well as their dependence on parameters and processes is indispensable. Model systems with well-defined properties are advantageous for gaining mechanistic information. The model electrocatalyst described in the previous section is ideal to investigate fuel cell relevant degradation mechanisms. It consists of platinum clusters which were produced in a laser vaporization source and deposited onto a defined carbon substrate like the amorphous film on a TEM grid. They are less complex than industrial catalysts because the clusters are homogeneously distributed, exhibit a narrow particle size distribution and are supported by a defined substrate. In contrast to common model catalysts, i.e. polycrystalline materials and single crystals, they consist of supported platinum nanoparticles. Since this model system is very close to real conditions, it is ideal to study induced degradation processes in detail. First results regarding the behavior of supported platinum clusters under exposure to different electrochemical treatments and environments are presented in the following paper. The clusters were deposited onto carbon supported TEM grids and statistically analyzed using TEM images, revealing a random particle distribution. For the investigation, the TEM grids were employed as working electrodes in the electrochemical cell and subjected to potentiostatic or potential cycling conditions in acid electrolyte saturated with argon, oxygen or carbon monoxide. In order to follow occurring changes, TEM images were taken before and after the electrochemical treatment and compared. It is shown that the samples are stable at potentials below $0.55 V_{\text{RHE}}$. However, upon cycling to a potential of $1.05 V_{\text{RHE}}$, migration of the nanoparticles on the surface was induced in all cases. Consequently, the interaction of the particles to the support is not strong enough to inhibit migration of the clusters upon potential cycling. In argon and oxygen atmosphere, this mobility leads to coalescence of the particles whereas in the electrolyte saturated with carbon monoxide coalescence is inhibited leading to distinctive structures.

Although this investigation shows that the model catalyst is not stable under operative conditions of a fuel cell, interesting aspects about the degradation behavior were obtained. Particle migration and coalescence have shown to be the main degradation mechanisms and no dissolution or Ostwald ripening was observed. Furthermore, the inhibition of coalescence in the presence of carbon monoxide is an interesting fact which can possibly be further developed for the selective utilization of this effect. In future, more detailed studies about the dependence of degradation processes on particle size distributions and distances between particles, using this model electrocatalyst, are planned. Additionally, this kind of study facilitates the application of

different types of supports in order to specifically study the interaction between the particles and the support, which significantly influences catalyst degradation.

Electrochemically induced nanocluster migration

K. Hartl, M. Nesselberger, K.J.J. Mayrhofer, S. Kunz, F.F. Schweinberger, G. Kwon, M. Hanzlik, U. Heiz, and M. Arenz

Electrochimica Acta, 2010, Volume 56, Issue 2, Pages 810-816

Permanent weblink:

<http://dx.doi.org/10.1016/j.electacta.2010.10.005>

Reprinted from *Electrochimica Acta*, 56, 2, K. Hartl, M. Nesselberger et al., Electrochemically induced nanocluster migration, 810, Copyright (2010), with permission from Elsevier.



Electrochemically induced nanocluster migration

Katrin Hartl^{a,d}, Markus Nesselberger^d, Karl J.J. Mayrhofer^c, Sebastian Kunz^a, Florian F. Schweinberger^a, GiHan Kwon^a, Marianne Hanzlik^b, Ueli Heiz^a, Matthias Arenz^{d,*}

^a Lehrstuhl Physikalische Chemie, Technische Universität München, Lichtenbergstr. 4, D-85748 Garching, Germany

^b Institut für Elektronenmikroskopie, Technische Universität München, Lichtenbergstr. 4, D-85748 Garching, Germany

^c MPI für Eisenforschung, Abt. Grenzflächenchemie und Oberflächentechnik, Max-Planck-Straße 1, D-40237 Düsseldorf, Germany

^d Department of Chemistry, CS06, University of Copenhagen, Universitetsparken 5, DK-2100 Copenhagen Ø, Denmark

ARTICLE INFO

Article history:

Received 9 June 2010

Received in revised form 1 October 2010

Accepted 2 October 2010

Available online 28 October 2010

Keywords:

Nanocluster migration

Electrocatalysis

PEM fuel cells

Platinum

Degradation mechanism

ABSTRACT

In the presented study the influence of electrochemical treatments on size-selected Pt nanoclusters (NCs) supported on amorphous carbon is investigated by means of transmission electron microscopy (TEM). Well-defined Pt NCs are prepared by an ultra-high vacuum (UHV) laser vaporization source and deposited with low kinetic energy (≤ 10 eV/cluster) onto TEM gold grids covered by a thin (2 nm) carbon film. After transfer out of UHV Pt NCs are verified to be uniform in size and randomly distributed on the support. Subsequently, the TEM grids are employed as working electrodes in a standard electrochemical three electrode setup and the Pt nanoclusters are subjected to different electrochemical treatments. It is found that the NC arrangement is not influenced by potential hold conditions (at 0.40 V vs. RHE) or by potential cycling in a limited potential window ($V_{\max} = 0.55$ V vs. RHE). Upon potential cycling to 1.05 V vs. RHE, however, the NCs migrate on the carbon support. Interestingly, migration in oxygen or argon saturated electrolyte leads to NC coalescence, a mechanism discussed for being responsible for performance degradation of low temperature fuel cells, whereas in carbon monoxide saturated electrolyte the Pt NC agglomerate, but remain separated from each other and thus form distinctive structures.

© 2010 Elsevier Ltd. All rights reserved.

1. Introduction

Due to their unique physical and chemical properties, supported nanoclusters (NCs) are of considerable interest with respect to potential applications in manifold research areas such as optics, electronics, sensor technology and heterogeneous (electro-) catalysis. The specific characteristics of NCs, however, may exhibit a strong dependence on the particle size distribution, the mean interparticle distance, the exact arrangement of the NCs, as well as the interaction of the NCs with the support. Therefore, the re-arrangement of metallic nanoparticles induced by preparation procedures [1–6], temperature treatment [7,8], electron beam irradiation [9,10] or due to aging effects [11] represents a fundamental issue in nanoscience.

Specifically platinum particles supported on carbon substrates constitute one of the most important catalytic systems, considering its application in fuel cells where it facilitates the direct conversion of chemical into electric energy [12]. In studies concerning the stability of such catalysts it is demonstrated that the active sur-

face area of Pt decreases over time. Three different mechanisms are discussed in literature regarding this degradation: Pt dissolution, particle migration and concomitant coalescence, and particle detachment [13,14]. In half-cell measurements, Pt dissolution leads to electrochemical Ostwald ripening, i.e. Pt dissolution and the subsequent re-deposition of Pt-ions onto larger particles following the Gibbs–Thomson effect. In contrast to the gas phase Ostwald ripening processes, in electrochemistry no indications of atomic diffusion of Pt particles on the support are found. It is noteworthy, that in proton exchange membrane fuel cells (PEMFCs), alternative to electrochemical re-deposition, the Pt ions can also be reduced by hydrogen gas diffusing from the anode electrode [14]. In the case of particle migration, whole particles diffuse over the support surface and may coalesce after their collision. Thus both processes, electrochemical Ostwald ripening as well as migration and coalescence lead to the formation of larger Pt particles. To which extent the respective mechanisms contribute to observed losses in surface area in applied systems is of great importance for the development of efficient and durable PEMFCs and thus a topic of ongoing research [15].

In the presented work we utilize size-selected Pt NCs deposited onto an amorphous carbon support as a model system for investigating the degradation of PEM fuel cell catalysts. The Pt NCs

* Corresponding author. Tel.: +45-35320002.

E-mail address: m.arenz@kemi.ku.dk (M. Arenz).

are prepared by a laser vaporization source and deposited with low kinetic energies onto carbon coated TEM gold grids. By characterizing the Pt nanocluster arrangements with transmission electron microscopy (TEM) before and after electrochemical potential cycling treatments their behavior on the carbon support is studied in detail.

2. Experimental

2.1. Sample preparation

Platinum NCs are produced by a high frequency laser vaporization cluster source which is described in detail in ref. [16]. In short, by focusing the second harmonic of a Nd:YAG laser (*Spitlight DPSS, 100 Hz, InnoLas*) onto a rotating Pt disk a metal plasma is produced which is thermalized by a helium pulse. During supersonic expansion of the helium-metal vapor into the vacuum nucleation occurs and nanoclusters are formed. The NC beam is guided by home-built ion optics to a bender, which consists of an electric quadrupole, where the positively charged nanocluster ions are separated from negatively charged and neutral ones. In addition, at the bender the NC ions are mass-selected as only NCs within a certain mass range exhibit the trajectory path through the exit hole of the bender. Subsequently, these pre-selected NCs are guided through a quadrupole mass spectrometer (QMS; *ABB extrel; mass limit 9000 amu*), which can be operated by two different modes: Either in an ion guide transmission mode, or in a mass-resolving mode. The latter mode provides an extremely accurate mass-selecting device and depending on the applied resolution clusters with an exact number of atoms can be produced; however, the transmission of the particle beam is limited to masses below 9000 amu. In the present work the QMS was mainly operated in transmission mode and size-selection was achieved by means of the bender system. This allowed the preparation of clusters that are large enough in size to enable the use of TEM as a characterization method. After passing the QMS the particle beam is deposited with low kinetic energy (≤ 10 eV/nanocluster) onto a TEM gold grid covered by an amorphous carbon film. For the electrochemical characterization by cyclic voltammetry (CV) the NC were deposited onto a glassy carbon (GC) disk of a rotating disk electrode. The TEM grid and GC disk, respectively, were mounted on a home-built sample holder at the end of a manipulator, which allows the control of the deposition potential (kinetic energy of nanocluster beam) as well as the measurement of the neutralization current. In order to replace the sample it is transferred into a vacuum lock by means of the manipulator and automatically the latter gets separated from the vacuum chamber by closing a pneumatic gate. Thus, ventilation of the lock to ambient conditions and subsequent replacement of the TEM grid/GC disk is possible. All samples have been prepared with similar settings at the bender and the mass spectrometer, but the deposition time, which defines the coverage of the nanoclusters on the grid, was varied. The gold TEM grid is coated with a holey carbon film covered with a 2 nm extra layer of amorphous carbon (*Quantifoil, Germany*) which serves as a support for the nanoclusters.

2.2. Electrochemical treatment and analysis procedure

The proceeding is very similar to the recently developed IL-TEM method [17,18]. The basic idea is to utilize TEM gold grids as working electrodes in electrochemical measurements. Thus NC samples can be compared before and after electrochemical treatments. The procedure was as follows: First, the prepared sample is examined via TEM at a JEM 2010 microscope (*JEOL, Japan*) with an acceleration voltage of 120 kV and a magnification of 160k. Subsequently,

the electrochemical treatment is accomplished and after drying of the sample a second TEM investigation follows. The electrochemical treatments were conducted in an all-Teflon three-compartment electrochemical cell [19,20], using a home-built Potentiostat. A saturated Calomel electrode (SCE), separated by an electrolytic bridge from the main cell compartment was used as reference electrode, however, all potentials are given with respect to the reversible hydrogen potential (RHE), which was measured with a polycrystalline Pt rotating disc electrode for every experiment. A graphite rod was used as counter electrode. The electrolyte was prepared using Millipore Milli-Q®-water (>18.3 M Ω cm, TOC <5 ppb) and concentrated HClO₄ (*suprapure; Merck, Germany*). The TEM grid was contacted by a gold wire and immersed into the electrolyte as working electrode. For the treatments the potential was cycled between 0.06 and 1.06 V vs. RHE with 0.05 V s⁻¹ in 0.1 mol dm⁻³ HClO₄ for 2400 s (60 cycles). During the treatment the electrolyte was continuously saturated with the respective gas indicated in the text. After the electrochemical treatment the TEM grid was dried under a gentle nitrogen stream and transferred back for the TEM analysis.

2.3. Statistical analysis

The center-of-particle and particle size distribution were evaluated using the image processing program *ImageJ* developed at the *National Institutes of Health*. The average diameter of the NCs represents the Feret's diameter and was determined in two different ways, in each case assuming a spherical shape: one value represents the average diameter of all NCs, whereas the other one is received from a Gaussian fit of the frequency distribution assuming that the larger diameters result from agglomerated NCs. The latter is considered as the diameter of the NCs just before deposition.

For the nearest-neighbor distribution (NND) the centre coordinates of the particles were determined with *ImageJ* and the cumulative frequency distribution was calculated from the particle distances using self-programmed software. In order to know whether this distribution can be assumed as a random distribution, the experimental curve was compared to a theoretical one. The latter was determined using the formula of Ref. [21] for the exclusion probability for impenetrable hard discs and subtracting it from unity. As the theoretical distribution is a function of the particle volume fraction, it was calculated for each image separately. The borders of significance are calculated according to the Kolmogorov–Smirnov test [22] using a statistical significance of five percent.

3. Results and discussion

At the beginning of the experiments, an electrochemical characterization of the Pt NCs was performed by cyclic voltammetry. In Fig. 1 it is demonstrated that the CVs of the NC samples exhibit the typical features of Pt in acid electrolyte. At low potentials hydrogen adsorbs/desorbs from the Pt surface [V] ~ 0.05 – 0.35 V vs. RHE, whereas between ~ 0.35 – 0.70 V vs. RHE only capacitive currents due to the charging/de-charging of the double layer are observed. The formation of oxygenated species and their reduction occurs at potentials >0.70 V vs. RHE. The observed voltammograms were stable, indicating the absence of significant loss in Pt surface area during the experiments.

In Fig. 2a, a TEM micrograph of a typical as-prepared Pt NC sample is shown. The NCs are uniform in size (2.09 ± 0.30 nm) and well separated on the support. Only very few coalesced NCs are observed at such low NC coverage. A statistical analysis of the nearest neighbor distribution of the NCs (Fig. 2b) reveals

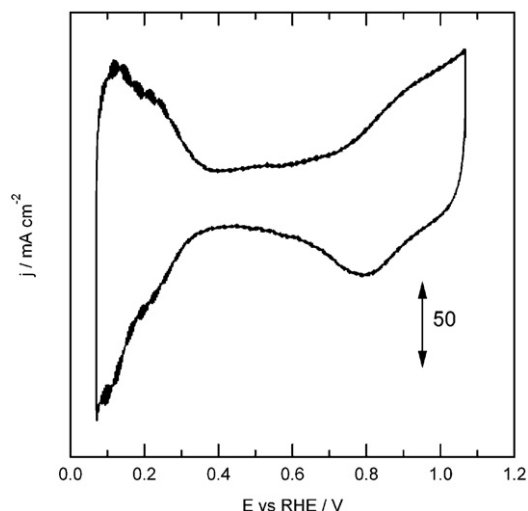


Fig. 1. Cyclic voltammogram of a Pt/C cluster probe recorded in a rotating disk electrode setup in 0.1 M HClO₄ solution with a scan rate of 0.1 V s⁻¹.

that the Pt NCs exhibit a random distribution on the support. At higher NC coverage the number of coalesced particles increases, however, the NC are still randomly distributed (see Fig. 3). No agglomerated structures due to particle–particle interactions, such as the ones reported previously [1,3,4,6], were found. This indicates that the coalesced Pt clusters are formed due to direct collisions of NCs during deposition and no significant NC migration occurs on the support prior to the electrochemical measurements.

In order to investigate the influence of different electrochemical treatments on the Pt NC arrangement the samples were analyzed by TEM before and after treatment. It was found that the NCs (cluster size as well as random distribution) are not influenced by potential hold conditions at 0.40 V vs. RHE or by potential cycling in a limited potential window ([V]=0.06–0.56 V vs. RHE) (not shown). Potential cycling in an extended potential window ([V]=0.06–1.06 V vs. RHE), however, leads to NC migration (see

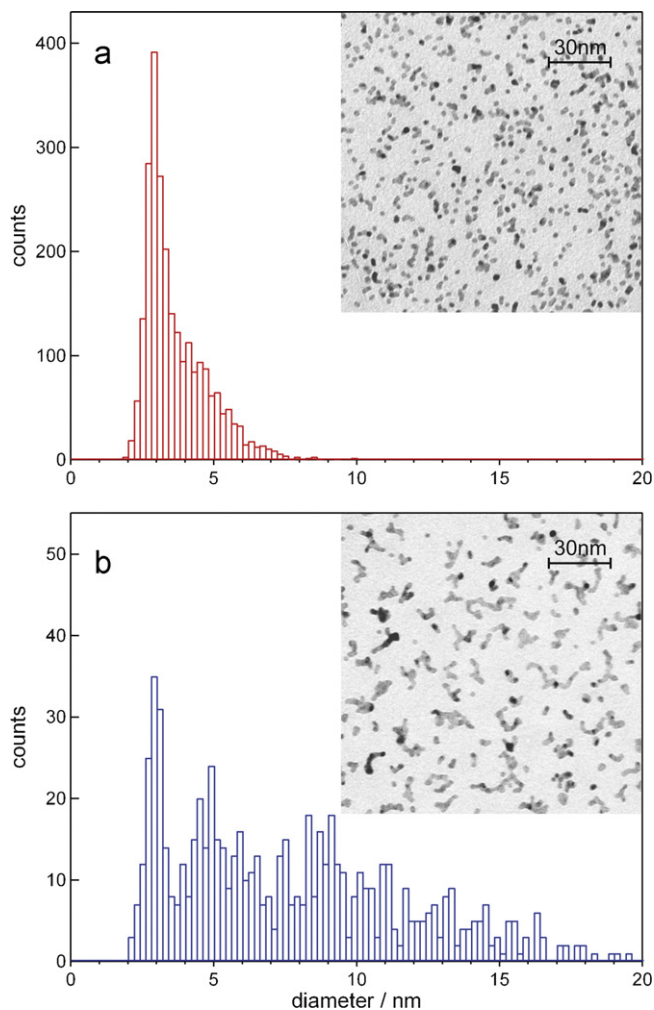


Fig. 3. TEM micrographs with corresponding histograms of the particle size distribution before (a) and after electrochemical treatment (b). The treatment consisted of 60 potential cycles between 0.06 and 1.06 V vs. RHE in oxygen saturated 0.1 mol dm⁻³ HClO₄ solution at a sweep rate of 0.05 V s⁻¹.

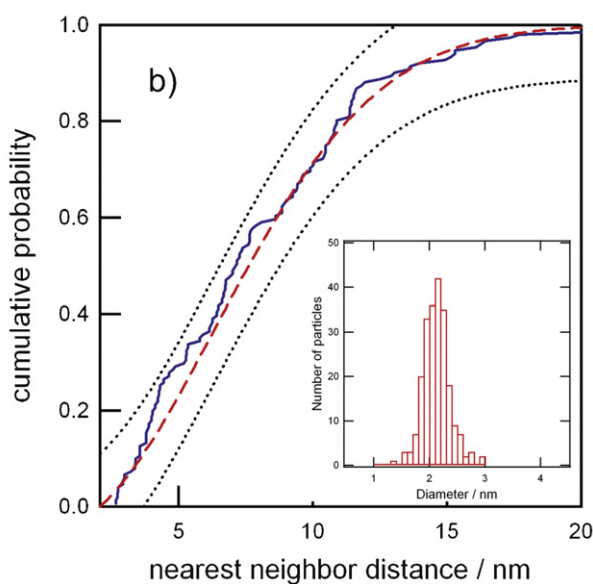
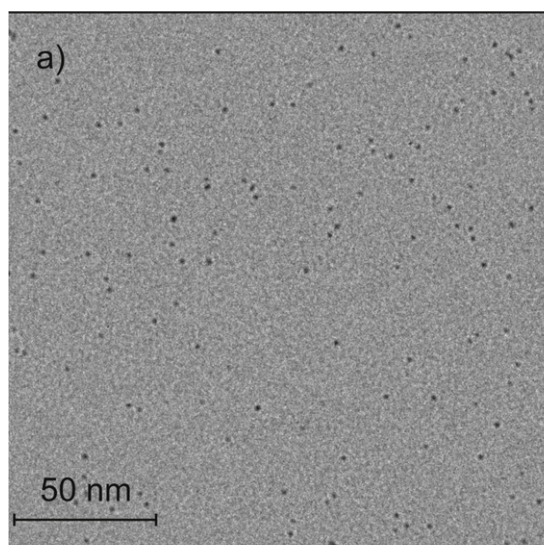


Fig. 2. Representative TEM micrograph of an as-prepared Pt nanocluster sample at low coverage (a). In part (b) the determined cumulative nearest neighbor distribution (blue line) is compared to its theoretical curve assuming a random distribution (red dashed line); significance calculated according to the Kolmogorov–Smirnov test using a statistical significance of five percent (black dotted line). In the inset the histogram of the particle size is shown. (For interpretation of the references to color in this figure legend, the reader is referred to the web version of the article.)

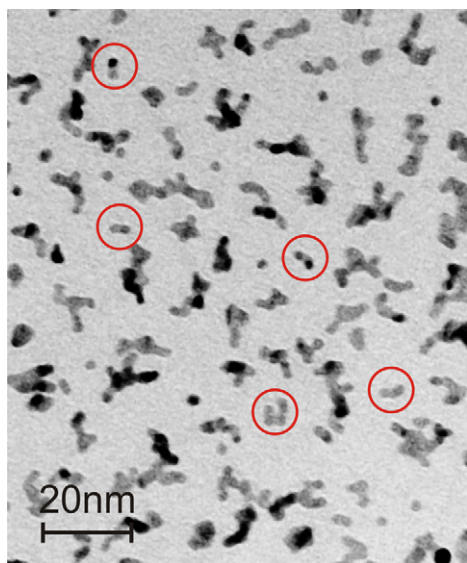


Fig. 4. TEM micrograph of a sample with electrochemically induced agglomeration of the nanoclusters. The width of the branched structures closely resembles the diameter of the as-prepared individual Pt NCs. In many cases the single NCs can still be identified in the coalesced particles as highlighted by the circles.

Fig. 3). The representative TEM micrographs along with the respective particle histograms show that in the as-prepared sample the NCs exhibit only a small degree of agglomeration, i.e. the particle diameter of the individual NCs is well discernible together with a rather broad shoulder towards larger diameters. The fitted diameter of the individual NC is 2.8 ± 0.3 nm with an average of all NCs of 3.5 nm. After potential cycling in oxygen saturated solution, the NCs clearly have formed coalesced, branched structures, similar to the ones observed in previous studies performed in hot concentrated phosphoric acid [23]. It is noteworthy, that in argon saturated electrolyte the same behavior is observed as for the presented case. The formed nanocluster-agglomerates exhibit dimensions of up to 20 nm and are randomly distributed on the amorphous carbon substrate, i.e. no preferred surface sites are discernable. Furthermore, no apparent particle detachment is discernable as observed in previous experiments on industrial high surface area catalysts exposed to very high potentials (1.4 V vs. RHE) [17]. The particle density is not affected by the treatment as shown by analyzing the surface area fraction of Pt on the carbon films (16.7% and 16.6% before and after the treatment, respectively). From measurements with the high surface area catalysts it is known that once a particle is detached from the support, in an electrochemical half-cell with excess electrolyte most particles are washed into solution and only a tiny fraction re-attaches on the support [17].

In the TEM micrographs of the treated sample no thermodynamically favored spheres can be identified and the width of the branched structures closely resembles the diameter of the as-prepared individual Pt NCs. In some cases even the spherical shape of individual NCs is still clearly discernable in the coalesced structures as highlighted in Fig. 4. It is therefore concluded that the observed structures are a consequence of the migration and coalescence of intact Pt NCs on the support. Pt dissolution and concomitant electrochemical Ostwald ripening can be excluded to play a significant role. In the histograms of the treated samples no tailing to the end of small particle diameters is discernable, as would be expected in the case of Pt dissolution due to the favorable consumption of smaller Pt NCs [24]. Migration of whole particles on a support is reported in literature in general due to temperature activated diffusion, i.e. due to heating of the sam-

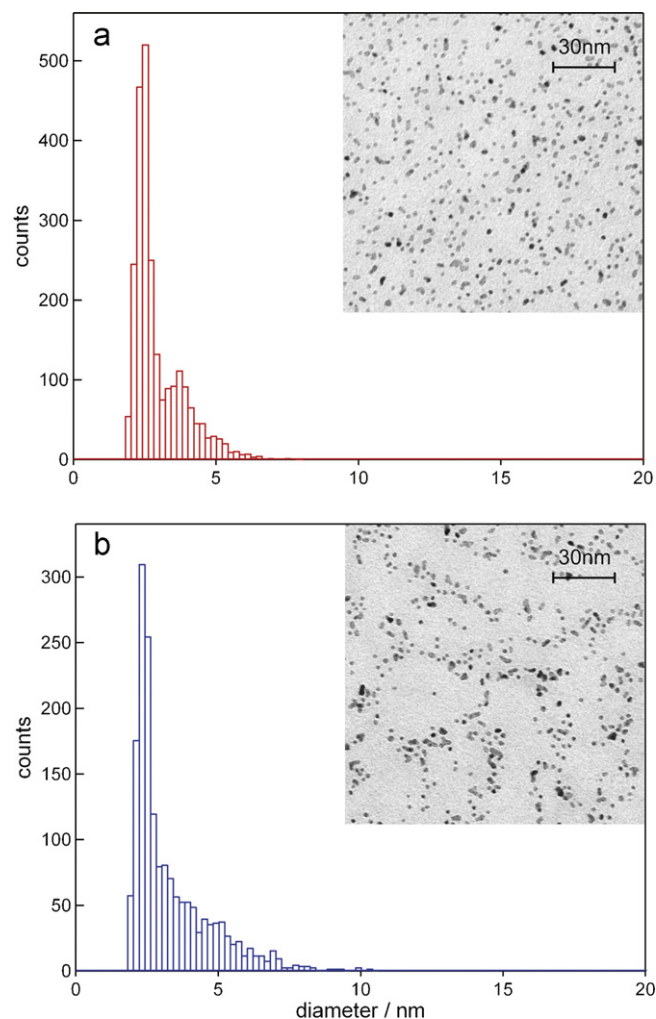


Fig. 5. TEM micrographs with corresponding histograms of the particle size distribution before (a) and after electrochemical treatment (b). The treatment consisted of 60 potential cycles between 0.06 and 1.06 V vs. RHE in carbon monoxide saturated $0.1 \text{ mol dm}^{-3} \text{ HClO}_4$ solution at a sweep rate of 0.05 V s^{-1} .

ples [7,8] and electron beam irradiation [9,10]. Here the process is most likely not temperature activated as all measurements are performed at room temperature and the potential window of the potential cycling has a decisive influence if NC diffusion is observed or not, i.e. an unchanged random particle distribution is observed when limiting the upper potential window to the double layer region. Although, the driving force for migration is not entirely clear at this point, a possible mechanism might be the continuous change of the wetting/nonwetting behavior of the Pt NCs on the carbon support. Such a behavior is known for example upon change of the reaction gases for Ag on a Sapphire [25] as well as for small Cu clusters on a ZnO support [26]. In the gas phase the wetting behavior is related to the metal/vapor, substrate/vapor and metal/substrate interfacial energies [27]. In electrochemistry it is known from previous work that during an oxidative treatment of carbon surfaces by potential cycling towards high potentials oxygen species from the water are incorporated into the carbon surface, inducing a change in the hydrophobicity [28,29]. At the same time the surface of the Pt NCs changes from a reduced to an oxide covered state upon potential cycling, thus weakening the bonding of the Pt NCs to the substrate [30,31]. Consequently, in the presented investigations the hydrophobic/hydrophilic interaction of Pt NCs and carbon support is repeatedly changed, which might diminish the adhesive force of the Pt NCs. Thus during the

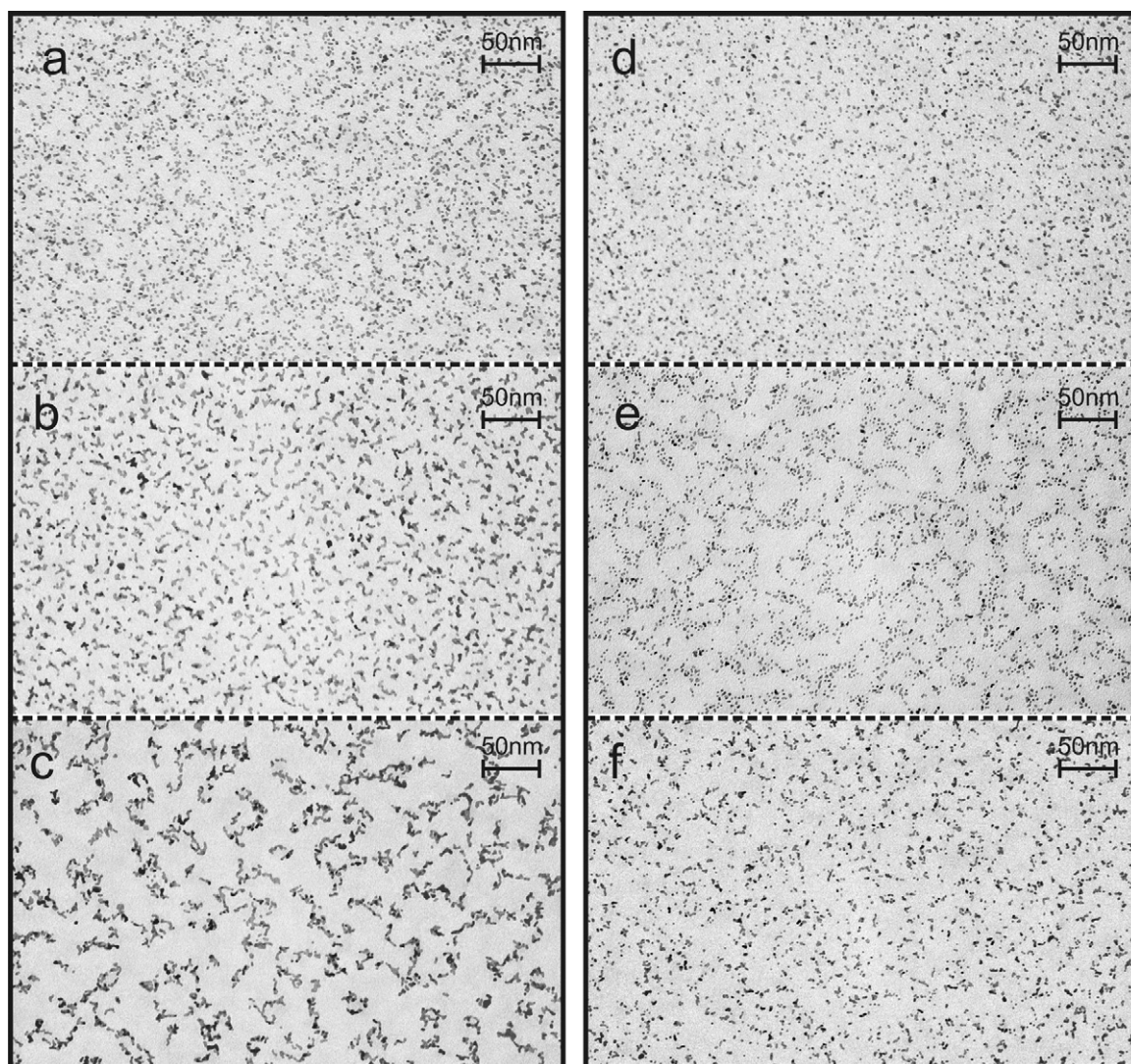


Fig. 6. Sequence of TEM micrographs of nanocluster samples which were electrochemically treated in oxygen as well as in carbon monoxide saturated solution, however, in a different order. Micrograph a and d show the initial NC samples. For sequence a, b, c the order was first oxygen and then CO saturated solution. For sequence d, e, and f the order was first CO and then oxygen saturated solution. The respective treatment consisted of 60 potential cycles between 0.06 and 1.06 V vs. RHE at a sweep rate of 0.05 V s^{-1} .

treatment the NC mobility is changed leading to the observed behavior similar to a Brownian motion. This explanation is in agreement with the observations that a certain threshold potential for particle migration exists, the migration is independent of the gas dissolved in the electrolyte solution (see also below), and that in the applied potential range no complete carbon oxidation to CO_2 occurs.

Interestingly, although Pt NCs migrate upon potential cycling in CO saturated electrolyte as well (see statistical evaluation of the nearest-neighbor distribution in the supporting information), no coalesced structures are observed after such a treatment. As demonstrated in Fig. 5 applying the same experimental protocol as for oxygen saturated electrolyte (Fig. 3), potential cycling in CO saturated solution does not induce any significant change in the particle size distribution, i.e. despite the fact that the Pt NCs form agglomerates, the average particle size remains constant at 2.8 nm. This surprising finding is independent of the prehistory of the sample and can be found for coalesced structures as well. In Fig. 6 it is shown that cycling a NC sample first in oxygen and afterwards in carbon monoxide saturated solution (sequence a–c) induces NC coalescence in the first treatment, while the coalesced

structures align in a pattern during the second treatment. Apparently, no further coalescence is induced. If a NC is treated in reversed order (sequence d–f), first particle alignment without coalescence is induced and then coalescence. Furthermore, after cycling in carbon monoxide saturated solution in certain cases even ring-shaped structures were observed (see Fig. 7). While exact NC alignment mechanism is not known, no indications were found that the structures are due to the drying conditions or that they depend on the initial structure of the carbon film. In contrast to potential cycling in oxygen or argon saturated solution, where the Pt NCs appear to coalesce according to a “hit and stick”-model [32], i.e. the NCs stick upon collisions at the point of impact, in CO saturated solution the Pt NC seem to exhibit a “passivation” layer which prevents cluster coalescence. A possible explanation could be repulsive forces due to the dipole of adsorbed CO molecules. It is well-known that carbon monoxide adsorbs very strongly on platinum forming an ordered adlayer with repulsive dipole-dipole coupling [33]. At this point, however, this is a speculative assumption. Future investigation will focus on the particle “passivation” in more detail, as it might lead to new ideas for strategies avoiding particle coalescence in applied systems.

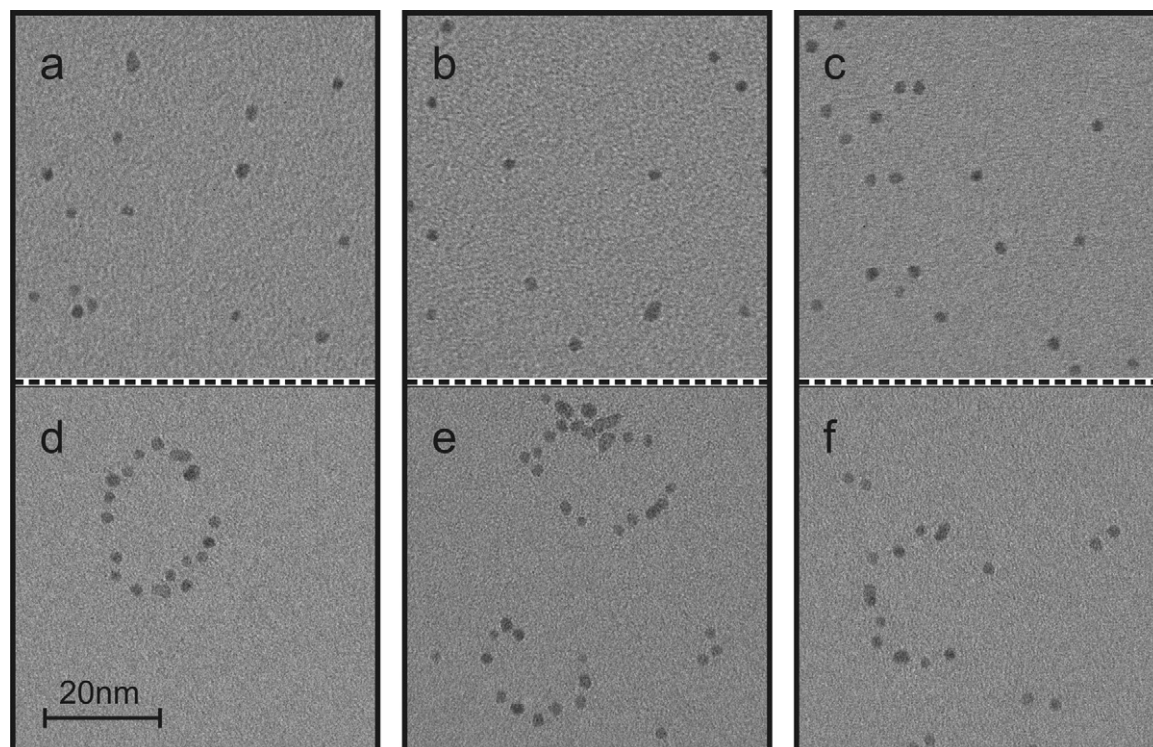


Fig. 7. TEM images of a sample with low Pt NC coverage before (a–c) and after (d–f) the electrochemical treatment in a carbon monoxide purged electrolyte. The treatment consisted of 60 potential cycles between 0.06 and 1.06 V vs. RHE in carbon monoxide saturated 0.1 mol dm⁻³ HClO₄ solution at a sweep rate of 0.05 V s⁻¹.

4. Conclusions

In conclusion, UHV prepared Pt nanoclusters supported on the amorphous carbon film of TEM gold grids were utilized to gain insight into different catalyst degradation mechanisms. The results demonstrate that upon the applied potential cycling treatment no Pt dissolution occurs. In contrast to an electrochemical Ostwald ripening mechanism, the treatment induces a migration of whole Pt nanoclusters on the support. In O₂ or Ar saturated solution the nanoclusters coalesce according to a “hit and stick”-model, whereas upon potential cycling in carbon monoxide saturated electrolyte coalescence is suppressed. The NCs stay separated and align in certain patterns depending on the cluster coverage.

Acknowledgements

This work was supported by the DFG through the Emmy-Noether project ARE852/1-1. Katrin Hartl and Sebastian Kunz acknowledge the German FCI for a chemistry funds scholarship, Karl J.J. Mayrhofer the Austrian FWF for an Erwin-Schrödinger Scholarship. H.A. Gasteiger is acknowledged for the critical reading of the manuscript and bringing some of the references to our attention.

Appendix A. Supplementary data

Supplementary data associated with this article can be found, in the online version, at doi:10.1016/j.electacta.2010.10.005.

References

- [1] R. Alayan, L. Arnaud, M. Broyer, E. Cottancin, J. Lerme, S. Marhaba, J.L. Vialle, M. Pellarin, *Phys. Rev. B* 76 (2007).
- [2] J.X. Huang, F. Kim, A.R. Tao, S. Connor, P.D. Yang, *Nat. Mater.* 4 (2005) 896.
- [3] D. Tainoff, L. Bardotti, F. Tournus, G. Guiraud, O. Boisron, P. Melinon, *J. Phys. Chem. C* 112 (2008) 6842.
- [4] A. Lando, N. Kebaili, P. Cahuzac, C. Colliex, M. Couillard, A. Masson, M. Schmidt, C. Brechignac, *Eur. Phys. J. D* 43 (2007) 151.
- [5] B. Yoon, V.M. Akulin, P. Cahuzac, F. Carlier, M. de Frutos, A. Masson, C. Mory, C. Colliex, C. Brechignac, *Surf. Sci.* 443 (1999) 76.
- [6] L. Bardotti, P. Jensen, A. Hoareau, M. Treilleux, B. Cabaud, *Phys. Rev. Lett.* 74 (1995) 4694.
- [7] M. Jose-Yacamán, C. Gutierrez-Wing, M. Miki, D.Q. Yang, K.N. Piyakis, E. Sacher, *J. Phys. Chem. B* 109 (2005) 9703.
- [8] M. Wanner, R. Werner, D. Gerthsen, *Surf. Sci.* 600 (2006) 632.
- [9] M. Flueli, P.A. Buffat, J.P. Borel, *Surf. Sci.* 202 (1988) 343.
- [10] H.M. Zheng, R.K. Smith, Y.W. Jun, C. Kisielowski, U. Dahmen, A.P. Alivisatos, *Science* 324 (2009) 1309.
- [11] R. Popescu, R. Schneider, D. Gerthsen, A. Bottcher, D. Löffler, P. Weis, M.M. Kappes, *Surf. Sci.* 603 (2009) 3119.
- [12] N.M. Markovic, P.N. Ross, *CatTech* 4 (2000) 110.
- [13] R. Borup, J. Meyers, B. Pivovar, Y.S. Kim, R. Mukundan, N. Garland, D. Myers, M. Wilson, F. Garzon, D. Wood, P. Zelenay, K. More, K. Stroh, T. Zawodzinski, J. Boncella, J.E. McGrath, M. Inaba, K. Miyatake, M. Hori, K. Ota, Z. Ogumi, S. Miyata, A. Nishikata, Z. Siroma, Y. Uchimoto, K. Yasuda, K.I. Kimijima, N. Iwashita, *Chem. Rev.* 107 (2007) 3904.
- [14] P.J. Ferreira, G.J. la O, Y. Shao-Horn, D. Morgan, R. Makharia, S. Kocha, H.A. Gasteiger, *J. Electrochem. Soc.* 152 (2005) A2256.
- [15] K. Sasaki, M. Shao, R. Adzic, *Dissolution and stabilization of platinum in oxygen cathodes*, in: F.N. Büchi, M. Inaba, T.J. Schmidt (Eds.), *Polymer Electrolyte Fuel Cell Durability*, Springer, New York, 2009.
- [16] U. Heiz, F. Vanolli, L. Trento, W.D. Schneider, *Rev. Sci. Instrum.* 68 (1997) 1986.
- [17] K.J.J. Mayrhofer, J.C. Meier, S.J. Ashton, G.K.H. Wiberg, F. Kraus, M. Hanzlik, M. Arenz, *Electrochem. Commun.* 10 (2008) 1144.
- [18] K.J.J. Mayrhofer, S.J. Ashton, J.C. Meier, G.K.H. Wiberg, M. Hanzlik, M. Arenz, *J. Power Sources* 185 (2008) 734.
- [19] K.J.J. Mayrhofer, G.K.H. Wiberg, M. Arenz, *J. Electrochem. Soc.* 155 (2008) P1.
- [20] K.J.J. Mayrhofer, S.J. Ashton, J. Kreuzer, M. Arenz, *Int. J. Electrochem. Sci.* 4 (2009) 1.
- [21] S. Torquato, B. Lu, J. Rubinstein, *Phys. Rev. A* 41 (1990) 2059.
- [22] J. Lehn, H. Wegmann, *Einführung in die Statistik*, 5th ed., B.G. Teubner Verlag, Wiesbaden, 2006.
- [23] G.A. Gruver, R.F. Pascoe, H.R. Kunz, *J. Electrochem. Soc.* 127 (1980) 1219.
- [24] M.S. Wilson, F.H. Garzon, K.E. Sickafus, S. Gottesfeld, *J. Electrochem. Soc.* 140 (1993) 2872.
- [25] D. Chatain, F. Chabert, V. Ghetta, J. Fouletier, *J. Am. Ceram. Soc.* 77 (1994) 197.

- [26] J.D. Grunwaldt, A.M. Molenbroek, N.Y. Topsoe, H. Topsoe, B.S. Clausen, *J. Catal.* 194 (2000) 452.
- [27] Z.M. Wang, P. Wynblatt, D. Chatain, *Interface Sci.* 7 (1999) 173.
- [28] B.J. Hwang, Y.W. Tsai, J.F. Lee, P. Borthen, H.H. Strehblow, *J. Synchrotron. Radiat.* 8 (2001) 484.
- [29] K.H. Kangasniemi, D.A. Condit, T.D. Jarvi, *J. Electrochem. Soc.* 151 (2004) E125.
- [30] C. Bittencourt, M. Hecq, A. Felten, J.J. Pireaux, J. Ghijsen, M.P. Felicissimo, P. Rudolf, W. Drube, X. Ke, G. Van Tendeloo, *Chem. Phys. Lett.* 462 (2008) 260.
- [31] X.W. Yu, S.Y. Ye, *J. Power Sources* 172 (2007) 133.
- [32] T.A. Witten, L.M. Sander, *Phys. Rev. Lett.* 47 (1981) 1400.
- [33] M.W. Severson, C. Stuhlmann, I. Villegas, M.J. Weaver, *J. Chem. Phys.* 103 (1995) 9832.

6.2 Improved Catalyst Durability by Support Modifications

In the degradation process of electrocatalysts, not only the particles itself, but also the support plays an important role. The application of graphitized carbon as catalyst support, for example, is known to enhance the durability of electrocatalysts by reducing the carbon corrosion rate [51]. In addition to the durability of the support itself, the strength of particle-support interaction influences particle detachment and migration with concomitant coalescence, both processes leading to loss in active surface area. Much effort in terms of optimization of electrocatalysts is dedicated to improvements of the support durability. However, not many reports on how to improve the particle-support interaction are available.

6.2.1 IL-TEM investigations on the degradation mechanism of Pt/C electrocatalysts with different carbon supports

The physicochemical properties of carbon blacks, which are commonly used as supports in electrocatalysts, are strongly influenced by the presence of surface groups. These groups are mainly incorporated into the carbon during the manufacturing process. The most significant kinds of surface groups are the ones containing oxygen, like phenol, carbonyl, carboxyl, quinone or lactone functional groups. They affect wettability, chemical reactivity, electrical and catalytic properties of the carbon black and therefore influence the binding strength to particles and adsorbates. [35]

It has been shown that potential cycling to high potentials generates oxygen functional groups at the carbon surface, inducing a change of the physicochemical properties [67, 68]. In cyclic voltammetry, only electroactive oxygen surface groups, such as the quinone/hydroquinone couple, are detectable. These are frequently used as an index of the degree of surface oxidation of the carbon material [11].

Nowadays, a standard modification in order to gain higher durability of a carbon black is its graphitization. By this means, the carbon corrosion rate in MEA tests is lowered by a factor of 2-3 [51]. For further improvements of electrocatalyst stability other approaches concerning modifications of the catalyst substrate are developed. In the following paper, a catalyst designed for high durability is investigated regarding its active surface area loss and the occurring degradation processes upon an accelerated stress test. Therefore, electrochemical in combination with IL-TEM experiments were performed.

The surface of the carbon support of the catalyst of interest had been modified using transition metals in order to improve its resistance to oxidation. In comparison with a similar catalyst without support modification, the difference in degradation behavior upon a potential cycling stress test was determined. It was shown that the

reduced loss in active surface area of the catalyst with the modified support arises from a limited particle detachment process. Coalescence of adjacent particles occurs for both samples, but after an initial loss in active surface area the modified catalyst seems to be stabilized in contrast to the reference catalyst. Since the characterization of the bare carbon supports showed that the capability of total oxidation to carbon dioxide is comparable for the two applied catalysts, the modification apparently strengthens the anchoring of the particles on the support and in this way inhibits their detachment. Additionally, from a mechanistic point of view, one can draw the conclusion that total oxidation of the carbon support does not play a decisive role in the particle detachment mechanism.

IL-TEM investigations on the degradation mechanism of Pt/C electrocatalysts with different carbon supports

K. Hartl, M. Hanzlik and M. Arenz

Energy & Environmental Science, 2011, Volume 4, Issue 1, Pages 234 - 238

Permanent weblink:

<http://dx.doi.org/10.1039/C0EE00248H>

Reproduced by permission of The Royal Society of Chemistry.

IL-TEM investigations on the degradation mechanism of Pt/C electrocatalysts with different carbon supports†

Katrin Hartl,^{ac} Marianne Hanzlik^b and Matthias Arenz^{*c}

Received 9th July 2010, Accepted 23rd September 2010

DOI: 10.1039/c0ee00248h

Utilizing our recently developed method of identical location transmission electron microscopy (IL-TEM) in combination with electrochemical surface area determination, the degradation behavior of different carbon supported Pt catalysts for polymer electrolyte membrane fuel cells (PEMFCs) is investigated. Two different Pt based catalysts supported on a low surface area (LSA) carbon are compared to a Pt catalyst with standard high surface area (HSA) carbon support. One of the LSA carbon supports is of conventional type, while the other is modified by a transition metal. Relative to the standard, both catalysts with LSA carbon support exhibit improved degradation behavior in terms of loss in active surface area upon accelerated stress tests. The catalyst with transition metal modified carbon support thereby exhibits by far superior improvements. The characterization of the bare carbon supports indicates that the observed differences between both catalysts with LSA carbon support are not related to the resistance of the support to complete oxidation to carbon dioxide. Instead, the IL-TEM results reveal that the improved properties of the catalyst with transition metal modified support are due to a stabilization of the Pt particles attached to the support. Particle detachment thus can be drastically reduced and the degradation is limited to a migration and coalescence or sintering mechanism.

1. Introduction

Due to their high efficiency converting chemical into electric energy polymer electrolyte membrane fuel cells (PEMFCs) play an important role in the widely discussed effort of substituting conventional vehicle motors by electric power-trains. Substantial progress has been made on many technical aspects concerning a commercial large-scale deployment of PEMFCs. The

manufacturing of fuel cell stacks, their implementation in vehicles, and longtime field trials are nowadays standard practice. However, in order to render PEMFCs commercially viable for such demanding applications as electric vehicles their cathode electrocatalyst still needs improvements in terms of both activity¹ and perhaps more importantly, stability.^{2,3}

The standard catalysts for PEM fuel cells are Pt-based nanoparticles on a high surface area (HSA) carbon support.⁴ In recent years the main research effort was to improve the power output per amount of Pt used in a fuel cell, *i.e.* the mass activity of the catalyst. It is now demonstrated by many experimental and theoretical investigations that the crucial cathode reaction—the oxygen reduction reaction—can be considerably increased by alloying platinum with a second transition metal such as Co, Ni, or Cu.^{5–7}

Much less is known about catalyst degradation. Despite the fact that several studies in PEM as well as phosphoric acid (PA) fuel cells showed that catalyst degradation is one of the major

^aLehrstuhl Physikalische Chemie, Technische Universität München, Lichtenbergstr. 4, D-85748 Garching, Germany

^bZentrum für Elektronenmikroskopie, Technische Universität München, Lichtenbergstr. 4, D-85748 Garching, Germany

^cDepartment of Chemistry, CS06, University of Copenhagen, Universitetsparken 5, DK-2100 Copenhagen Ø, Denmark
E-mail: m.arenz@kemi.ku.dk

† Electronic supplementary information (ESI) available: CO stripping curves for the ECSA determination of the catalysts. See DOI: 10.1039/c0ee00248h

Broader context

Fuel cells are an efficient alternative to conventional power sources such as combustion engines. Instead of producing first heat, which has to be further transformed into mechanical energy, fuel cells convert chemical energy directly into useful electrical energy. An essential part of a fuel cell is the catalyst, where the chemical reactions take place. In general catalysts are composed of an active component of high surface to mass ratio, *e.g.* nanoparticles, and a support. In today's low temperature fuel cells, the active component of the catalyst must contain platinum, a rare and expensive metal. Thus there is a strong incentive to minimize the amount of platinum as well as to enhance the durability of the catalyst. Despite the significant progress in recent years, further breakthroughs are required. In order to optimize the durability of catalysts a detailed understanding of the degradation mechanism as a function of the applied conditions is necessary. The approach of identical location transmission electron microscopy (IL-TEM), recently developed in our group, combines accelerated stress tests with a detailed insight of the behaviour of single catalyst nanoparticles. Therefore this methodology offers a useful tool to screen the behaviour of fuel cell catalysts in an efficient way.

reasons for gradual performance losses, this topic only recently gained increased attention. In general the cause of catalyst degradation is related to a loss in accessible surface area of the active catalyst components.³ In addition, recent work also suggests that the de-alloying of Pt-alloy catalysts due to segregation and concomitant dissolution of non-noble components inflicts a continuous detrimental effect on the performance of low temperature fuel cells.^{8–10} For the loss in electrochemically active surface area (ECSA) of Pt in PEM fuel cells there are three fundamentally different mechanisms discussed.¹¹ That is Pt dissolution, the migration and concomitant coalescence of Pt nanoparticles on the carbon support, and the detachment of Pt nanoparticles from the support. Pt dissolution can be further sub-divided into two processes, resulting either in Pt re-deposition onto larger particles (electrochemical Ostwald ripening) or in the precipitation of Pt crystallites close to the membrane electrolyte due to reduction by hydrogen gas diffusing through the membrane. In addition to these three processes concerning Pt also the complete oxidation of the carbon support to carbon dioxide can occur under certain conditions, which results in the loss of electrical contact of the Pt nanoparticles. In general it is assumed that a combination of these mechanisms occurs and that the degradation resistance of a catalyst can be improved by supports less prone towards total oxidation, *i.e.* that the particle detachment is linked to the oxidation of the support to carbon dioxide. Therefore, conventional high surface area supports are replaced by graphitized or low surface area carbons.

In the presented work the degradation behavior of two Pt based electrocatalysts, labeled as catalysts I and II, on low surface area (LSA) carbon supports is compared to a Pt based catalyst with standard high surface area (HSA) carbon, called standard. The two catalysts pursue different degradation mitigation strategies. For catalyst I the LSA carbon support was used in its original form, for catalyst II the LSA carbon support was modified by a transition metal prior to Pt impregnation. The bare carbon supports are characterized towards their corrosion resistance in membrane electrode assembly (MEA) tests, which indicate that the corrosion resistance of the carbon support of both catalysts is quite similar. The degradation of the synthesized Pt based catalysts is scrutinized by a combination of electrochemical half-cell measurements and identical location transmission electron microscopy (IL-TEM).

2. Experimental

2.1. Catalyst samples

The three investigated catalysts consisted of Pt nanoparticles about 3 nm in size supported on different carbon supports. As standard a catalyst with standard HSA carbon and 46 wt% Pt content was used, catalyst I has 27.8 wt% Pt content and is supported on a LSA carbon (CI), catalyst II has 29.8 wt% Pt content and is supported on a LSA carbon (CII) which was additionally modified by a transition metal. Catalysts I and II were synthesized, including the transition metal modification, by BASF, Germany. The BET surface areas of the LSA carbons were 30 and 53 m² g⁻¹, for catalysts I and II, respectively. After modification, the BET surface area of the LSA carbon support utilized for the synthesis of catalyst II was reduced to 28 m² g⁻¹.

2.2. Stability test of carbon supports

The corrosion stability of the bare carbon supports was characterized in membrane electrode assembly (MEA) tests according to the procedure described in ref. 12. In short, carbon electrodes were prepared by casting a carbon/PTFE ink onto a highly hydrophobized carbon paper and subsequently hot-pressed together with a standard Pt-containing GDE (gas diffusion electrode) on a Celtec® membrane. The corrosion tests were carried out in 50 cm² single cell setups using specially coated graphite plates. The Pt-containing GDE acted as the reference and counter electrodes, whereas the carbon electrodes acted as working electrodes. The corrosion tests were performed at 1.2 V vs. RHE at 180 °C. The reference electrode was continuously purged by 10% H₂ in N₂ and the working electrode was purged by N₂ containing 5% water partial pressure. The carbon loss was determined by detecting the CO₂ release in the fuel cell exhaust.

2.3. Electrochemical half-cell measurements

The electrochemical measurements were conducted in a three-compartment electrochemical Teflon-cell,¹³ using a rotating disc electrode (RDE) setup (Radiometer Analytical, France) and a home-built potentiostat. A saturated Calomel electrode (SCE), separated by an electrolytic bridge from the working electrode compartment, was used in each experiment. However, all potentials are given with respect to the reversible hydrogen potential (RHE), which was measured for every experiment. A graphite rod was used as a counter electrode. The electrolyte, 0.1 M HClO₄, was prepared using Millipore Milli Q® water and concentrated HClO₄ (Suprapure; Merck, Germany). In order to prepare a catalyst suspension the catalyst powders were dispersed ultrasonically for at least 10 minutes in ultrapure Millipore Milli Q® water to a concentration of 0.14 mg_{Pt} ml⁻¹. Prior to preparation of a thin catalyst film onto the polished glassy carbon tip of a RDE, the catalyst suspension was sonicated for additional 3 minutes. Then 20 µl of the suspension were pipetted onto the RDE tip (5 mm diameter, 0.196 cm² geometrical surface area), resulting in a Pt loading of 14 µg_{Pt} cm⁻². The catalyst suspension on the glassy carbon electrode was dried in a nitrogen stream and the electrode tip was attached to a RDE. After transfer to the electrochemical cell, the tip was immersed under potential control at 0.05 V into argon-saturated 0.1 M HClO₄ solution. The potential was then continuously cycled between 0.05 V and 1.0 V until a stable cyclovoltammogram was recorded. All measurements were performed at room temperature with iR-compensation of the solution resistance. The ECSA was determined by CO-stripping in Ar purged solution, after saturating the surface with CO at a potential of 0.05 V. As degradation treatment the potential of the electrodes was cycled between 0.4 and 1.4 V_{RHE} with a scan speed of 1 V s⁻¹. Each treatment procedure consisted of 3600 cycles, corresponding to 2 h. In some cases the treatment was repeated. The ECSA was determined before, at halftime, and at the end of the treatment procedures.

2.4. Identical location transmission electron microscopy (IL-TEM)

For the IL-TEM¹⁴ investigations the catalyst suspension was diluted by a factor of 1 : 10. A gold finder grid (400 mesh; Plano,

Germany) was coated with an amorphous carbon film. The hydrophilicity of the carbon film, which is necessary for a uniform distribution of the catalyst particles, develops during a glow discharge exposure to an oxygen plasma. After this pre-treatment, 5 μl of catalyst suspension were pipetted onto the gold finder grid. In order to keep the catalyst loading as low as possible (to avoid overlapping of catalyst particles), the drop was delicately absorbed off the grid after approximately 10 seconds, using filter paper. The grid was dried, and then investigated using a JEM 2010 microscope (JEOL, Japan) with an accelerating voltage of 120 kV and a magnification of 150 k. TEM micrographs were recorded before and after the treatment procedures, *i.e.* 3600 potential cycles between 0.4 and 1.4 V_{RHE} with a scan rate of 1 V s^{-1} , on identical locations of the catalyst.

3. Results and discussion

3.1. Stability of bare carbon support materials

In order to investigate the intrinsic corrosion resistance of the carbon support materials MEA tests of the bare carbons were performed prior to the synthesis, *i.e.* supporting of Pt nanoparticles onto them. The carbon loss of the different samples determined by detecting the CO_2 release in the fuel cell exhaust is plotted in Fig. 1. It is seen that under the applied conditions in the first five hours all LSA carbon samples exhibit higher corrosion resistance than the standard HSA carbon Vulcan XC72 which loses 50% of its mass. Furthermore, it is obvious that the transition metal modification of the initially poorly performing LSA carbon CII leads to a considerably improved corrosion resistance. The decrease in mass over time is almost identical for the LSA carbon CI and the modified LSA carbon CII. Thus the resistance towards complete oxidation of their support materials is similar for both catalysts I and II.

3.2. Electrochemical characterization of ECSA loss

In order to determine the ECSA loss of the synthesized catalysts I and II upon accelerated degradation tests, they were exposed to potential cycling treatments in an electrochemical half-cell. The

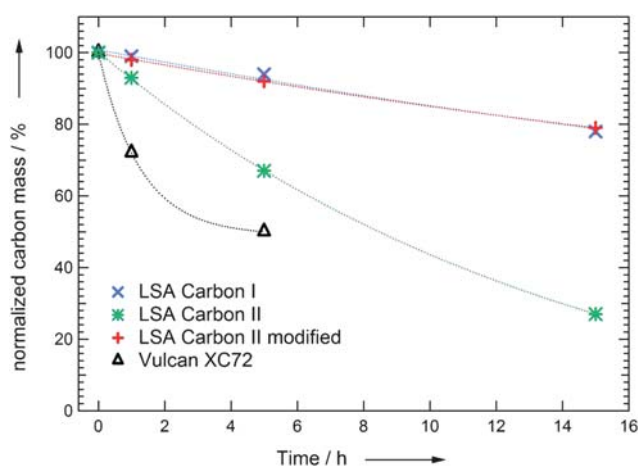


Fig. 1 Corrosion test of carbon supports before Pt impregnation. Dotted lines show exponential fits and are considered only as a guide for the eye.

treatments consisted of potential cycling between 0.4 and 1.4 V_{RHE} with a scan rate of 1 V s^{-1} . The cyclovoltammograms (CVs) of the particular catalysts in the initial state as well as after 2 and 4 hours of treatment are shown in Fig. 2. In its initial state the CV of catalyst I (Fig. 2a) exhibits the typical features of a Pt/C catalyst.¹⁵ The under potential deposition of hydrogen (H_{upd}) and the formation of OH and oxides on the Pt nanoparticles are well discernible and lie in the expected potential regions. Furthermore, it is evident from the reduced features in the CV that after potential cycling the ECSA of the catalyst is considerably decreased. By comparison the initial CV of catalyst II (Fig. 2b) clearly shows a modified signature and the typical Pt features are diminished due to the influence of the transition metal. Furthermore, the capacitance of the support is larger than for catalyst I. Based on the CVs the ECSA loss during degradation treatment is considerably inhibited compared to catalyst I. The inhibited Pt features, however, hamper a precise ECSA evaluation. In order to study the Pt surface area loss more accurately, CO stripping experiments were conducted (see ESI†). Thus determined ECSA values for the pristine catalysts are $52 \text{ m}^2 \text{ g}_{\text{Pt}}^{-1}$ and $67 \text{ m}^2 \text{ g}_{\text{Pt}}^{-1}$ for I and II, respectively. In Fig. 3 the ECSA loss due to the potential cycling treatment of the catalysts I and II is compared to the one of a standard high surface area Pt catalyst with similar particle size ($\sim 3 \text{ nm}$). Both electrocatalysts supported on a LSA carbon exhibit an improved performance in the degradation test compared to the standard catalyst. Furthermore, it is evident that catalyst II exhibits a much less

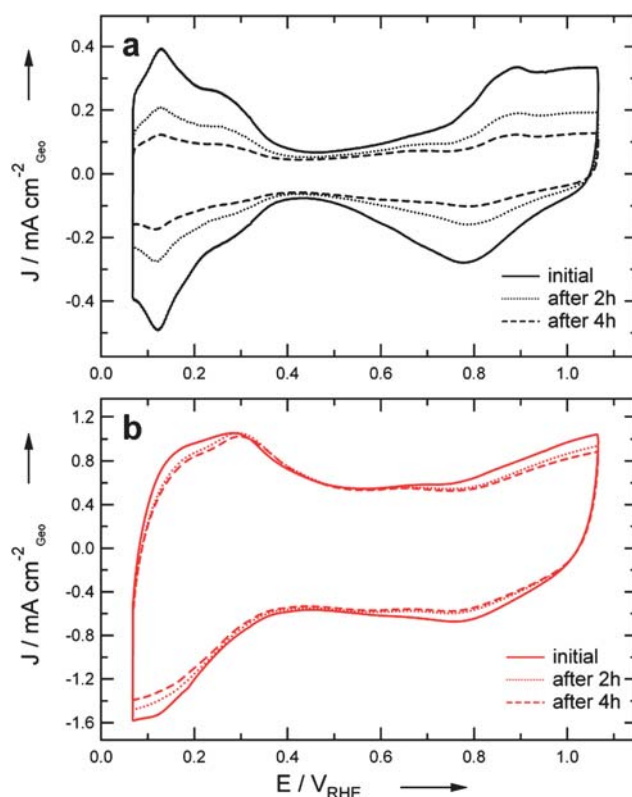


Fig. 2 CVs of catalyst I (a) and catalyst II (b) in their initial state as well as after 2 h and 4 h accelerated degradation treatment. The treatment consisted of potential cycling between 0.4 and 1.4 V_{RHE} at 1 V s^{-1} in argon saturated 0.1 M HClO_4 .

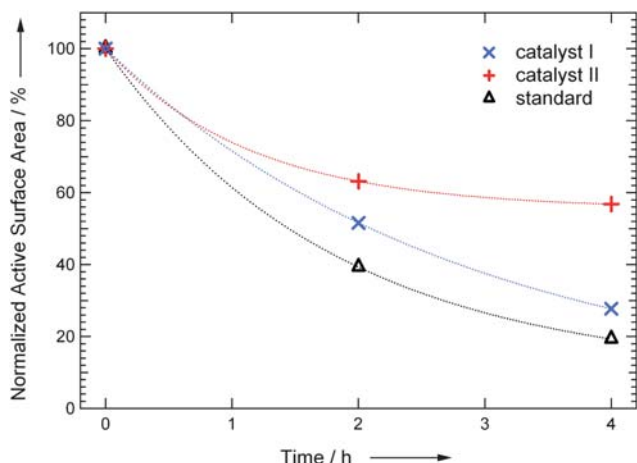


Fig. 3 ECSA loss of catalysts I and II due to accelerated degradation treatment by potential cycling between 0.4 and 1.4 V_{RHE} at $1 V s^{-1}$ determined by CO stripping measurements. Measurements of the standard catalyst are shown for comparison.

pronounced ECSA loss than catalyst I, especially after the first degradation treatment. The slowed-down ECSA loss in the second treatment indicates that catalyst II experiences an initial degradation process, but is afterwards stabilized. Catalyst I by comparison exhibits a continuous time-dependent degradation profile, similar as the standard catalyst, but inhibited.

3.3. IL-TEM analysis

In order to examine the degradation process in detail, IL-TEM measurements were performed. In accordance with the electrochemical determination of the ECSA loss, the TEM micrographs of identical locations of catalyst I before and after potential cycling (see Fig. 4) demonstrate that the accelerated degradation treatment results in a considerable reduction in the amount of Pt nanoparticles on the carbon support. It is noteworthy in this respect that after the treatment individual Pt particles can be found on the amorphous carbon film of the TEM grid indicating a particle detachment process rather than the dissolution of Pt

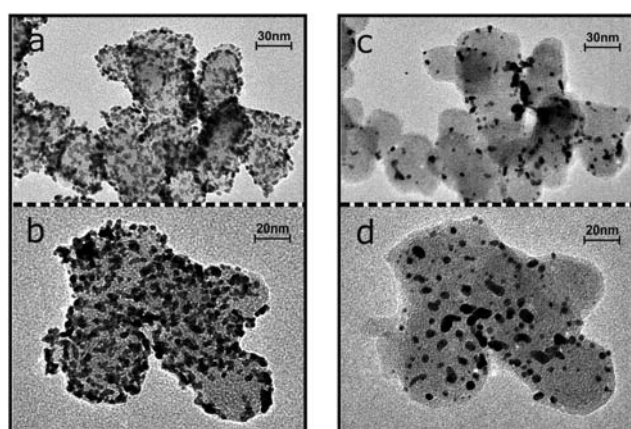


Fig. 4 IL-TEM of two representative areas of catalyst I before (a and b) and after (c and d) 2 h accelerated degradation treatment consisting of potential cycling between 0.4 and 1.4 V_{RHE} at $1 V s^{-1}$.

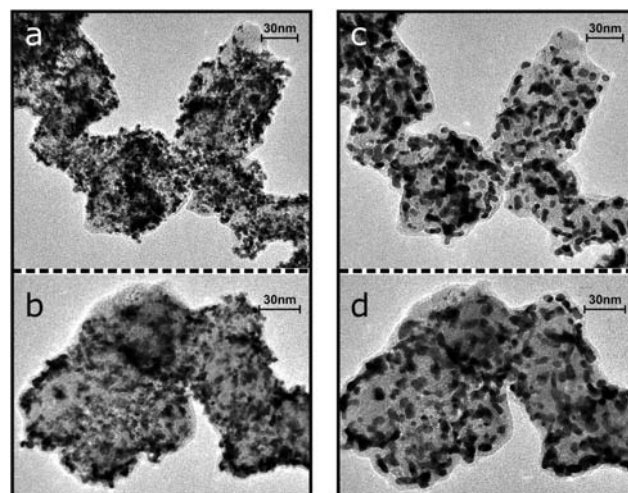


Fig. 5 IL-TEM of two representative areas of catalyst II before (a and b) and after (c and d) 2 h accelerated degradation treatment consisting of potential cycling between 0.4 and 1.4 V_{RHE} at $1 V s^{-1}$.

nanoparticles. At the same time no changes in the carbon support are discernible. In addition to particle detachment, the growth of larger Pt particles is evident as well. The formation of larger Pt nanoparticles seems to be increased in areas of high particle density. A preference for small particles to disappear,¹⁷ however, is not evident. The IL-TEM measurements thus indicate that under the applied accelerated degradation treatment the ECSA loss of catalyst I is a result of a particle detachment process superimposed by migration and coalescence and/or electrochemical Ostwald ripening. The particle detachment process on catalyst I is similar to the one observed in our previous study of a Pt catalysts with HSA carbon support.¹⁶ In the previous study, however, despite a larger ECSA loss the observed particle growth was considerably lower.

The IL-TEM micrographs of catalyst II are shown in Fig. 5. The micrographs of the identical locations of catalyst II clearly show that the loss in particles upon the accelerated degradation treatment is greatly reduced as compared to catalyst I. This finding is in line with the ECSA determination by CO stripping. While the loss in active material is considerably reduced and especially no significant particle detachment is apparent from the IL-TEM measurements, some changes in the catalyst are discernible. As an effect of the treatment, small Pt particles coalesce and form larger particles similar to a melting process. The large particles seem to be stabilized on the carbon support. As for catalyst I, for catalyst II no significant change in the carbon support is observed upon the treatment.

3.4. Comparison of the catalysts

Compared to the standard, catalysts I and II exhibit an improved performance in terms of ECSA loss. By comparison to the previous IL-TEM investigations¹⁶ the measurements indicate that the main degradation mechanism of particle detachment upon cycling treatment is still active for catalyst I with a conventional LSA carbon support. Most loss in ECSA is correlated to particle detachment, not Pt dissolution, in line with the observation of Pt particles on the carbon film of the TEM

grids after treatment. In addition to particle detachment, there is a second, minor mechanism active, which is responsible for the Pt particle growth. Although it is difficult to distinguish between Pt dissolution and re-deposition, *i.e.* electrochemical Ostwald ripening, and a particle migration and coalescence mechanism, the fact that no preferential disappearance of small Pt particles is observed supports a migration and coalescence mechanism.^{18,19}

By comparison, the properties of catalyst II with a transition metal modified LSA carbon support are fundamentally changed. The combination of the ECSA loss determination together with the IL-TEM investigations unambiguously shows that the Pt nanoparticles are stabilized on the support. The particle detachment process is considerably inhibited and is not the main degradation mechanism anymore. Upon the accelerated degradation treatment the catalyst initially experiences a pronounced degradation (however, less than the other catalysts), but is then stabilized. The IL-TEM investigations indicate that the initial degradation is a result of the fusion of adjacent Pt particles to form larger stabilized particles. Hence, this process slows down with time—as would be expected—and thus leads to a considerable inhibition of the ECSA loss as observed in the second treatment of the electrochemical measurement. As for catalyst I the distinction between Ostwald ripening, and particle migration and coalescence is difficult, but no preferential disappearance of small Pt particles is observed.

Interestingly, the corrosion tests of the pure carbon supports demonstrate that the resistance of the CI carbon and the modified CII carbon towards complete oxidation to carbon dioxide is almost identical. This finding indicates that the complete oxidation of the carbon support to carbon dioxide does not play a decisive role in the particle detachment process, which is observed on catalyst I but not on catalyst II. This interpretation is consistent with the fact that in the IL-TEM measurements no change in the carbon support is apparent upon cycling treatment.

4. Conclusion

In conclusion, the behavior of two different electrocatalysts developed for degradation mitigation has been investigated by means of electrochemical and IL-TEM measurements. The carbon supports of both catalysts, a conventional and a transition metal modified LSA carbon, exhibit a similar corrosion resistance towards complete oxidation to carbon dioxide. The synthesized catalysts of similar Pt loadings and particle size, however, show a distinctively different degradation behavior. Upon exposure to accelerated degradation treatments the catalyst with an unmodified LSA carbon support exhibits a somewhat improved degradation resistance as compared to a standard. The mechanism responsible for the major loss in active surface area, *i.e.* a particle detachment process, however, is the same as that found in the previous studies. By comparison, the transition metal modified carbon support clearly leads not only to an inhibited ECSA loss, but furthermore results in

a drastic change of the main degradation mechanism. The results indicate that after an initial degradation caused by the fusion of adjacent particles, the catalyst is stabilized against further treatment. The particle detachment process is successfully suppressed. Interestingly, the suppression of particle detachment is not correlated to the resistance of the support towards the complete oxidation to carbon dioxide.

Acknowledgements

This work was supported by the German DFG through the Emmy-Noether project ARE852/1-1. Katrin Hartl acknowledges the German FCI for a chemistry funds scholarship. Dr. Ekkehard Schwab and Dr. Claudia Querner of BASF are acknowledged for the supply of the catalyst samples and the carbon corrosion tests.

References

- 1 T. R. Ralph and M. P. Hogarth, *Platinum Met. Rev.*, 2002, **46**, 3–14.
- 2 J. Greeley, I. E. L. Stephens, A. S. Bondarenko, T. P. Johansson, H. A. Hansen, T. F. Jaramillo, J. Rossmeisl, I. Chorkendorff and J. K. Nørskov, *Nat. Chem.*, 2009, **1**, 552–556.
- 3 R. Borup, J. Meyers, B. Pivovar, Y. S. Kim, R. Mukundan, N. Garland, D. Myers, M. Wilson, F. Garzon, D. Wood, P. Zelenay, K. More, K. Stroh, T. Zawodzinski, J. Boncella, J. E. McGrath, M. Inaba, K. Miyatake, M. Hori, K. Ota, Z. Ogumi, S. Miyata, A. Nishikata, Z. Siroma, Y. Uchimoto, K. Yasuda, K. I. Kimijima and N. Iwashita, *Chem. Rev.*, 2007, **107**, 3904–3951.
- 4 H. A. Gasteiger, S. S. Kocha, B. Sompalli and F. T. Wagner, *Appl. Catal. B*, 2005, **56**, 9–35.
- 5 S. Mukerjee and S. Srinivasan, *J. Electroanal. Chem.*, 1993, **357**, 201–224.
- 6 V. R. Stamenkovic, B. S. Mun, M. Arenz, K. J. J. Mayrhofer, C. A. Lucas, G. F. Wang, P. N. Ross and N. M. Markovic, *Nat. Mater.*, 2007, **6**, 241–247.
- 7 P. Mani, R. Srivastava and P. Strasser, *J. Phys. Chem. C*, 2008, **112**, 2770–2778.
- 8 H. R. Haas and M. T. Davis, *ECS Trans.*, 2009, **25**, 1623–1631.
- 9 K. J. J. Mayrhofer, V. Juhart, K. Hartl, M. Hanzlik and M. Arenz, *Angew. Chem., Int. Ed.*, 2009, **48**, 3529–3531.
- 10 K. J. J. Mayrhofer, K. Hartl, V. Juhart and M. Arenz, *J. Am. Chem. Soc.*, 2009, **131**, 16348–16349.
- 11 P. J. Ferreira, G. J. la O', Y. Shao-Horn, D. Morgan, R. Makharia, S. Kocha and H. A. Gasteiger, *J. Electrochem. Soc.*, 2005, **152**, A2256–A2271.
- 12 T. J. Schmidt, *ECS Trans.*, 2006, **1**, 19–31.
- 13 K. J. J. Mayrhofer, G. K. H. Wiberg and M. Arenz, *J. Electrochem. Soc.*, 2008, **155**, P1–P5.
- 14 K. J. J. Mayrhofer, S. J. Ashton, J. C. Meier, G. K. H. Wiberg, M. Hanzlik and M. Arenz, *J. Power Sources*, 2008, **185**, 734–739.
- 15 T. J. Schmidt, H. A. Gasteiger, G. D. Stab, P. M. Urban, D. M. Kolb and R. J. Behm, *J. Electrochem. Soc.*, 1998, **145**, 2354–2358.
- 16 K. J. J. Mayrhofer, J. C. Meier, S. J. Ashton, G. K. H. Wiberg, F. Kraus, M. Hanzlik and M. Arenz, *Electrochem. Commun.*, 2008, **10**, 1144–1147.
- 17 Y. Shao-Horn, W. C. Sheng, S. Chen, P. J. Ferreira, E. F. Holby and D. Morgan, *Top. Catal.*, 2007, **46**, 285–305.
- 18 C. G. Granqvist and R. A. Buhrman, *J. Catal.*, 1976, **42**, 477–479.
- 19 M. S. Wilson, F. H. Garzon, K. E. Sickafus and S. Gottesfeld, *J. Electrochem. Soc.*, 1993, **140**, 2872–2877.

6.3 Bimetallic Particles for Electrocatalysis

The application of bimetallic catalysts in fuel cells is beneficial in two respects: first of all, the amount of platinum can be reduced and secondly, it has been shown that alloying of platinum with other transition metals enhances the specific activity towards the oxygen reduction reaction by a factor of about 2-3 compared to pure platinum [6, 7, 8, 9]. Both aspects contribute to an improved mass activity of the catalyst which is most important regarding the commercial application of fuel cells. The reason for the activity enhancement is usually ascribed to geometrical modifications like a decreased Pt-Pt bond distance and changes in the electronic structure with respect to an increased Pt d-band vacancy [4]. Furthermore, there are reports about the stability of platinum bimetallic nanoparticles to be superior to the one of plain platinum [52].

Ideally, only the catalytically active metal of a bimetallic particle is located at the surface where the reactions take place. Therefore, core-shell systems consisting of an inexpensive core surrounded by a platinum shell are promising candidates as fuel cell catalysts.

In this chapter, two different approaches with respect to bimetallic core-shell electrocatalysts are presented and characterized. The first one is an unsupported chemically synthesized Au-Pt core-shell catalyst with an average particle diameter of about 30 nm which exhibits an activity comparable to Pt bulk material. The other one is a commercial carbon supported Pt-Co alloy catalyst with a particle size of 4-5 nm, from which a core-shell structure is electrochemically induced by surface segregation, resulting in a highly active oxygen reduction catalyst. Afterwards, the stability of the in-situ generated core-shell structure, as well as the core-shell structure of the same alloy catalyst generated by chemical leaching, is investigated by cyclic voltammetry in alkaline solution.

6.3.1 AuPt core-shell nanocatalysts with Pt bulk activity

As mentioned above, high activity and a low amount of platinum represent two major requirements for commercially viable electrocatalysts. One promising approach in this respect is the application of core-shell particles, where the catalytically active material is located at the surface of an inner core of a different composition [69, 70, 10]. The core-shell concept facilitates a high utilization of Pt and by-passes the unfavorable particle size effect of Pt nanoparticles [4, 66].

One highly active core-shell catalyst described in the literature consists of a gold core and a platinum shell [71, 72]. The synthesis of these particles is typically performed by an electrochemical underpotential deposition of a copper monolayer onto gold nanoparticles. Subsequently, copper is replaced by the more noble platinum in a

spontaneous redox process [71]. The copper adlayer is thereby oxidized by Pt cations in the electrolyte, which are reduced and simultaneously deposited. Considering the necessity of potential control during the whole procedure and its intricateness, its drawback is obvious: this synthesis procedure is not upscalable for commercial applications.

In the following paper, a new synthesis procedure for AuPt core-shell particles is introduced which distinguishes itself as being upscalable and uses only basic chemicals. The synthesis of the particles, which was conducted by a cooperation partner, was thereby optimized based on their characterization using TEM analysis and RDE measurements. In this respect, cyclic voltammetry is proven to be a powerful surface sensitive technique for the investigation of the surface composition of a bimetallic system. After first poor results, the synthesis route was optimized leading to uniform, flat, and complete Pt layers around a spherical gold core. Electrocatalytic measurements showed that the specific activity of these particles towards the oxygen reduction reaction equals the one of polycrystalline Pt.

AuPt core-shell nanocatalysts with Pt bulk activity

K. Hartl, K.J.J. Mayrhofer, M. Lopez, and M. Arenz

Electrochemistry Communications, 2010, Volume 12, Issue 11, Pages 1487-1489

Permanent weblink:

<http://dx.doi.org/10.1016/j.elecom.2010.08.013>

Reprinted from Electrochemistry Communications, 12, 11, K. Hartl, K.J.J. Mayrhofer et al., AuPt core-shell nanocatalysts with Pt bulk activity, 1487, Copyright (2010), with permission from Elsevier.



AuPt core–shell nanocatalysts with bulk Pt activity

Katrin Hartl ^{a,e}, Karl J.J. Mayrhofer ^b, Marco Lopez ^c, Dan Goia ^d, Matthias Arenz ^{e,*}

^a Technische Universität München, Germany

^b Max Planck Institute for Iron Research, Germany

^c Umicore AG & Co KG, Germany

^d Clarkson University, USA

^e University of Copenhagen, Department of Chemistry, Universitetsparken 5, 2100 Copenhagen, Denmark

ARTICLE INFO

Article history:

Received 3 August 2010

Received in revised form 13 August 2010

Accepted 16 August 2010

Available online 22 August 2010

Keywords:

Core–shell catalyst

Oxygen reduction reaction

Fuel cell

ABSTRACT

In the presented work, the evaluation of an unsupported AuPt core–shell catalyst for the oxygen reduction reaction is introduced. Applying only basic chemicals in an upscalable synthesis route, it is demonstrated that uniform, flat, and complete Pt layers around a spherical Au core are obtained. The electrocatalytic measurements show that the surface area specific activity of the AuPt core–shell catalyst towards the important oxygen reduction reaction equals the one of polycrystalline bulk Pt. To our knowledge, this is the first time that the unfavorable particle size effect of Pt nanoparticles could be by-passed for a nanoscale catalyst.

© 2010 Elsevier B.V. All rights reserved.

1. Introduction

Energy conversion technology, in particular with regard to powering automobiles, is the challenge of the 21st century. With crude oil reserves being constrained and too valuable to be burned as fossil fuels, an efficient alternative must be found in the near future. One contemplated scenario is to store or generate onboard electric energy by batteries or fuel cells and to use electrical power-trains. However, in order to render PEMFCs commercially viable for such demanding large scale applications, the improvement of electrocatalysts for the cathodic oxygen reduction reaction (ORR) is crucial. The application of core–shell particles, where the catalytically active metal is located at the surface of an interior of a different composition, is a promising approach in this respect [1–6].

2. Experimental

The core–shell AuPt particles were obtained from Umicore AG & Co KG. They were synthesized according to processes developed by Clarkson University in cooperation with Umicore [7]. Stable dispersions of highly crystalline gold nanoparticles made according to the procedure reported by Goia et al. [8] were used as core material in the first step. The size of the obtained gold nanoparticles was approx. 30 nm. In a subsequent step, an amount of platinum equivalent to 20% of the weight of gold was added as hexachloroplatinic acid solution to the gold dispersion, which was then heated to 70–80 °C. At this

temperature, Pt(IV) species were reduced by adding 0.01 M ascorbic acid solution to reduce the Pt under gentle mixing.

The TEM micrographs were recorded with a JEOL JEM 2010 instrument at Clarkson University. The carbon supported high surface area catalysts were supplied by Umicore AG & Co KG. The electrochemical measurements were conducted in a three-compartment electrochemical Teflon-cell, using a fully automated rotating disk electrode setup (Radiometer Analytical, France) with a home built potentiostat. A saturated Calomel electrode and a graphite rod were used as reference and counter electrode, respectively. The electrolyte was prepared using Millipore Milli Q® water and HClO₄ (Suprapure; Merck, Germany).

3. Results and discussion

The AuPt nanocatalyst was synthesized using a two-step wet chemical process consisting of the preparation of the Au core particles in the first, and the deposition of a continuous thin Pt shell in the second. The size of the obtained AuPt particles is ~30 nm, so that for the investigated composition of 80 wt.% Au/20 wt.% Pt, the platinum shell consists of approximately three atomic layers. The obtained core–shell particles are displayed in Fig. 1a. For comparison, the same composition AuPt core–shell particles without uniform layer by layer deposition but formation of Pt clusters on the Au shell are shown as well (Fig. 1b). The synthesis of uniform Pt layers is also evident in the electrochemical characterization. In the cyclic voltammogram (see Fig. 1c) of the uniform core–shell nanocatalyst only typical Pt features can be observed, whereas in the case of a fragmented Pt shell with small Pt clusters characteristic Au oxidation and reduction peaks occur

* Corresponding author. Tel.: +45 353 20002.

E-mail address: m.arenz@kemi.ku.dk (M. Arenz).

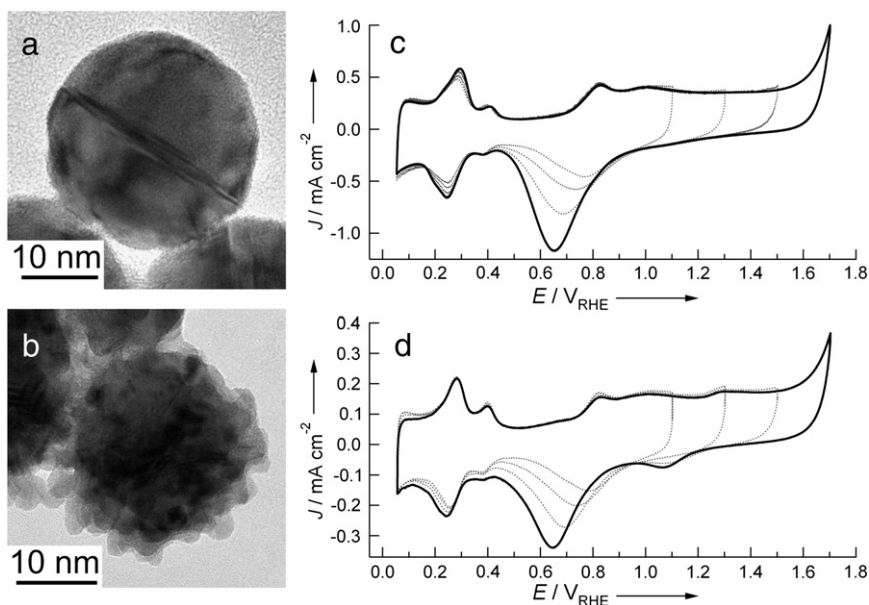


Fig. 1. TEM micrographs (a,b) and cyclic voltammetry (CV) (c,d) of AuPt core-shell particles with a closed shell (a,c) and with a fragmentary shell (b,d).

at 1.3 and 1.05 V_{RHE} [9], respectively (see Fig. 1d), indicating that both Pt and Au are electrochemically accessible at the particle surface.

The electrocatalytic performance of the ORR is evaluated in thin film rotating disk electrode (RDE) measurements, with normalization of the reaction rate to the catalyst surface area (specific activity, SA) as well as to the applied catalyst mass (mass activity, MA). Therefore, first the Pt surface area of the catalyst was determined for a series of samples with different loadings in so-called CO-stripping experiments by oxidizing a pre-adsorbed CO adlayer (see Fig. 2). From the slope of the linear relationship of the measured charge density with the applied catalyst loading the electrochemically active surface area (ECA) can be calculated (inset of Fig. 2). Assuming a charge density of $390 \mu\text{C cm}^{-2}$ for CO oxidation ($2e^-$) on polycrystalline Pt [10], the slope corresponds to an ECA of $28.2 \text{ m}^2/\text{g}_{\text{Pt}}$ for the AuPt nanocatalyst. It is noteworthy in this respect that the linear relationship is an essential criterion indicating that for all applied catalyst loadings the whole catalyst surface is electrochemically accessible.

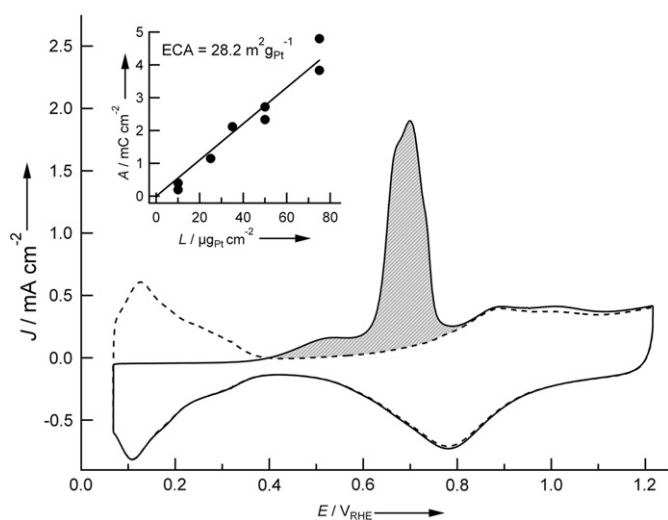


Fig. 2. CO-stripping experiment with following CV (dashed line) for AuPt core-shell particles with a loading of $37.5 \mu\text{g}_{\text{Pt}} \text{ cm}^{-2}$. The shaded area indicates the charge corresponding to the surface area of the catalyst. The inset shows the determination of the ECA by a linear fit of the plot of active surface area values against the referring catalyst loadings L .

In order to determine the kinetics of the oxygen reduction reaction, polarization curves in oxygen saturated 0.1 M HClO_4 electrolyte were recorded for different catalyst loadings. The Tafel plot of a representative measurement is depicted in Fig. 3 together with measurements of two state-of-the-art carbon supported high surface area Pt and Pt_3Co catalysts. For different loadings of the AuPt catalyst an average SA of 2.06 mA cm^{-2} is obtained at $0.90 V_{\text{RHE}}$. Note, that the relatively high standard deviation (see inset) originates from the fact that at $0.90 V_{\text{RHE}}$, where the SA is typically assessed in literature, the ORR current for the AuPt system almost reaches the diffusion-limited potential region. For such highly active systems it would thus be more appropriate to compare the current densities at $0.925 V_{\text{RHE}}$.

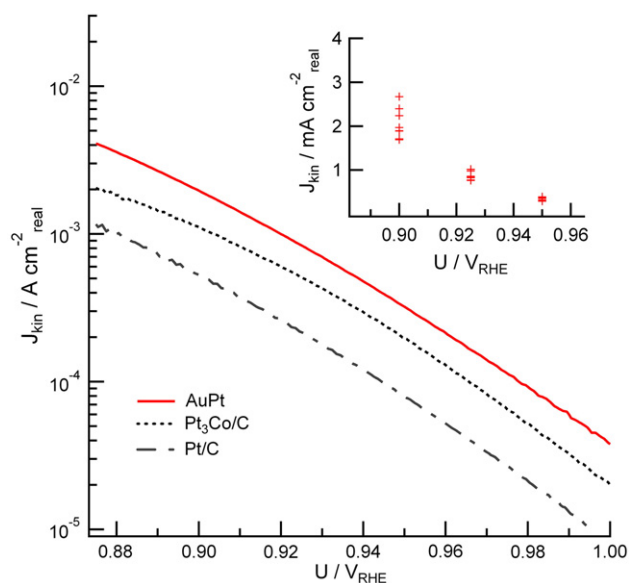


Fig. 3. Tafel plots of the specific ORR activities of the AuPt core-shell particles, in comparison to two state-of-the-art carbon supported catalysts (Pt/C and $\text{Pt}_3\text{Co}/\text{C}$). The inset shows the SA of AuPt for different catalyst loadings ranging from 10 to $75 \mu\text{g}_{\text{Pt}} \text{ cm}^{-2}$; from the respective eight individual measurements it can be seen that the statistical error at $0.9 V_{\text{RHE}}$ is much higher than at 0.925 or $0.95 V_{\text{RHE}}$, due to the fact that the measured current in the RDE measurements approaches the diffusion-limited value.

Table 1

Comparison of the electrochemical surface area ECA and the ORR activities in 0.1 M HClO₄ expressed as specific activities (SA) at 0.9 and 0.925 V_{RHE} and mass activities (MA) at 0.9 V_{RHE} of different electrode samples. The errors of the SA and ECA for the AuPt catalyst are standard deviations of eight individually measured values. The MA error is calculated using these values.

	AuPt	Pt poly	Pt/C	Pt ₃ Co/C
SA @ 0.9 V _{RHE} [mA cm ⁻²]	2.06 ± 0.35	2.1	0.54	1.05
SA @ 0.925 V _{RHE} [mA cm ⁻²]	0.88 ± 0.10	0.84	0.22	0.50
MA @ 0.9 V _{RHE} [A mg _{Pt} ⁻¹]	0.58 ± 0.10	Not defined	0.53	0.81
ECA [m ² /g _{Pt}]	28.2 ± 1.3	Not defined	98.5	77.5

In Table 1 the catalytic activity for the ORR of the AuPt nanoparticles is compared to state-of-the-art carbon supported high surface area Pt and Pt₃Co catalysts and, as a benchmark, bulk Pt. The SA of the AuPt is equal to that of polycrystalline Pt, while, in line with previous reports, the carbon supported Pt and Pt₃Co catalysts exhibit a SA reduced by a factor of approximately 4 and 2, respectively. To our knowledge, this is the first time that on a nanoparticle system the SA of polycrystalline bulk Pt could be conserved, which is not even the case for Pt black catalysts, see ref. [11]. Gasteiger et al. therein report a SA of unsupported Pt black particles in the size range of 30–50 nm reduced by the factor of 2 compared to polycrystalline Pt, which could be confirmed in our laboratory. It has to be noted, however, that due to the large particle size in this AuPt core–shell model catalyst, the mass activity is slightly lower than for the state-of-the-art Pt₃Co sample supplied by Umicore. Still, the AuPt core–shell catalysts evaluated represent a promising model system for a new concept of PEM fuel cell electrocatalysts with great potential. Compared to results for carbon supported Pt-alloy systems previously reported from other research groups, the mass activity of the AuPt core–shell catalyst is even slightly improved (0.49 A mg_{Pt}⁻¹ obtained for Pt₂₀Cu₂₀Co₆₀/C at 0.9 V_{RHE} [4]).

Future studies have to be directed towards catalyst optimization by varying the particle size, shell thickness and, certainly, the core material. For instance, a non-noble metal core can be used instead of gold in order to reduce material costs, as long as its degradation properties are acceptable [12].

4. Conclusions

We present the electrocatalytic evaluation of an unsupported core–shell catalyst with superior characteristics. The resulting AuPt

core–shell catalysts exhibit an outstanding SA towards the oxygen reduction reaction, thus offering great potential for further improvements in the performance and the costs of PEM fuel cells. The measurements show that an equal specific activity towards the oxygen reduction reaction as for polycrystalline Pt could be achieved for a nanoscale catalyst, thus by-passing the unfavorable particle size effect of Pt nanoparticles [11,13]. Moreover, the synthesis methods developed by Clarkson University and Umicore AG & Co KG [7] yield highly uniform, flat, and complete Pt layers around a metal core. At the same time it stands out by being upscalable to larger amounts for industrial applications, and by using only basic chemicals.

Acknowledgement

This work was supported by the DFG through the Emmy-Noether project ARE852/1-1 and Umicore AG & Co KG. Katrin Hartl thanks the German FCI which supports her with a Chemie Fonds Scholarship.

References

- [1] J. Zhang, F.H.B. Lima, M.H. Shao, K. Sasaki, J.X. Wang, J. Hanson, R.R. Adzic, *Journal of Physical Chemistry. B* 109 (2005) 22701.
- [2] J.L. Zhang, M.B. Vukmirovic, Y. Xu, M. Mavrikakis, R.R. Adzic, *Angewandte Chemie. International Edition* 44 (2005) 2132.
- [3] M. Inaba, *ECS Transactions* 25 (2009) 573.
- [4] R. Srivastava, P. Mani, N. Hahn, P. Strasser, *Angewandte Chemie. International Edition* 46 (2007) 8988.
- [5] J. Greeley, I.E.L. Stephens, A.S. Bondarenko, T.P. Johansson, H.A. Hansen, T.F. Jaramillo, J. Rossmeisl, I. Chorkendorff, J.K. Nørskov, *Nature Chemistry* 1 (2009) 552.
- [6] K.J.J. Mayrhofer, V. Juhart, K. Hartl, M. Hanzlik, M. Arenz, *Angewandte Chemie. International Edition* 48 (2009) 3529.
- [7] WO 2008/025750A1, WO 2008/025751A1 (to Umicore AG & Co KG).
- [8] D. Andrescu, T.K. Sau, D.V. Goia, *Journal of Colloid and Interface Science* 298 (2006) 742.
- [9] L.D. Burke, P.F. Nugent, *Gold Bulletin* 30 (1997).
- [10] K.J.J. Mayrhofer, D. Strmcnik, B.B. Blizanac, V. Stamenkovic, M. Arenz, N.M. Markovic, *Electrochimica Acta* 53 (2008) 3181.
- [11] H.A. Gasteiger, S.S. Kocha, B. Sompalli, F.T. Wagner, *Applied Catalysis B: Environmental* 56 (2005) 9.
- [12] K.J.J. Mayrhofer, K. Hartl, V. Juhart, M. Arenz, *Journal of the American Chemical Society* 131 (2009) 16348.
- [13] K.J.J. Mayrhofer, B.B. Blizanac, M. Arenz, V.R. Stamenkovic, P.N. Ross, N.M. Markovic, *The Journal of Physical Chemistry. B* 109 (2005) 14433.

6.3.2 Adsorbate-Induced Surface Segregation for Core-Shell Nanocatalysts

Alloys of platinum with other non-noble transition metals are a promising class of electrocatalysts regarding their higher activity at lower costs compared to pure platinum catalysts [6, 7, 8, 9]. Polycrystalline Pt₃Co exhibits the highest specific activity among the alloys of platinum with other non-noble transition metals of this kind [6]. In order to guarantee an optimal utilization only the catalytically active Pt metal should be present at the surface where the reactions take place. Furthermore, as cobalt is not stable upon acid contact it would otherwise be leached from the surface [73]. The thereby generated cobalt ions might diffuse into the membrane electrolyte and lead to severe problems like a decreased conductivity [4]. Therefore, this kind of catalyst is typically exposed to a pre-leaching procedure before its application in a fuel cell. By treating the catalyst with concentrated acid at elevated temperatures, cobalt is dissolved and completely removed from the surface [70].

However, Stamenkovic *et al.* showed that the surface composition of such alloys can be modified into a Pt top-layer by temperature annealing of bulk material. Furthermore, there are reports about a change of surface composition of alloys in response to reactive environments [74]. Concerning the latter study, Tao *et al.* observed reversible segregation processes of Rh-Pd alloy nanoparticles in response to oxidizing and reducing reactive environments in the gas phase.

In order to displace cobalt atoms from the surface of a commercial Pt₃Co/C electrocatalyst into the interior core, an in-situ adsorbate-induced surface segregation procedure was developed. The decisive part of the process is the exposure of the alloy catalyst to a carbon monoxide environment. This treatment can be accomplished in two ways: first, the catalyst can be modified in a gas phase treatment. The catalyst is thereby placed into a rotary evaporator which is filled with ambient pressure of CO and heated to 473K for three hours. At this temperature, no corrosion of the carbon support takes place. Secondly, an electrochemical treatment can be applied. Thereby, the catalyst is dried onto a glassy carbon disc electrode and subjected to potential cycling in CO-saturated alkaline electrolyte for 60 min. The potential is cycled with a slow scan rate from potentials within the H_{upd}-range until the initial part of the CO oxidation. This treatment is known to induce a structural change of the surface creating a flatter surface and a concomitant reduction of defect sites [75, 76]. Related to the similar temperature induced effect, this process is called "CO annealing".

Both treatments lead to core-shell particles consisting of a Pt shell around an alloy core. The modification can be followed by cyclic voltammetry in alkaline solution due to vanishing of characteristic cobalt features in the cyclovoltammogram and the

CO-stripping curve. The activity of these particles is even higher than the one of the leached catalyst leading to an improvement compared to the standard Pt catalyst by a factor of 2-3. In further studies it could be shown by analytic measurements using ICP-OES that other than for the leaching process no traces of cobalt can be found in the electrolyte. This finding confirms the induced segregation mechanism. The difference in activity between the leached and the CO annealed catalyst could be due to an enrichment of cobalt in the upper layers below the Pt top layer, as was also found for bulk alloys [6].

In the following paper, the preparation procedures, the characterization and a comparison of the activities of Pt₃Co/C core-shell catalysts are illustrated.

Adsorbate-Induced Surface Segregation for Core-Shell Nanocatalysts

K.J.J. Mayrhofer, V. Juhart, K. Hartl, M. Hanzlik, and M. Arenz

Angewandte Chemie International Edition, 2009, Volume 48, Issue 19, Pages
3529 - 3531

Permanent weblink:

<http://dx.doi.org/10.1002/anie.200806209>

This is the pre-peer reviewed version of the following article: *Angew. Chem. Int. Ed.* (2009) 48, 19, 3529; reproduced with permission from Wiley-VCH.

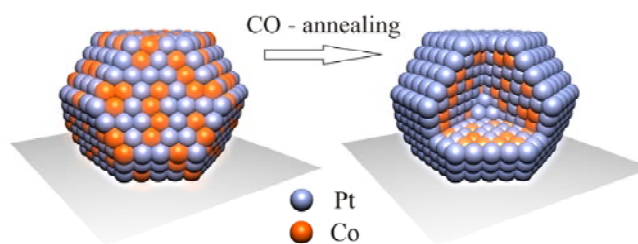
Adsorbate-induced surface segregation for core-shell nanocatalysts

Karl J.J. Mayrhofer ^{*}, Viktorija Juhart, Katrin Hartl, Marianne Hanzlik and Matthias Arenz ^{*}

A reduction in the amount of noble metal in catalysts is of great importance for many industrial applications considering the continuously rising price of precious metals. One approach is to decrease the size of catalyst particles down into the nanometer range, in order to primarily increase the specific surface area per mass, but also to benefit from a change in the electronic structure ^[1]. Core-shell catalyst structures containing an inexpensive, non-noble core surrounded by a noble metal shell can bring about further improvements in this respect. Ideally, only the catalytically active metal is located at the surface on which reactions take place to guarantee an optimal utilization; while the reaction rate should not suffer from the inactive core material. For alloys of Pt with other transition metals, a promising class of fuel cell cathode catalyst ^[2,3], core-shell structures can be achieved by either high-temperature annealing ^[4], chemical leaching of the non-noble material ^[5], or electrochemical deposition techniques ^[6,7]. All of these methods, however, exhibit significant disadvantages including the loss in active surface area and material, the formation of an incomplete noble metal shell, and the necessity for potential control during preparation. We present a novel preparation procedure of such core-shell nanoparticles with a Pt-shell that overcomes all these issues by using an adsorbate-induced surface segregation effect.

It is well known in literature that depending on the heat of segregation and the surface mixing energy, the composition of the surface of a bimetallic system can be very different from the bulk ^[8]. This effect is additionally dependant upon the chemical potential of the gas phase, since strong bonding of adsorbates will result in a gain in energy of the system. As a consequence, for bimetallic systems an enrichment at the surface of the component that binds a certain adsorbate more strongly may occur ^[9-11]. Here, this process was applied to modify an un-leached, carbon supported Pt₃Co alloy high surface area catalyst (HSAC) in order to increase the utilization of Pt in the particles with an average diameter of approximately 5 nm. For this purpose the catalyst was subject to either a gas phase treatment, or an electrochemical treatment in a three-electrode cell.

In the first case the plain catalyst powder was placed into a rotary evaporator, which was then repeatedly evacuated and filled with CO to eliminate residual oxygen. The distiller was then filled with ambient pressure of CO and heated to 200 °C for three hours. This temperature was sufficiently high to accelerate the surface segregation process without initiating the corrosion of the carbon support (see supporting information). For the electrochemical treatment a suspension of the catalyst was dried onto a rotating disc working electrode (RDE), which was then subjected to a potential cycling in CO saturated alkaline electrolyte, so-called CO-annealing ^[12]. Since the adsorption enthalpy of CO on Pt is somewhat higher than on Co ^[13], Pt segregates to the surface of the nanoparticles, and correspondingly displaces Co to the core. Both applied methods lead to the same core-shell structure, i.e. when the adsorbed CO becomes fully oxidized a Pt_xCo_y alloy core with a Pt-shell structure remains (see scheme 1).



Scheme 1. Adsorbate-induced surface segregation on bimetallic nanoparticles.

Such a surface annealing effect can be easily observed on polycrystalline and single crystal model systems using surface sensitive techniques, for instance low-energy ion scattering ^[14-16], however, for the applied high surface area catalysts it is in general more complicated. In order to determine the surface condition of the catalyst nanoparticles, we used cyclic voltammetry in alkaline electrolyte as a surface sensitive tool. By analysis of the adsorption/desorption properties in argon purged electrolyte and comparison to a plain Pt HSAC (see Figure 1A), it is evident that the pre-treated catalyst surface consists of both, Pt and Co atoms, whilst after CO-annealing a Pt-shell layer containing no Co atoms has been formed on the particle surface. The broad current peaks observed at a potential of 0.7 V_{RHE} in the anodic and 0.5 V_{RHE} in the cathodic scan ascribed to the oxidation of Co²⁺ on the surface to Co³⁺ ^[17-19], are no longer present after the treatment with CO, so that the latter CV is closely resembling that of Pt. Moreover, the findings from the CO-stripping experiment (Figure 1B) are consistent with a change in the surface composition. The early onset of the oxidation of adsorbed CO and the additional oxidation peak at low potentials (0.4 V_{RHE}) are an unambiguous sign of Co surface atoms. In comparison, the CO-annealed catalyst behaves like a plain Pt HSAC and is inferior in oxidizing the adsorbed CO, due to the lack of bifunctional reaction centres.

[*] Dr. K.J.J. Mayrhofer, M.Sc. V. Juhart, M.Sc. K. Hartl, Dr. M. Hanzlik[†], Dr. M. Arenz
Physikalische Chemie
[†] Institut für Elektronenmikroskopie
Technische Universität München
Lichtenbergstr.4, D-85748 Garching
Tel: (+49) 89289 13294; Fax: (+49) 89289 13389
Corresponding author's e-mail addresses:
karl.mayrhofer@mytum.de; matthias.arenz@mytum.de
Homepage: <http://www.phys.chemie.tu-muenchen.de>

[**] This work was supported by the DFG through the Emmy-Noether project ARE852/1-1. Karl J.J. Mayrhofer thanks the Austrian FWF, which supports him with an Erwin-Schrödinger Scholarship. We thank Dr. T. Tada from Tanaka Kikinzoku Kogyo for the supply of the catalyst.



Supporting information for this article is available under <http://www.angewandte.org> or from the authors.

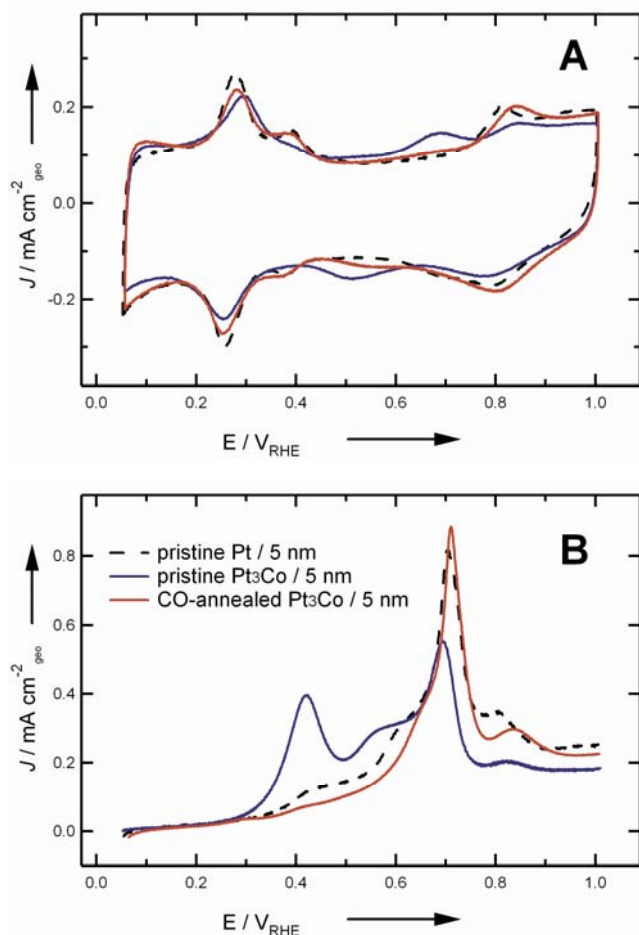


Figure 1. Cyclic voltammetry (A) and CO stripping (B) of Pt₃Co (red), CO-annealed Pt₃Co (blue) catalyst in alkaline electrolyte purged with argon. A plain Pt HSAC catalyst is shown for comparison (black dashed, factor 0.7).

The core-shell nanoparticles were also investigated as possible catalyst candidates for oxygen reduction, which is a key reaction in fuel cell technology. From previous studies on polycrystalline and single-crystal model systems it is well known that alloying Pt with a first-row transition metal leads to an increase in specific activity by a factor of 2-4^[15]. A similar improvement in catalytic activity could be observed on the CO-annealed Pt₃Co high-surface area catalyst in this study (see Table 1). The activity normalized to the mass of Pt of the pristine Pt₃Co catalyst in alkaline electrolyte is comparable to that of a plain Pt HSAC catalyst. After a CO-annealing treatment, however, the mass activity increases significantly by a factor of 2.5-3, with a slightly better performance obtained with the gas-phase CO-annealed catalyst. This is an additional confirmation that the utilization of the active noble metal at the surface has improved, supporting our interpretation of the cyclic voltammetry and CO stripping data. Assuming that the obtained core-shell structure is chemically stable under the reaction conditions, the amount of noble metal applied and consequently the overall cost of a fuel cell could be decisively reduced.

ORR	Pt / 5 nm	Pt ₃ Co ^[a]	Pt ₃ Co ^[b]	Pt ₃ Co ^[c]
0.900 V _{RHE}	0.12	0.13	0.29	0.36
0.875 V _{RHE}	0.23	0.26	0.55	0.65

Table 1. Comparison of the ORR activities in 0.1 M KOH [mA μg_{Pt}⁻¹] at two particular potentials ([a] pristine catalyst; [b] in-situ CO-annealed; [c] gas-phase CO-annealed). The error of the absolute values is ±15 %.

Investigations of the nanoparticle treatment via transmission electron microscopy of identical locations (IL-TEM)^[20, 21] are demonstrated in Figure 3. The shape of the carbon support stays unaltered after the CO annealing process, so that the identical locations can be retrieved readily. No significant variation between the position and structure of the as-received and CO-annealed catalyst particles can be seen and the particle size remains the same. Unfortunately, no elemental contrast due to the core-shell modification could be obtained, as is possible with aberration-corrected high-angle annular dark field STEM^[22].

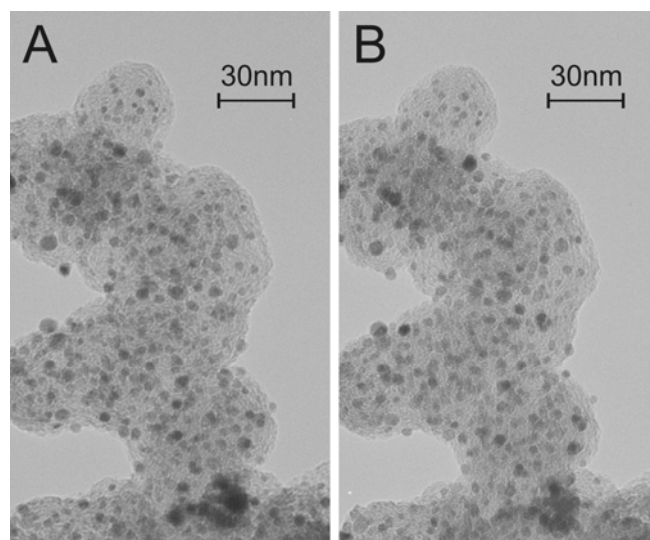


Figure 3. IL-TEM investigation of the Pt₃Co catalyst before (A) and after (B) CO-annealing.

The unaltered particle size is a clear sign that CO-annealing is a gentle preparation procedure for Pt-shell nanocatalyst structures, especially, when compared to high-temperature annealing or chemical leaching techniques^[4]. Combined with the information from the electrochemical surface characterization we can conclude that a Pt shell can be formed around a Pt_xCo_y core by adsorbate induced surface segregation. The result is a highly active catalyst with very promising potential, not only for the oxygen reduction but also for other reactions requiring noble metal surfaces. Future investigations will focus on the stability of the core-shell structure under various applied conditions, as well as on the further reduction in the content of the noble metal in the catalyst.

Experimental Section

The electrochemical measurements were conducted in a three-compartment electrochemical Teflon-cell, using a rotating disc electrode setup (*Radiometer Analytical, France*) and potentiostat (*Bank, Germany*). A saturated Calomel electrode and graphite rod were used as reference and counter electrodes, respectively. The electrolyte was prepared using Millipore Milli Q[®] water and KOH pellets (*Suprapure; Merck, Germany*). IL-TEM micrographs were recorded before and after the gas phase CO-annealing procedure on the identical catalyst locations using a JEM 100CX microscope (*JEOL, Japan*) with an accelerating voltage of 100 kV. For experimental details regarding TEM and the catalyst film preparation see supporting information.

Keywords: core shell catalyst · Pt shell · surface segregation · CO annealing · ORR · fuel cell

- [1] S. B. A. Hamid, R. Schlögl, *Angewandte Chemie International Edition* **2004**, *43*, 1628.
- [2] V. Poncec, *Applied Catalysis A: General* **2001**, *222*, 31.
- [3] V. R. Stamenkovic, B. Fowler, B. S. Mun, G. Wang, P. N. Ross, C. A. Lucas, N. M. Markovic, *Science* **2007**, *315*, 493.
- [4] S. Koh, J. Leisch, M. F. Toney, P. Strasser, *J. Phys. Chem. C* **2007**, *111*, 3744.
- [5] R. Srivastava, P. Mani, N. Hahn, P. Strasser, *Angewandte Chemie International Edition* **2007**, *46*, 8988.
- [6] J. Zhang, F. H. B. Lima, M. H. Shao, K. Sasaki, J. X. Wang, J. Hanson, R. R. Adzic, *Journal of Physical Chemistry B* **2005**, *109*, 22701.
- [7] S. Papadimitriou, A. Tegou, E. Pavlidou, S. Armyanov, E. Valova, G. Kokkinidis, S. Sotiropoulos, *Electrochimica Acta* **2008**, *53*, 6559.
- [8] A. Christensen, A. V. Ruban, P. Stoltze, K. W. Jacobsen, H. L. Skriver, J. K. Nørskov, F. Besenbacher, *Physical Review B* **1997**, *56*, 5822.
- [9] J. Nerlov, I. Chorkendorff, *Catalysis Letters* **1998**, *54*, 171.
- [10] V. Poncec, *Surface Science* **1979**, *80*, 352.
- [11] Y. Yin, R. M. Rioux, C. K. Erdonmez, S. Hughes, G. A. Somorjai, A. P. Alivisatos, *Science* **2004**, *304*, 711.
- [12] M. Arenz, K. J. J. Mayrhofer, V. R. Stamenkovic, B. Blizanac, T. Tada, N. M. Markovic, P. N. Ross, *Journal of the American Chemical Society* **2005**, *127*, 6819.
- [13] Y. Gauthier, M. Schmid, S. Padovani, E. Lundgren, V. Bus, G. Kresse, J. Redinger, P. Varga, *Physical Review Letters* **2001**, *87*, 036103.
- [14] U. Bardi, B. C. Beard, P. N. Ross, *Journal of Catalysis* **1990**, *124*, 22.
- [15] V. R. Stamenkovic, B. S. Mun, K. J. J. Mayrhofer, P. N. Ross, N. M. Markovic, *J. Am. Chem. Soc.* **2006**, *128*, 8813.
- [16] K. S. Shpiro, N. S. Telegina, V. M. Gryaznov, K. M. Minachev, Y. Rudny, *Catalysis Letters* **1992**, *12*, 375.
- [17] F. H. B. Lima, E. A. Ticianelli, *Electrochimica Acta* **2004**, *49*, 4091.
- [18] H. T. Duong, M. A. Rigsby, W.-P. Zhou, A. Wieckowski, *The Journal of Physical Chemistry C* **2007**, *111*, 13460.
- [19] M. Pourbaix, *Atlas of electrochemical equilibria in aqueous solutions*, 2nd English ed ed., National Association of Corrosion Engineers, Houston, **1974**.
- [20] K. J. J. Mayrhofer, S. J. Ashton, J. C. Meier, G. K. H. Wiberg, M. Hanzlik, M. Arenz, *Journal of Power Sources* **2008**, *185*, 734.
- [21] K. J. J. Mayrhofer, J. C. Meier, S. J. Ashton, G. K. H. Wiberg, F. Kraus, M. Hanzlik, M. Arenz, *Electrochemistry Communications* **2008**, *10*, 1144.
- [22] S. Chen, P. J. Ferreira, W. Sheng, N. Yabuuchi, L. F. Allard, Y. Shao-Horn, *Journal of the American Chemical Society* **2008**, *130*, 13818.

6.3.3 Degradation of Carbon-Supported Pt Bimetallic Nanoparticles by Surface Segregation

As shown in the last section, core-shell particles can be formed in-situ from alloy particles by means of a reductive treatment in a carbon monoxide environment. This raises the question if this modification is reversible by an oxidative treatment, similar to the Rh-Pd-system described by Tao *et al.* [74].

Furthermore, if the reverse segregation would be initiated upon operating conditions in a PEM fuel cell, the cobalt which emerges at the particle surface would be dissolved in the acid environment. This leaching process can essentially lower the overall performance of the fuel cell as described by Gasteiger *et al.* [4].

As mentioned above, the long-term stability of an electrocatalyst is probably even more important for the implementation in commercially viable fuel cells than its initial activity. For the described Pt₃Co/C catalyst, this includes the stability of the core-shell structure which can be either generated by a leaching process or by "CO annealing". In this respect, the highly positive cathodic potentials during the operation of a PEM fuel cell, especially during start/stop cycles, pose a challenge on account of the oxidizing reactive environment.

In the following paper, both the leached and the CO annealed core-shell Pt₃Co/C catalyst are studied in terms of their long-term stability. For that purpose, cyclic voltammetry and CO stripping in alkaline electrolyte are used for the characterization of the surface composition of the particles. These methods distinguish themselves as being very surface sensitive. However, since cobalt is not stable upon acid contact, the measurements had to be conducted in alkaline electrolyte. By exposing the core-shell catalysts to an oxidative electrochemical potential cycling treatment and simultaneously following the change of the characteristic features using cyclic voltammetry, it is unambiguously shown that an increasing amount of cobalt segregates to the particle surface. Consequently, the oxidative treatment induces the segregation of cobalt to the surface.

In acid electrolyte, a comparable treatment is investigated by following the concentration of cobalt in the catalyst with time of treatment, using ICP-OES. By this means, it is demonstrated that the amount of cobalt in the particles decreases steadily. Consequently, in acid electrolyte, the segregation process is induced by the treatment analogous to the behavior in alkaline solution. Since cobalt is not stable upon acid contact, it dissolves as soon as it reaches the particle surface leading to a decrease in cobalt concentration. This process might lead to depletion of cobalt in the particles and in a fuel cell, conductivity problems might occur due to cobalt ions diffusing into the membrane electrolyte.

Degradation of Carbon-Supported Pt Bimetallic Nanoparticles by Surface Segregation

K.J.J. Mayrhofer, K. Hartl, V. Juhart, and M. Arenz

Journal of the American Chemical Society, 2009, Volume 131, Issue 45, Pages
16348 - 16349

Permanent weblink:

<http://dx.doi.org/10.1021/ja9074216>

Reprinted from J. Am. Chem. Soc., 2009, 131, 45, 16348 with permission from
(Copyright 2010) American Chemical Society.

Degradation of Carbon-Supported Pt Bimetallic Nanoparticles by Surface Segregation

Karl J. J. Mayrhofer,* Katrin Hartl, Viktorija Juhart, and Matthias Arenz*

Lehrstuhl Physikalische Chemie, Technische Universität München, D-85748 Garching, Germany

Received September 2, 2009; E-mail: karl.mayrhofer@mytum.de; matthias.arenz@mytum.de

In addition to their activity, the long-term stability of nanoparticle (NP) catalysts is of major importance for their large-scale implementation. Accordingly, the persistence of electrocatalysts in low-temperature fuel cells plays a decisive role in their success as future energy conversion systems. However, the highly positive cathodic potentials, the acidic environment of the membrane electrolyte, and extensive load-cycle changes during mobile applications are challenging even for Pt, the catalyst material of choice in polymer electrolyte membrane (PEM) fuel cells.¹

Alloying Pt with other transition metals has already been proven to be beneficial for the activity of the oxygen reduction reaction (ORR).^{2–5} Furthermore, the stability of Pt bimetallic or multimetallic NPs is often suggested to be superior to that of plain Pt NPs.⁶ While it has been shown that the amount of dissolution of the non-noble component is enhanced under potential cycling relative to potential hold conditions,⁷ it is generally assumed that after the non-noble component has been leached from the surface, the remaining core–shell structure is stabilized against further degradation processes.⁸ Moreover, it has even been suggested that alloying can prevent particle agglomeration under certain conditions.^{9,10} However, the segregation of atoms to the surface of particles under reactive conditions, which is crucial for other catalytic systems,^{11–14} has not been studied to date. In this communication, we present data on the degradation of a Pt bimetallic NP catalyst indicating that continuous surface segregation even at room temperature is detrimental to the stability of the composition of these types of catalysts in fuel cell applications.

The degradation of a bimetallic Pt NP catalyst was studied in alkaline solution utilizing an unleached carbon-supported PtCo catalyst. The nominal atomic ratio was 3:1 Pt/Co, and the average particle size was ~ 5 nm. In contrast to the case of an acid electrolyte, transition metals such as Fe, Ni, and Co are not leached from the electrode but remain stable in alkaline solution.⁷ The oxidation state of the atoms on the surface thereby depends on the applied potential and can easily be determined by cyclic voltammetry as a surface-sensitive technique. Thus, cyclic voltammograms (CVs) recorded in alkaline solution can provide semiquantitative information on the composition of the outermost atomic layer of the electrode material (Figure 1) and can be applied to detect changes due to surface segregation induced by an electrochemical treatment (Figure 2).

As demonstrated in Figure 1, the CVs of (A) unleached Pt₃Co and (B) acid-leached Pt₃Co samples provide the first evidence of their different surface composition. Typical features for Pt electrodes, underpotentially deposited hydrogen (H_{upd}) in the potential region of 0.05 V_{RHE} and 0.4 V_{RHE} , and adsorption/desorption of oxygenated species above 0.7 V_{RHE} are slightly reduced for the unleached Pt₃Co. Instead, a well-defined current peak couple emerges at ~ 0.7 and 0.5 V_{RHE} in the positive- and negative-going scans, respectively. On the basis of the Pourbaix diagram of Co, this peak couple can be attributed to the change in the oxidation

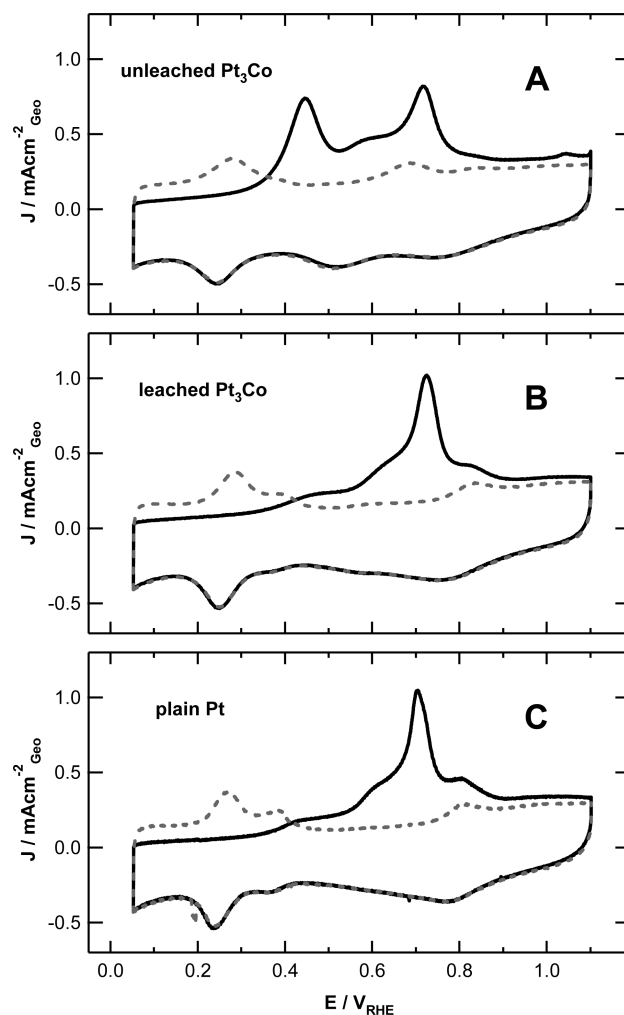


Figure 1. CVs in Ar-purged 0.1 M KOH electrolyte recorded at a scan rate of 50 $mV s^{-1}$ at room temperature (gray dashed curves) for (A) an unleached Pt₃Co catalyst, (B) a leached Pt₃Co catalyst, and (C) a plain Pt catalyst for comparison. Black solid lines are CO-stripping curves for the same catalysts.

state of Co surface atoms from 2+ to 3+.¹⁵ In contrast, the Co features do not appear in the CV of the leached Pt₃Co, which is virtually identical to that of plain Pt (Figure 1C). Further confirmation of the different surface composition can be obtained from the oxidation behavior of a preadsorbed CO monolayer in Figure 1 [so-called CO stripping (solid black lines)]. Again the leached Pt₃Co and plain Pt catalysts behave very similarly, with CO oxidation starting at ~ 0.3 V_{RHE} and a broad shoulder that evolves into a peak at ~ 0.7 V_{RHE} . In the CO stripping curve of the unleached Pt₃Co, however, a second peak at 0.45 V_{RHE} occurs, while the intensity of the peak at 0.7 V_{RHE} diminishes. This can be attributed to the

oxidation of adsorbed CO on Pt in the vicinity of oxidized Co surface atoms, which occurs at lower potentials than on a plain Pt surface as a result of a bimetallic promotion effect.

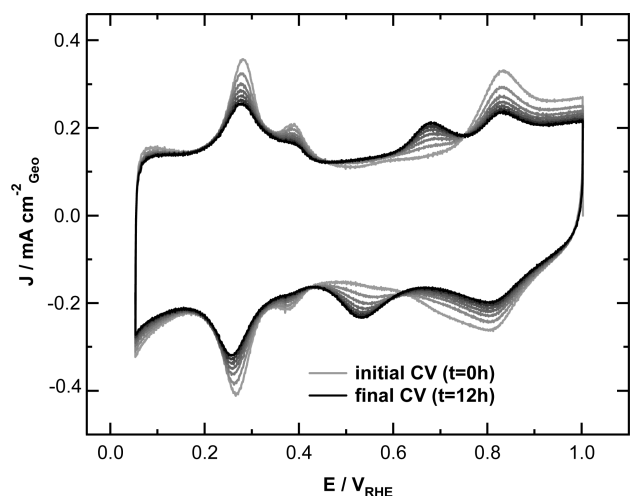


Figure 2. CV series (50 mV s^{-1} scan rate at room temperature) testing the stability of a leached Pt_3Co catalyst in Ar-purged 0.1 M KOH electrolyte. The gradual segregation of Co atoms to the surface due to potential cycling is demonstrated by displaying one CV recorded every 2 h between the initial CV (brightest gray solid curve) and the final CV after 12 h (dark solid curve).

Since different surface compositions of the nanoparticle catalysts can be distinguished unambiguously by cyclic voltammetry in alkaline electrolyte, changes upon electrochemical treatment also can now be probed in situ. In previous work, the long-term deterioration of the performance has been claimed to be negligible after an initial leaching of the surface alloying material.⁶ A different picture evolves, however, from studying a leached Pt_3Co catalyst by overnight potential cycling (50 mV s^{-1} scan rate between 0.05 and $1.0 \text{ V}_{\text{RHE}}$), as shown in Figure 2. The initial CV resembles that of a plain Pt surface, as described in Figure 1. The increasing Co features in the CVs recorded every 2 h thereafter clearly indicate the gradual accumulation of Co surface atoms on the NPs. Additionally, the CO stripping curves before and after the experiment (not shown) also change in a manner consistent with Figure 1. Because of alternating formation and reduction of an oxide layer during the potential treatment, the surface composition and the chemical state of the NPs change with time. In contrast to our recent study, where Pt segregated to the surface under the influence of a reducing CO atmosphere,¹⁶ the dynamic oxidizing conditions in this case induce quite the opposite effect of Co segregating toward the surface. It is interesting to note that milder treatments such as a constant-potential hold do not lead to such a severe effect; on the other hand, for instance, increasing the positive potential limit can dramatically accelerate the surface segregation. Moreover, repeating the experiment after subsequent leaching of the segregated Co from the surface causes segregation of additional internal Co atoms. Our investigations suggest that the surface segregation is initiated by the oxophilic character of Co, but roughening of the NP surface by subsurface oxygen might also be conducive.^{14,17}

In view of these results, it is expected that surface segregation also occurs in the acidic environment of PEM fuel cells, leading to continuous dealloying of PtCo catalysts due to Co dissolution.

Indeed, initial investigations of the surface segregation process induced by potential cycling in acid electrolyte suggest such a behavior. As demonstrated by means of ICP–OES, the ratio of Co to Pt atoms in the catalyst decreases with the number of potential cycles (see the Supporting Information). Additional investigations utilizing the recently developed IL-TEM methodology¹⁸ in combination with EDX are on the way.

In summary, we have qualitatively demonstrated by electrochemical investigations in alkaline electrolyte that even at room temperature, continuous surface segregation can occur for Pt bimetallic catalysts under certain conditions. Particularly when the potential is cycled in typical fuel cell cathode application ranges, Co atoms segregate to the surface of Pt_3Co NPs. Since in the acidic environment of PEM fuel cells any non-noble alloying material at the surface immediately dissolves into the electrolyte, such catalysts are expected to degrade steadily during operation until only Pt NPs remain. As a consequence, in order to fulfill key durability requirements for PEM fuel cells, specific attention to strategies for stabilization of the catalyst structure is required.^{19,20}

Acknowledgment. This work was supported by the DFG through the Emmy-Noether Project ARE852/1-1. K.J.J.M. expresses his gratitude to the Austrian FWF for an Erwin-Schrödinger Scholarship. K.H. thanks the German FCI for a Chemistry Funds Scholarship. The authors acknowledge G. K. H. Wiberg, S. J. Ashton, and T. Soini for their support and Dr. T. Tada of Tanaka Kikinzoku Kogyo for supplying the catalysts.

Supporting Information Available: Complete ref 1 and experimental details on the catalyst sample, electrochemical measurements, and catalyst treatment. This material is available free of charge via the Internet at <http://pubs.acs.org>.

References

- (1) Borup, R.; et al. *Chem. Rev.* **2007**, *107*, 3904.
- (2) Toda, T.; Igarashi, H.; Uchida, H.; Watanabe, M. *J. Electrochem. Soc.* **1999**, *146*, 3750.
- (3) Stamenkovic, V. R.; Mun, B. S.; Arenz, M.; Mayrhofer, K. J. J.; Lucas, C. A.; Wang, G. F.; Ross, P. N.; Markovic, N. M. *Nat. Mater.* **2007**, *6*, 241.
- (4) Chen, S.; Ferreira, P. J.; Sheng, W.; Yabuuchi, N.; Allard, L. F.; Shao-Horn, Y. *J. Am. Chem. Soc.* **2008**, *130*, 13818.
- (5) Koh, S.; Leisch, J.; Toney, M. F.; Strasser, P. *J. Phys. Chem. C* **2007**, *111*, 3744.
- (6) Antolini, E.; Salgado, J. R. C.; Gonzalez, E. R. *J. Power Sources* **2006**, *160*, 957.
- (7) Duong, H. T.; Rigsby, M. A.; Zhou, W. P.; Wieckowski, A. *J. Phys. Chem. C* **2007**, *111*, 13460.
- (8) Srivastava, R.; Mani, P.; Hahn, N.; Strasser, P. *Angew. Chem., Int. Ed.* **2007**, *46*, 8988.
- (9) Mukerjee, S.; Srinivasan, S. *J. Electroanal. Chem.* **1993**, *357*, 201.
- (10) Gasteiger, H. A.; Kocha, S. S.; Sompalli, B.; Wagner, F. T. *Appl. Catal., B* **2005**, *56*, 9.
- (11) Ponc, V. *Surf. Sci.* **1979**, *80*, 352.
- (12) Nerlov, J.; Chorkendorff, I. *Catal. Lett.* **1998**, *54*, 171.
- (13) Oh, S. G.; Rodriguez, N. M.; Baker, R. T. K. *J. Catal.* **1992**, *136*, 584.
- (14) Tao, F.; Grass, M. E.; Zhang, Y. W.; Butcher, D. R.; Renzas, J. R.; Liu, Z.; Chung, J. Y.; Mun, B. S.; Salmeron, M.; Somorjai, G. A. *Science* **2008**, *322*, 932.
- (15) Pourbaix, M. *Atlas of Electrochemical Equilibria in Aqueous Solutions*, 2nd English ed.; Association of Corrosion Engineers: Houston, TX, 1974.
- (16) Mayrhofer, K. J. J.; Juhart, V.; Hartl, K.; Hanzlik, M.; Arenz, M. *Angew. Chem., Int. Ed.* **2009**, *48*, 3529.
- (17) Greeley, J.; Norskov, J. K. *J. Phys. Chem. C* **2009**, *113*, 4932.
- (18) Mayrhofer, K. J. J.; Meier, J. C.; Ashton, S. J.; Wiberg, G. K. H.; Kraus, F.; Hanzlik, M.; Arenz, M. *Electrochem. Commun.* **2008**, *10*, 1144.
- (19) Greeley, J.; Stephens, I. E. L.; Bondarenko, A. S.; Johansson, T. P.; Hansen, H. A.; Jaramillo, T. F.; Rossmeisl, J.; Chorkendorff, I.; Norskov, J. K. *Nat. Chem.* **2009**, *1*, 552.
- (20) Mayrhofer, K. J. J.; Arenz, M. *Nat. Chem.* **2009**, *1*, 518.

JA9074216

6.4 Conclusion

In this chapter, different concepts towards the improvement of cathode catalysts in PEM fuel cells regarding their activity and stability were presented. The electrocatalyst consisting of platinum clusters deposited onto carbon substrates represents a novel, well-defined model system which can be used to study the influence of the carbon substrate, the particle density, the average particle size and the particle size distribution on the performance and durability of the catalyst. In this respect, degradation mechanisms can be studied in detail using IL-TEM and in this way related to different catalyst properties. The results are the basis for the development of future electrocatalysts.

Furthermore, it was shown that the carbon support has a great influence on the durability and the degradation processes of the electrocatalyst. IL-TEM measurements demonstrated an inhibition effect of particle detachment due to a modification of the carbon support of a Pt/C electrocatalyst using transition metals. Additionally, the results indicate that total oxidation of the carbon support is not the decisive factor with respect to the particle detachment mechanism.

Since bimetallic electrocatalysts received much attention in recent years, two catalysts of this kind are presented. First of all, unsupported core-shell AuPt particles are introduced as oxygen reduction catalyst. This catalyst is a promising concept for future electrocatalysts, consisting of an inner core of a different composition than platinum, which the shell is composed of. In this way, the active material is located at the surface, where the reactions take place, while the core material is shielded to the acid environment. Ideally, the inner material should be as cheap as possible in order to minimize the costs, but the system also has to be stable. In previous works, AuPt core-shell catalysts were reported to be highly active towards the oxygen reduction reaction [71]. However, the conventional synthesis route is complex and not upscalable. Therefore, a new synthesis method, suitable for large scale applications, was developed and optimized on the basis of TEM and electrochemical characterizations. The highly active AuPt core-shell catalyst can be taken as a model system which can be further improved by applying cheaper core materials than gold. One possibility could be the approach described by Zhang *et al.* [69], where a CoAu alloy is used as core material. Before the deposition of the platinum layer, the alloy particles are tempered forming a gold skin around a cobalt core. This structure could be taken as a starting point for the new synthesis route.

In addition, a commercially available Pt₃Co/C electrocatalyst was modified in-situ to a core-shell structure and characterized in detail. This core-shell structure consisting of a Pt shell around an alloy core is usually obtained by chemically leaching of the cobalt from the surface. Cyclic voltammetry and CO stripping in alkaline electrolyte were proven to be suitable to determine the surface composition of the alloy

catalyst. It was demonstrated, that the core-shell structure can be generated in-situ by a reductive treatment in carbon monoxide atmosphere. Thereby, surface segregation was induced and the resulting catalyst was even superior in activity towards the ORR compared to the one prepared by chemical leaching. However, both core-shell catalysts were also investigated regarding their stability upon operative conditions of a fuel cell. Cyclic voltammetry in alkaline electrolyte as well as elemental analysis showed that the reverse segregation process is induced upon an accelerated stress test. Cobalt segregates to the surface and, in an acidic environment, dissolves into the electrolyte or into the membrane, respectively. Consequently, for the development of improved bimetallic electrocatalysts, stability, including inhibited surface segregation, is of major importance besides activity aspects. Greeley *et al.* introduced a computational approach for the evaluation of possible alloy catalyst candidates. These catalysts have to form a Pt overlayer with an ORR activity higher than that of Pt and they should be as stable as possible. As indicators, the adsorption strength of an oxygen atom to the surface for predicting the ORR activity and the heat of alloy formation for the tendency of surface segregation, which determines the stability [10], are used. Following these predictions, new promising candidates might be found.

In general, in order to render commercially viable PEM fuel cells, their efficiency as well as their lifetime has to be improved. Some promising concepts and starting points for reaching this goal were presented in this chapter.

Chapter 7

Conclusion

In the presented work, three main topics were investigated. The first part (chapter 4) focused on accelerated stress tests using potential cycling in an electrochemical cell. It was discussed how the experimental parameters influence the obtained results and what precautionary measures have to be taken into account in order to ensure reproducible results. For example, it was shown that organic impurities originating from the synthesis of the catalyst have to be removed prior to the measurement by means of an electrochemical cleaning procedure, i.e. a continuous potential cycling process. The cleaning leads to an apparent increase in active surface area, which has to be accounted for in stress tests. Inorganic contaminants like chlorides were demonstrated to have a great influence on electrochemical measurements as well, and significantly accelerate the loss in active surface area. As a consequence, the avoidance of even trace amounts of chlorides in the fuel cell system is an important issue. Experiments with convection indicated the influence of mass transfer on the loss in active surface area. Two scenarios are possible: on the one hand, the convection accelerates the transport of dissolved platinum ions and detached platinum particles from the surface into the bulk solution and by this means prevent their redeposition. On the other hand, the degradation is enhanced due to the increased effective concentration of contaminations, like chlorides, at the catalyst surface. Additionally, it was demonstrated that the applied scan rate as well as the choice of electrolyte significantly affects the rate of degradation. The outcome of accelerated stress tests strongly depends on small details of the procedure, thus limiting the comparability of reported results. Based on this finding, the implementation of standardized test procedures might be beneficial.

In the second part, the durability and degradation behavior of standard oxygen reduction electrocatalysts were scrutinized and related to different properties of the catalysts. For this purpose, the results obtained by RDE measurements were compared to IL-TEM investigations. Five different high surface area catalysts were evaluated and the influence of platinum loading, particle size, carbon support and

use of alloyed particles on the degradation behavior was discussed. Upon a potential cycling treatment, particle detachment was found to occur for all catalyst samples and to be the predominant mechanism for the catalyst with larger particles (4-5 nm), which was synthesized from another catalyst with smaller particles by applying a heat treatment. Coalescence is dominant for the catalysts with smaller particle sizes (2-3 nm), whereas no indication for coalescence was found for the larger particles, possibly due to a stabilizing effect of the heat treatment. Changing platinum loadings from 20% to 50% did not influence the results. The graphitized carbon support seems to minimize particle detachment in comparison with amorphous carbon black and to retard particle migration leading to non-spherical coalesced particle shapes. The investigation of the Pt₃Co/C catalyst indicated leaching of the non-noble transition metal cobalt from the alloy particles resulting in particle shrinking. Furthermore, potentiostatic measurements at elevated temperatures were presented. It was found that by raising the temperature, the carbon support begins to degrade significantly, leading to its thinning and partial vanishing. This degradation effect can be related to the phenomenon of the collapse of the whole catalyst layer in a fuel cell.

The detailed investigations demonstrate that IL-TEM in combination with RDE measurements is a powerful tool to scrutinize degradation mechanisms of electrocatalysts. IL-TEM facilitates an insight into microscopic processes. Its application was verified for potential cycling and potentiostatic measurements at room temperature as well as elevated temperatures close to fuel cell conditions. In order to develop a more precise correlation between degradation mechanisms and specific properties based on the synthesis procedure, it would be beneficial to investigate in-house synthesized catalysts. In this case, all synthesis parameters would be known and could be controlled and communicated.

A starting point in this respect is represented by the application of well-defined model electrocatalysts which were introduced as one of the concepts towards high-performance catalysts presented in the third part (chapter 6). The production of the electrocatalysts under UHV conditions, including the generation of platinum clusters in a laser vaporization source as well as their mass selection and deposition onto a carbon substrate, were described in detail. By TEM analysis, migration of particles during the deposition procedure was excluded. Furthermore, samples with different particle size distributions and particle densities were characterized by means of TEM and electrochemical analysis. The determined electrochemically active surface area could thereby be linearly correlated with the integrated deposition current, which reflects the number of deposited clusters. The voltammetric features of the CV and the CO stripping experiments were in accordance with a platinum surface and the specific activity towards the oxygen reduction reaction could be determined.

By applying a potential cycling treatment, migration of whole particles on the surface of the carbon support was induced. The environment, i.e. the gas with which the electrolyte was saturated, influenced whether coalescence occurred (in oxygen or argon) or if it was suppressed (in carbon monoxide). In the latter case, the particles stayed separated and aligned in certain patterns depending on the cluster coverage. Based on these first investigations, further insights into the mechanisms of reactions and degradation can be gained by varying particle size distributions, particle densities, support materials and measurement details.

Another concept towards high-performance catalysts concerning the improvement of the catalyst durability is the modification of its carbon support with transition metals. In order to scrutinize this phenomenon on a microscopic scale, RDE measurements in combination with IL-TEM were employed. The results indicated an induced inhibition of particle detachment in comparison to a non-modified electrocatalyst.

One of the most promising approaches in catalyst development suggested in the literature is the application of bimetallic catalysts, especially core-shell catalysts. Based on electrochemical and TEM characterizations, the synthesis of unsupported AuPt core-shell particles was optimized by a cooperation partner leading to a highly active oxygen reduction electrocatalyst. This synthesis distinguishes itself as being upscalable in contrast to competing synthesis procedures. The concept of core-shell particles facilitates a high platinum utilization, and at the same time, it bypasses the negative particle size effect. Accordingly, the AuPt core-shell particles exhibit an activity towards the oxygen reduction reaction which is comparable to the one of polycrystalline platinum.

In addition to the chemically synthesized core-shell catalyst, the possibility of in-situ generation of a core-shell structure using a standard alloy Pt₃Co/C catalyst was demonstrated. An electrochemical treatment in carbon monoxide atmosphere thereby induced surface segregation. The resulting electrocatalyst exhibits a high specific activity towards the oxygen reduction reaction combined with a low amount of noble metal. However, also the reverse segregation process upon an accelerated stress test was demonstrated for in-situ prepared as well as for chemically leached Pt₃Co core-shell particles. This finding is in accordance with the observation of shrinking alloy particles described in chapter 5. It can be assumed that the same process might occur in a fuel cell upon operation, leading to dissolution of cobalt emerging at the surface. Diffusion of the cobalt ions into the membrane electrolyte might then cause conductivity problems.

As a result of the identified difficulties, activity and stability aspects of electrocatalysts should not be considered independently from one another, i.e. highly active catalysts, which do not degrade under operating conditions of a fuel cell, have to

be found. A theoretical approach for bimetallic electrocatalysts was suggested by Greeley *et al.*. In their calculations, both the activity towards the oxygen reduction reaction and the tendency towards surface segregation are optimized in order to obtain catalysts characterized by a high activity as well as stability.

In conclusion, IL-TEM in combination with RDE measurements was proven to be advantageous compared to conventional techniques used for degradation studies. It therefore has the potential to be established as a standard technique in fuel cell research for the mechanistic investigation of catalyst degradation. Furthermore, fundamental insights into the correlation between activity and degradation behavior and parameters and processes were gained. Such knowledge constitutes a basis for further development of highly efficient and durable electrocatalysts.

List of Figures

2.1	Time dependent potential of cyclic voltammetry and circuit of three-electrode setup	6
2.2	Schematic drawing of a rotating disc electrode and the radial flow of liquid during rotation	10
2.3	Procedure of IL-TEM	16
2.4	Procedure of relocation in IL-TEM	17
3.1	Preparation procedure of the catalyst film on the working electrode	22
3.2	Schematic drawing of the applied electrochemical Teflon cell	23
4.1	CVs before and after an electrochemical cleaning procedure	28
4.2	Scan rate dependent decrease in surface area	30
4.3	Comparison between degradation measurements in sulfuric and perchloric acid as electrolyte	31
4.4	Comparison of the CVs with and without added chlorides	32
4.5	Chloride concentration dependent loss of active surface area	33
4.6	Rotation and loading dependence of the loss of active surface area	34
4.7	Change of the characteristic CV in the presence of chlorides due to rotation.	35
5.1	Scheme of the different degradation mechanisms occurring in a fuel cell	38
5.2	Total loss of active surface area of the different electrocatalysts upon potential cycling	41
5.3	Time-dependent decrease of active surface area during the degradation treatment	42
5.4	IL-TEM images of the catalyst <i>Pt3nm</i>	44
5.5	IL-TEM images of the catalyst <i>Pt20%</i>	45
5.6	Particle size distributions for <i>Pt3nm</i> and <i>Pt20%</i> in each case before and after the degradation treatment	47
5.7	IL-TEM images of the catalyst <i>Ptgraph</i>	49
5.8	IL-TEM images of the catalyst <i>Pt5nm</i>	51
5.9	Analysis of IL-TEM images of the catalyst <i>Pt5nm</i>	52
5.10	Amount of produced CO ₂ of <i>Pt5nm</i> and <i>Pt3nm</i> during potential cycling	54
5.11	DEMS investigation of <i>Pt5nm</i> and <i>Pt3nm</i> : ECA against carbon loss	54
5.12	IL-TEM images of the catalyst <i>Pt₃Co</i>	57

5.13	Analysis of IL-TEM images of the catalyst Pt_3Co	58
5.14	CO stripping curves before and after a potentiostatic treatment of $Pt5nm$ at elevated temperatures	60
5.15	CO stripping curves of polycrystalline Pt after different treatments	61
5.16	ECA loss as function of the applied potential for two different temperatures	62
5.17	IL-TEM images of the catalyst $Pt5nm$ upon a potentiostatic treatment at $1.2 V_{RHE}$ and 333K	63
5.18	IL-TEM images of the catalyst $Pt5nm$ upon a potentiostatic treatment at $1.3 V_{RHE}$ and 348K	64
5.19	Further IL-TEM images of the catalyst $Pt5nm$ upon a potentiostatic treatment at $1.3 V_{RHE}$ and 348K	65
5.20	IL-TEM images of the catalyst $Pt5nm$ upon a potentiostatic treatment at $1.4 V_{RHE}$ and 348K	65

List of Tables

5.1	Characterization of the applied electrocatalysts	41
5.2	Statistical evaluation of the changes in number of particles and particle diameters for <i>Pt3nm</i> and <i>Pt20%</i> from identical regions using the images of IL-TEM	46
5.3	Attribution of degradation mechanisms to the electrocatalysts	56

References

- [1] K. Kordesch and G. Simader. *Fuel cells and their applications*. VCH Weinheim, 1996.
- [2] M. Gasik. *Materials for fuel cells*. Woodhead Publishing Ltd., Cambridge, England, 2008.
- [3] T.R. Ralph and M.P. Hogarth. Catalysis for low temperature fuel cells. Part I. The cathode challenges. *Platinum Metals Review*, 46(1):3–14, 2002.
- [4] H.A. Gasteiger, S.S. Kocha, B. Sompalli, and F.T. Wagner. Activity benchmarks and requirements for Pt, Pt-alloy, and non-Pt oxygen reduction catalysts for PEMFCs. *Applied Catalysis B: Environmental*, 56(1-2):9–35, 2005.
- [5] R. Schlögl and S.B. Abd Hamid. Nanocatalysis: mature science revisited or something really new? *Angewandte Chemie International Edition*, 43(13):1628–1637, 2004.
- [6] V.R. Stamenkovic, B.S. Mun, M. Arenz, K.J.J. Mayrhofer, C.A. Lucas, G. Wang, P.N. Ross, and N.M. Markovic. Trends in electrocatalysis on extended and nanoscale Pt-bimetallic alloy surfaces. *Nature Materials*, 6(3):241–247, 2007.
- [7] T. Toda, H. Igarashi, and M. Watanabe. Role of electronic property of Pt and Pt alloys on electrocatalytic reduction of oxygen. *Journal of the Electrochemical Society*, 145:4185, 1998.
- [8] S. Mukerjee and S. Srinivasan. Enhanced electrocatalysis of oxygen reduction on platinum alloys in proton exchange membrane fuel cells. *Journal of Electroanalytical Chemistry*, 357(1-2):201–224, 1993.
- [9] P. Mani, R. Srivastava, and P. Strasser. Dealloyed Pt-Cu core-shell nanoparticle electrocatalysts for use in PEM fuel cell cathodes. *The Journal of Physical Chemistry C*, 112(7):2770–2778, 2008.
- [10] J. Greeley, I.E.L. Stephens, A.S. Bondarenko, T.P. Johansson, H.A. Hansen, T.F. Jaramillo, J. Rossmeisl, I. Chorkendorff, and J.K. Nørskov. Alloys of platinum and early transition metals as oxygen reduction electrocatalysts. *Nature Chemistry*, 1(7):552–556, 2009.

-
- [11] R. Borup, J. Meyers, B. Pivovar, Y.S. Kim, R. Mukundan, N. Garland, D. Myers, M. Wilson, F. Garzon, D. Wood, et al. Scientific aspects of polymer electrolyte fuel cell durability and degradation. *Chemical reviews*, 107(10):3904–3951, 2007.
- [12] T.J. Schmidt, H.A. Gasteiger, G.D. Stäb, P.M. Urban, D.M. Kolb, and R.J. Behm. Characterization of High-Surface-Area Electrocatalysts Using a Rotating Disk Electrode Configuration. *Journal of the Electrochemical Society*, 145:2354–2358, 1998.
- [13] K.J.J. Mayrhofer, D. Strmcnik, B.B. Blizanac, V. Stamenkovic, M. Arenz, and N.M. Markovic. Measurement of oxygen reduction activities via the rotating disc electrode method: From pt model surfaces to carbon-supported high surface area catalysts. *Electrochimica Acta*, 53(7):3181–3188, 2008.
- [14] K. Sasaki, M. Shao, and R. Adzic. *Polymer Electrolyte Fuel Cell Durability, Dissolution and Stabilization of Platinum in Oxygen Cathodes*. Springer, New York, 2009.
- [15] K.J.J. Mayrhofer, S.J. Ashton, J.C. Meier, G.K.H. Wiberg, M. Hanzlik, and M. Arenz. Non-destructive transmission electron microscopy study of catalyst degradation under electrochemical treatment. *Journal of Power Sources*, 185(2):734–739, 2008.
- [16] A.J. Bard and L.R. Faulkner. *Electrochemical Methods, Fundamentals and Applications*. John Wiley and Sons, Inc., New York, second edition, 2001.
- [17] C.H. Hamann and W. Vielstich. *Elektrochemie*. Wiley/VCH, Weinheim, 2005. 4. vollständig überarbeitete Auflage.
- [18] R. Greef, R. Peat, L. M. Peter, D. Pletcher, and J. Robinson. *Instrumental Methods in Electrochemistry*. Ellis Horwood, Ltd., Chichester, 1985.
- [19] J. Hagen. *Industrial catalysis: a practical approach*. Wiley-VCH, Weinheim, 2006.
- [20] D. Linden and T.B. Reddy. *Handbook of batteries*. McGraw-Hill, New York, NY, third edition, 2001.
- [21] B.E. Conway and B.V. Tilak. Interfacial processes involving electrocatalytic evolution and oxidation of H₂, and the role of chemisorbed H. *Electrochimica acta*, 47(22-23):3571–3594, 2002.
- [22] N. M. Markovic, B. N. Grgur, C. A. Lucas, and P. N. Ross. Surface electrochemistry of CO on Pt(110)-(1x2) and Pt(110)-(1x1) surfaces. *Surface Science*, 384(1-3):L805–L814, 1997.
- [23] G. Jerkiewicz. Electrochemical Hydrogen Adsorption and Absorption. Part 1: Under-potential Deposition of Hydrogen. *Electrocatalysis*, pages 1–21.

- [24] D. Strmcnik, D. Tripkovic, D. van der Vliet, V. Stamenkovic, and N. M. Markovic. Adsorption of hydrogen on pt(111) and pt(100) surfaces and its role in the hor. *Electrochemistry Communications*, 10(10):1602–1605, 2008.
- [25] K. Kinoshita. *Electrochemical oxygen technology*. Wiley-Interscience, 1992.
- [26] R.L. Burwell. Manual of symbols and terminology for physicochemical quantities and units - appendix 2 - definitions, terminology and symbols in colloid and surface-chemistry, 2. heterogeneous catalysis. *Pure and Applied Chemistry*, 46(1):71–90, 1976.
- [27] S. Ashton. *The Design, Construction and Research Application of a Differential Electrochemical Mass Spectrometer (DEMS)*. Dissertation, TU München, 2011. in preparation.
- [28] L. Reimer and H. Kohl. *Transmission electron microscopy: physics of image formation*. Springer Verlag, New York, 2008.
- [29] S. Amelinckx, D. van Dyck, and J. van Landuyt. *Handbook of Microscopy: Methods I*. Wiley VCH, Weinheim, 1997.
- [30] Z. Siroma, K. Ishii, K. Yasuda, M. Inaba, and A. Tasaka. Stability of platinum particles on a carbon substrate investigated by atomic force microscopy and scanning electron microscopy. *Journal of Power Sources*, 171(2):524–529, 2007.
- [31] G. Wiberg. *The development of a state-of-the-art experimental setup demonstrated by the investigation of fuel cell reactions in alkaline electrolyte*. Dissertation, TU München, 2010. <http://nbn-resolving.de/urn/resolver.pl?urn:nbn:de:bvb:91-diss-20101008-993285-1-2>.
- [32] K.J.J. Mayrhofer, G.K.H. Wiberg, and M. Arenz. Impact of glass corrosion on the electrocatalysis on pt electrodes in alkaline electrolyte. *Journal of the Electrochemical Society*, 155:P1–P5, 2008.
- [33] K.J.J. Mayrhofer, S.J. Ashton, J. Kreuzer, and M. Arenz. An Electrochemical Cell Configuration Incorporating an Ion Conducting Membrane Separator between Reference and Working Electrode. *International Journal of Electrochemical Science*, 4(1):1–8, 2009.
- [34] H.R. Haas and M.T. Davis. Electrode and Catalyst Durability Requirements in Automotive PEM Applications: Technology Status of a Recent MEA Design and Next Generation Challenges. *ECS Transactions*, 25(1):1623–1631, 2009.
- [35] K. Kinoshita. *Carbon: electrochemical and physicochemical properties*. John Wiley Sons, New York, NY, 1988.
- [36] S. Henning. *The Electrochemical Degradation of a 3 nm carbon-supported Platinum Catalyst under Fuel Cell relevant conditions*. Master’s thesis, TU München, Munich, 2010.

- [37] S. Haslinger. *The Electrochemical Degredation of a Fuel Cell High Surface Area Carbon supported 5 nm Platinum Catalyst*. Master's thesis, TU München, Munich, 2010.
- [38] T.J. Schmidt, U.A. Paulus, H.A. Gasteiger, and R.J. Behm. The oxygen reduction reaction on a Pt/carbon fuel cell catalyst in the presence of chloride anions. *Journal of Electroanalytical Chemistry*, 508(1-2):41–47, 2001.
- [39] W.L. Marshall and E.V. Jones. Second Dissociation Constant of Sulfuric Acid from 25 to 350° Evaluated from Solubilities of Calcium Sulfate in Sulfuric Acid Solutions^{1, 2}. *The Journal of Physical Chemistry*, 70(12):4028–4040, 1966.
- [40] V. Stamenkovic, N.M. Markovic, and P.N. Ross. Structure-relationships in electrocatalysis: oxygen reduction and hydrogen oxidation reactions on Pt (111) and Pt (100) in solutions containing chloride ions. *Journal of Electroanalytical Chemistry*, 500(1-2):44–51, 2001.
- [41] A.P. Yadav, A. Nishikata, and T. Tsuru. Effect of halogen ions on platinum dissolution under potential cycling in 0.5 M H₂SO₄ solution. *Electrochimica Acta*, 52(26):7444–7452, 2007.
- [42] R.G. Bond and C.P. Straub. *Handbook of environmental control. Vol. III. Water supply and treatment*. Chemical Rubber Co., Cleveland, OH, 1974.
- [43] B.C.J. Zoeteman and F.J.J. Brinckman. *Human intake of minerals from drinking water in the European Communities. In: Hardness of drinking water and public health. Proceedings of the European Scientific Colloquium. Proceedings of the European Scientific Colloquium, Luxembourg, 1975*. Pergamon Press, Oxford, 1976.
- [44] A.B. Ofstad, M.S. Thomassen, J.L.G. de la Fuente, F. Seland, S. Møller-Holst, and S. Sunde. Assessment of Platinum Dissolution from a Pt/C Fuel Cell Catalyst: An Electrochemical Quartz Crystal Microbalance Study. *Journal of the Electrochemical Society*, 157:B621, 2010.
- [45] K. Matsuoka, S. Sakamoto, K. Nakato, A. Hamada, and Y. Itoh. Degradation of polymer electrolyte fuel cells under the existence of anion species. *Journal of Power Sources*, 179(2):560–565, 2008.
- [46] K.J.J. Mayrhofer, J.C. Meier, S.J. Ashton, G.K.H. Wiberg, F. Kraus, M. Hanzlik, and M. Arenz. Fuel cell catalyst degradation on the nanoscale. *Electrochemistry Communications*, 10(8):1144–1147, 2008.
- [47] Y. Shao-Horn, W.C. Sheng, S. Chen, P.J. Ferreira, E.F. Holby, and D. Morgan. Instability of supported platinum nanoparticles in low-temperature fuel cells. *Topics in Catalysis*, 46(3):285–305, 2007.

- [48] P.J. Ferreira, Y. Shao-Horn, D. Morgan, R. Makharia, S. Kocha, and H.A. Gasteiger. Instability of Pt/ C Electrocatalysts in Proton Exchange Membrane Fuel Cells. *Journal of the Electrochemical Society*, 152:A2256, 2005.
- [49] M.S. Wilson, F.H. Garzon, K.E. Sickafus, and S. Gottesfeld. Surface area loss of supported platinum in polymer electrolyte fuel cells. *Journal of the Electrochemical Society*, 140:2872–2877, 1993.
- [50] X. Yu and S. Ye. Recent advances in activity and durability enhancement of Pt/C catalytic cathode in PEMFC:: Part II: Degradation mechanism and durability enhancement of carbon supported platinum catalyst. *Journal of Power Sources*, 172(1):145–154, 2007.
- [51] P.T. Yu, W. Gu, J. Zhang, R. Makharia, F.T. Wagner, and H.A. Gasteiger. *Polymer Electrolyte Fuel Cell Durability, Carbon-Support Requirements for Highly Durable Fuel Cell Operation*. Springer, New York, 2009.
- [52] E. Antolini, J.R.C. Salgado, and E.R. Gonzalez. The stability of Pt-M (M= first row transition metal) alloy catalysts and its effect on the activity in low temperature fuel cells: A literature review and tests on a Pt-Co catalyst. *Journal of power sources*, 160(2):957–968, 2006.
- [53] K. Hartl, K.J.J. Mayrhofer, M. Hanzlik, and M. Arenz. Identical-location TEM investigations of Pt/C electrocatalyst degradation at elevated temperatures. in preparation.
- [54] O.V. Cherstiouk, A.N. Simonov, N.S. Moseva, S.V. Cherepanova, P.A. Simonov, V.I. Zaikovskii, and E.R. Savinova. Microstructure Effects on the Electrochemical Corrosion of Carbon Materials and Carbon Supported Pt Catalysts. *Electrochimica Acta*, 55(28):8453–8460, 2010.
- [55] A.P. Young, J. Stumper, and E. Gyenge. Characterizing the structural degradation in a PEMFC cathode catalyst layer: carbon corrosion. *Journal of The Electrochemical Society*, 156(8):B913–B922, 2009.
- [56] F. Maillard, S. Schreier, M. Hanzlik, E.R. Savinova, S. Weinkauff, and U. Stimming. Influence of particle agglomeration on the catalytic activity of carbon-supported Pt nanoparticles in CO monolayer oxidation. *Physical Chemistry Chemical Physics*, 7(2):385–393, 2004.
- [57] M. Wissler. Graphite and carbon powders for electrochemical applications. *Journal of power sources*, 156(2):142–150, 2006.
- [58] G.A. Gruver. The corrosion of carbon black in phosphoric acid. *Journal of The Electrochemical Society*, 125(10):1719–1720, 1978.
- [59] H.A. Gasteiger and N.M. Markovic. Just a Dream – or Future Reality? *Science*, 324(5923):48, 2009.

- [60] G. Mie. Articles on the optical characteristics of turbid tubes, especially colloidal metal solutions. *Annalen der Physik*, 330(3):377–445, 1908.
- [61] S. Gilb, K. Hartl, A. Kartouzian, J. Peter, U. Heiz, H.G. Boyen, and P. Ziemann. Cavity ring-down spectroscopy of metallic gold nanoparticles. *The European Physical Journal D-Atomic, Molecular, Optical and Plasma Physics*, 45(3):501–506, 2007.
- [62] U. Heiz and U. Landman. *Nanocatalysis*. Springer Verlag, Berlin, 2007.
- [63] A. Sanchez, S. Abbet, U. Heiz, W.D. Schneider, H. Häkkinen, R.N. Barnett, and U. Landman. When gold is not noble: nanoscale gold catalysts. *The Journal of Physical Chemistry A*, 103(48):9573–9578, 1999.
- [64] M. Haruta. When gold is not noble: catalysis by nanoparticles. *The Chemical Record*, 3(2):75–87, 2003.
- [65] K. Kinoshita. Particle size effects for oxygen reduction on highly dispersed platinum in acid electrolytes. *Journal of the Electrochemical Society*, 137:845, 1990.
- [66] K.J.J Mayrhofer, B.B. Blizanac, M. Arenz, V.R. Stamenkovic, P.N. Ross, and N.M. Markovic. The impact of geometric and surface electronic properties of Pt-catalysts on the particle size effect in electrocatalysis. *The Journal of Physical Chemistry B*, 109(30):14433–14440, 2005.
- [67] K.H. Kangasniemi, D.A. Condit, and T.D. Jarvi. Characterization of Vulcan electrochemically oxidized under simulated PEM fuel cell conditions. *Journal of the Electrochemical Society*, 151:E125, 2004.
- [68] B.J. Hwang, Y.W. Tsai, J.F. Lee, P. Borthen, and H.H. Strehblow. In situ EXAFS investigation of carbon-supported Pt clusters under potential control. *Journal of Synchrotron Radiation*, 8(2):484–486, 2001.
- [69] J. Zhang, F.H.B. Lima, M.H. Shao, K. Sasaki, J.X. Wang, J. Hanson, and R.R. Adzic. Platinum monolayer on nonnoble metal-noble metal core-shell nanoparticle electrocatalysts for O₂ reduction. *The Journal of Physical Chemistry B*, 109(48):22701–22704, 2005.
- [70] R. Srivastava, P. Mani, N. Hahn, and P. Strasser. Efficient oxygen reduction fuel cell electrocatalysis on voltammetrically dealloyed Pt–Cu–Co nanoparticles. *Angewandte Chemie International Edition*, 46(47):8988–8991, 2007.
- [71] S.R. Brankovic, J.X. Wang, and R.R. Adzic. Metal monolayer deposition by replacement of metal adlayers on electrode surfaces. *Surface science*, 474(1-3):L173–L179, 2001.
- [72] M. Inaba. Durability of Electrocatalysts in Polymer Electrolyte Fuel Cells. *ECS Transactions*, 25(1):573, 2009.

-
- [73] M. Pourbaix. *Atlas of electrochemical equilibria in aqueous solutions*. Pergamon Press Ltd., Oxford, 1966.
- [74] F. Tao, M.E. Grass, Y. Zhang, D.R. Butcher, J.R. Renzas, Z. Liu, J.Y. Chung, B.S. Mun, M. Salmeron, and G.A. Somorjai. Reaction-driven restructuring of Rh-Pd and Pt-Pd core-shell nanoparticles. *Science*, 322(5903):932, 2008.
- [75] D.S. Strmcnik, D.V. Tripkovic, D. van der Vliet, K.C. Chang, V. Komanicky, H. You, G. Karapetrov, J.P. Greeley, V.R. Stamenkovic, and N.M. Markovic. Unique Activity of Platinum Adislands in the CO Electrooxidation Reaction. *Journal of the American Chemical Society*, 130(46):15332–15339, 2008.
- [76] M. Arenz, K.J.J. Mayrhofer, V. Stamenkovic, B.B. Blizanac, T. Tomoyuki, P.N. Ross, and N.M. Markovic. The effect of the particle size on the kinetics of CO electrooxidation on high surface area Pt catalysts. *Journal of the American Chemical Society*, 127(18):6819–6829, 2005.

Acknowledgements - Danksagung

Mein besonderer Dank gilt an dieser Stelle meinem Betreuer Prof. Dr. Matthias Arenz, der mir die Bearbeitung dieses interessanten Themas im Rahmen meiner Doktorarbeit ermöglicht und mich in jeglicher Hinsicht unterstützt hat. Gleichzeitig möchte ich mich auch bei Prof. Dr. Ueli Heiz für die Ermöglichung meiner Doktorarbeit an der TU München bedanken und dafür, dass ich weiterhin so freundlich in seinem Lehrstuhl aufgenommen wurde.

Des Weiteren möchte ich folgenden Personen danken:

- Dr. Karl Mayrhofer, der mir vor allem in der Anfangsphase mit Rat und Tat zur Seite stand und mich mit großem Enthusiasmus in die Welt der Elektrokatalyse einführte,
- meinen Laborkollegen Sean, Gustav, Viktorija und insbesondere Markus für die gute Zusammenarbeit und die Bereicherung des Laboralltags,
- allen Mitgliedern der Heiz-Gruppe insbesondere Kathrin, Josef, Andreas, Brad, Yves, Martin, Andrew, Florian Sch., Sebastian, GiHan und Florian S. für die freundliche Atmosphäre und den Spaß,
- allen Mitgliedern der Nanokemi-Gruppe der Københavns Universitet, insbesondere Magni, Erling, Søren und Jakob für die schöne Zeit in Kopenhagen,
- Marianne Hanzlik vom Zentrum für Elektronenmikroskopie für die tolle Zusammenarbeit, die vielen langen und immer ergiebigen Diskussionen und für ihre sympathische hilfsbereite Art,
- der Feinmechanik- sowie der Elektronikwerkstatt für ihre exzellente Arbeit und die guten Ratschläge,
- meiner Familie und meinen Freunden für die einzigartige Unterstützung und den bedingungslosen Rückhalt während meines gesamten Studiums
- und schließlich danke ich meinem Ehemann Stefan für seine immerwährende Geduld und Unterstützung sowie für seine Liebe, die mein Leben Tag für Tag verschönert.

Curriculum Vitae

Katrin Gabriele Schlögl, née Hartl

Situlistr. 35
80939 München

Phone: +49.89.289.13401
Mobile: +49.179.1211869
Email: katrin.hartl@mytum.de

Born: 26th of December 1983 in Altötting, Germany
Nationality: German

Education

Doctoral thesis **since May 2008**

Chair for Physical Chemistry, Chemistry Department, Technische Universität München; Munich, Germany

Project	Identical location transmission electron microscopy in combination with rotating disc electrode measurements - the activity of fuel cell catalysts and its degradation
Research Stay	Copenhagen University, Denmark (June 2010 - January 2011)
Scholarship	Chemiefonds Scholarship of the "Fonds der Chemischen Industrie" (October 2008 - September 2010)
Supervisor	Prof. Dr. Matthias Arenz

Master Studies Chemistry **October 2006 - March 2008**

Technische Universität München; Munich, Germany

Major Subject	Physical Chemistry
Second Major	Catalysis and Reaction Technology
Master's Thesis	Optical Spectroscopy of Mass Selected Metal Clusters on SiO ₂
Supervisor	Prof. Dr. Ueli Heiz, Chair for Physical Chemistry
Award	Jürgen Manchot award for excellent final degree

Bachelor Studies Chemistry **October 2003 - August 2006***Technische Universität München; Munich, Germany*

Bachelor's Thesis Cavity Ringdown Spectroscopy of Supported Gold Nanoparticles
Supervisor Prof. Dr. Ueli Heiz, Chair for Physical Chemistry

School Education **September 1994 - June 2003***König-Karlmann-Gymnasium Altötting, Germany*

Major Subjects Mathematics, Physics
Degree Abitur

Further Experience**Practical internship** **August 2006 - October 2006***Wacker Chemie AG, Burghausen; Germany*

Investigation of the influence of different promoters in the Müller-Rochow process

Teaching **October 2008 - March 2010***Chemistry Department, Technische Universität München; Munich, Germany*

Tutorial for Spectroscopy and Photochemistry, Spectroscopy and Molecular Structure and Thermodynamics and Kinetics

Presentations and Talks**Talks:**

DPG Frühjahrstagung
Regensburg, Germany, March 2010

Fonds der Chemischen Industrie Treffen
Munich, Germany, February 2010

216th meeting of the Electrochemical Society (ECS)
Vienna, Austria, Oktober 2009

Poster presentations:

COST 41 Meeting
Munich, Germany, March 2010

"Electrochemistry: Crossing Boundaries", organized by GDCh
Gießen, Germany, Oktober 2008

Munich, 25th of May 2011

Publication List

1. Hartl, K., Hanzlik, M., and Arenz, M. (2011). IL-TEM investigations on the degradation mechanism of Pt/C electrocatalysts with different carbon supports. *Energy & Environmental Science* 4, 234-238.
2. Hartl, K., Mayrhofer, K.J.J., Lopez, M., Goia, D., and Arenz, M. (2010). AuPt core-shell nanocatalysts with bulk Pt activity. *Electrochemistry Communications* 12, 1487-1489.
3. Hartl, K., Nesselberger, M., Mayrhofer, K.J.J., Kunz, S., Schweinberger, F.F., Kwon, G., Hanzlik, M., Heiz, U., and Arenz, M. (2010). Electrochemically induced nanocluster migration. *Electrochimica Acta* 56, 810-816.
4. Kunz, S., Hartl, K., Nesselberger, M., Schweinberger, F.F., Kwon, G., Hanzlik, M., Mayrhofer, K.J.J., Heiz, U., and Arenz, M. (2010). Size-selected clusters as heterogeneous model catalysts under applied reaction conditions. *Physical Chemistry Chemical Physics* 12 (35), 10288-10291.
5. Hartl, K., Mayrhofer, K.J.J., and Arenz, M. (2009). Stability of Pt Alloy High Surface Area Catalysts. *ECS Transactions* 25 (1), 555.
6. Mayrhofer, K. J. J., Hartl, K., Juhart, V., and Arenz, M. (2009). Degradation of Carbon-Supported Pt Bimetallic Nanoparticles by Surface Segregation. *Journal of the American Chemical Society* 131, 16348.
7. Mayrhofer, K. J. J., Juhart, V., Hartl, K., Hanzlik, M., and Arenz, M. (2009). Adsorbate-Induced Surface Segregation for Core-Shell Nanocatalysts. *Angewandte Chemie - International Edition* 48, 3529-3531.
8. Gilb, S., Hartl, K., Kartouzian, A., Peter, J., Heiz, U., Boyen, H.G., and Ziemann, P. (2007). Cavity ring-down spectroscopy of metallic gold nanoparticles. *European Physical Journal D* 45, 501-506.